Chaperone Effects on Tau Amyloid Formation

Hannah E.R. Baughman

A dissertation

submitted in partial fulfillment of the

requirements for the degree of

Doctor of Philosophy

University of Washington

2019

Reading Committee:

Abhinav Nath, Chair

Rachel E. Klevit

Kelly K. Lee

Program Authorized to Offer Degree:

Medicinal Chemistry

University of Washington

Abstract

Chaperone Effects on Tau Amyloid Formation

Hannah E.R. Baughman

Chair of the Supervisory Committee:
Professor Abhinav Nath
Medicinal Chemistry

Tau is a microtubule-associated protein that forms insoluble amyloid fibrils in a set of neurodegenerative disorders termed tauopathies, which include Alzheimer's disease, frontotemporal dementia, and chronic traumatic encephalopathy. Molecular chaperones are proteins that act to prevent aberrant protein aggregation such as tau fibril formation. This dissertation characterizes the mechanisms by which chaperones interact with tau to counteract its aggregation, with particular focus on the small heat shock protein HspB1. Chapter 2 compares the effects of HspB1 on tau aggregation with the effects of another structurally-unrelated chaperone, Hsc70. Chapter 3 describes interactions between the disordered N-terminal region (NTR) and the structured alpha-crystallin domain (ACD) of HspB1. Both domains are involved in chaperone activity toward tau. Understanding how they interact with each other enables further structural characterization of interactions between HspB1 and tau in Chapter 4. Chapter 4 also identifies a way by which interactions between the NTR and ACD can be perturbed to improve HspB1 chaperone activity against tau.

TABLE OF CONTENTS

LIST OF FIGURES

ACKNOWLEDGEMENTS

I've been lucky to cross paths with a lot of great people during my time in graduate school, without whom this work would not have been possible. First, I would like to thank my two advisors, Abhi Nath and Rachel Klevit, for giving me the opportunity to pursue a challenging project that bridged their areas of expertise. They have offered tremendous support and been sources of inspiration and smart ideas while granting me the independence to make the project my own. Both have fostered collaborative environments within their labs, and I have benefited greatly from members of both labs. In particular, I would like to thank Amanda Clouser for first encouraging me to work on HspB1 and offering both mentorship and friendship since the day I arrived at the University of Washington. I would also like to thank Eleanor Vane, Chris Woods, Maria Janowska, Scott Delbecq, and Lisa Tuttle for helpful discussions, advice, and encouragement over the years. Finally, I would like to thank Hau Pham and Chloe Adams for their important contributions to the project as my mentees.

Over the course of my PhD, I have been a part of multiple scientific communities, including the Biological Physics, Structure, and Design program, the departments of Medicinal Chemistry and Biochemistry, and the Molecular Biophysics Training Program. I have had the opportunity to meet smart people from multiple fields, and my work has truly benefited as a result. I particularly want to thank my BPSD cohort, the BPSD program coordinator Erin Kirschner, and the members of my committee, Chip Asbury, Bill Atkins, Kelly Lee, and Ning Zheng.

I would like to thank my family for their support and encouragement throughout my life. Finally, I would like to thank Benjamin Basanta for his love and support and for being someone with whom I could celebrate, commiserate, and collaborate over the past six years ago.

Chapter 1. INTRODUCTION

1.1 PROTEIN AGGREGATION, AMYLOID FORMATION, AND MOLECULAR CHAPERONES

The cytoplasm of cells is densely packed, and proteins exist in close proximity to other proteins and additional macromolecules such as nucleic acids and lipids. The total concentration of macromolecules in the cytoplasm varies by cell type but is estimated to be 300-400 mg/ml or 30-40% of the total volume in *E. coli* cells (Zimmerman and Trach 1991). These crowded conditions facilitate interactions that drive vital biological processes (Zhou et al. 2008) but also can promote aberrant protein-protein interactions that result in protein aggregation (Van Den Berg et al. 1999; Munishkina et al. 2004; Uversky et al. 2002). Cellular stress events such as acidosis, oxidative stress, and temperature changes further increase the risk of aberrant protein aggregation (Tyedmers et al. 2010). Protein aggregation is typically detrimental and has been linked to numerous human diseases, including cataract formation, diabetes, and multiple neurodegenerative disorders.

Protein aggregation usually takes one of two forms: amorphous aggregation or amyloid formation. Amorphous aggregates are insoluble assemblies of proteins that associate in a manner that lacks regular order. By contrast, amyloid aggregates are highly ordered and are characterized by the formation of long, fibrillar assemblies with β sheet structure (Tyedmers et al. 2010). In amyloid fibrils, proteins align perpendicular to the fibril axis and form extended β strands mediated by backbone hydrogen bonds and sidechain contacts between protein subunits (Padmanabhan et al. 2017). These structures tend to be highly thermodynamically stable and may represent the global energetic minimum for many proteins (Baldwin et al. 2011). The formation of amyloid-type

aggregates is particularly common for intrinsically disordered proteins, in part because the aggregation-prone segments of these proteins tend to be solvent-exposed rather than buried within a folded core (Linding et al. 2004). Amyloid formation is associated with many protein aggregation diseases, including Alzheimer's Disease, Parkinson's Disease, and Huntington's Disease. Many factors potentially contribute to the toxicity of amyloid formation in disease, including loss of function of the proteins involved, gain of toxic function of fibrils or pre-fibrillar species, interference of aggregates with other intracellular processes, and loss of protein homeostasis. For many amyloid-forming proteins, pre-amyloid oligomeric species are thought to be most responsible for toxic effects (Chiti and Dobson 2006). While the role of amyloid formation in disease is well-documented, recent studies have also identified functional roles of amyloid forms of proteins, including antimicrobial activity and peptide hormone storage (Maji et al. 2009; Kumar et al. 2016). In some cases, amyloid formation by the same protein can play both functional and disease-associated roles. For example, Amyloid-β fibril formation is implicated in the development of Alzheimer's Disease but also was shown to have antimicrobial properties (Kumar et al. 2016).

Molecular chaperones are proteins that act to maintain protein homeostasis through interactions with unfolded, misfolded, and/or aggregation-prone proteins. Humans have multiple structurally-unrelated chaperone families, many of which contain multiple homologous members. In total, humans have approximately 200 distinct chaperones and co-chaperones (Hartl et al. 2011). Together, these form complex networks that act to target different clients and distinct phases of protein folding and protein aggregation processes. Some classes of chaperones, such as Hsp70, Hsp90, and chaperonins, use the energy of ATP hydrolysis to promote proper folding and drive re-folding of misfolded proteins. Others, including the Hsp104 family, use ATP to disaggregate

pre-formed fibrils. Others act in an ATP-independent manner to engage aggregation-prone proteins and delay or prevent their aggregation (Hartl et al. 2011). There is considerable overlap in these functional categories. For example, Hsp70 family members can disaggregate fibrils when acting in concert with Hsp40 and Hsp110 chaperones (Gao et al. 2015a) and have been shown to have ATP-independent anti-aggregation activity in addition to their refolding activity (Chaari et al. 2016; Kundel et al. 2018). Chaperones from different families interact extensively, and these interactions are often mediated by co-chaperones that serve as physical linkers. Chaperones also interact with the autophagy pathway and the ubiquitin-proteasome system to facilitate the degradation of unsalvageable proteins or protein aggregates (Hartl et al. 2011).

Together, a cell's chaperone proteins and the network of interactions between them serves as a defense system against aberrant protein aggregation. Many protein aggregation diseases are age-associated, indicating that the cell's chaperone machinery is able to prevent toxic aggregation for years, but its ability to maintain proteostasis is compromised over the course of a lifetime (Hartl et al. 2011). The work in this dissertation aims to further our understanding of how molecular chaperones act to prevent aberrant protein aggregation. It investigates interactions between the protein tau, which forms amyloid fibrils in a set of neurodegenerative disorders termed tauopathies, and the chaperone proteins HspB1 and Hsc70.

1.2 TAU BIOLOGY AND DISEASE IMPLICATIONS

Tau is a microtubule-associated protein abundantly expressed in neurons. In tauopathies, it is found to be hyperphosphorylated, dissociated from microtubules, and deposited amyloid fibrils. Tauopathies include Alzheimer's Diseases, Pick's Disease, chronic traumatic encephalopathy, progressive supranuclear palsy, corticobasal degeneration, agyrophilic grain disease, and frontotemporal dementia with parkinsonism linked to chromosome 17 (FTDP-17).

Although tauopathies differ in their clinical presentation and patterns of tau deposition, they all involve the formation of insoluble tau fibrils accompanied by neurodegeneration (Mandelkow and Mandelkow 2011). FTDP-17 is caused by inherited mutations in the tau gene, indicating that tau plays a causative role in the development of this disease (Wszolek et al. 2005). While the causes of tauopathies are subject to some debate and involve complicated interplay between additional cellular proteins and environmental factors, the fact that mutations in the tau gene are sufficient to cause disease strongly suggests that tau plays a central role in the development of most if not all tauopathies.

The biological function of tau remains poorly understood, but it is known to play roles in microtubule stability, neurite outgrowth, and hippocampal development. In healthy neurons, the concentration of tau is 1-2 μM, and most is associated with microtubules (Iqbal et al. 2010; Mandelkow and Mandelkow 2011). Knockout of tau in mice results in delayed hippocampal neuron development but does not cause physical abnormalities or impair the ability of the mice to reproduce, indicating that there may be some redundancy of its function (Dawson et al. 2001). Studies in human neurons indicate that tau plays roles in promoting neurite outgrowth and axonal development and can regulate axonal trafficking of organelles and other cargo (Stamer et al. 2002). Microtubules play important roles in neurons, particularly in axonal development and axonal trafficking, and these phenotypic effects of tau are likely due to interactions between tau and microtubules. In vitro, tau promotes tubulin polymerization and microtubule stability. Tubulin dimers interact with multiple sites within the tau protein and form a fuzzy complex that promotes tubulin assembly and microtubule polymerization (Li and Rhoades 2017). Tau binds to assembled microtubules in an elongated manner, spanning multiple tubulin subunits and promoting stability of the polymerized form (Kellogg et al. 2018).

Tau is intrinsically disordered in solution. It can be subdivided into four domains: an N-terminal projection domain, a proline-rich region, a microtubule-binding repeat region, and a short C-terminal region (Figure 1.1). Tau undergoes alternative splicing at two sites. The N-terminal projection domain can contain 0, 1, or 2 insertions, and isoforms are termed 0N, 1N, and 2N. The microtubule-binding repeat region can have either 4 repeats or 3 depending on whether the second repeat is present, which are denoted 3R and 4R. Therefore, six possible tau isoforms exist, the longest being tau2N4R and the shortest tau0N3R. Healthy adult brains typically contain equal proportions of 3R and 4R tau, and deviation from this balance in either direction has been linked to disease . Multiple disease-associated mutations have been shown to alter the splicing of the repeat domain of tau, including some silent mutations, indicating that imbalance of these isoforms is sufficient to cause disease (D'Souza et al. 1999). The tau fibrils that form in different tauopathies differ in the isoforms they contain. For example, Alzheimer's Disease fibrils contain all six tau isoforms (Goedert et al. 1989), whereas Pick's Disease fibrils only contain 3R tau (Falcon et al. 2018a). The presence of different isoforms could explain some differences in disease presentation and pathology observed in different tauopathies.

Fibril formation is driven by two aggregation-prone motifs, ^{275}VQIINK^{280} and ^{306}VQIVYK^{311}, which occur at the beginning of the second and third microtubule-binding repeats (Figure 1.1). These regions have β-strand propensity in solution, and tau constructs require at least one of them to form fibrils *in vitro* (von Bergen et al. 2000; Von Bergen et al. 2001; Mukrasch et al. 2005). The tau protein in disease fibrils is hyperphosphorylated and subject to extensive post-translational modifications (Mandelkow and Mandelkow 2011). Recombinant tau protein does not spontaneously form fibrils *in vitro* but requires extensive phosphorylation or the addition of a polyanionic compound to induce aggregation. Multiple polyanions, including heparin, RNA,

polyphosphate, and polyglutamate, have been shown to induce tau aggregation (Friedhoff et al. 1998; Kampers et al. 1996; Cremers et al. 2016). The role of these polyanions has been subject to some debate; however, it is clear that they promote structural rearrangement, the formation of elongation-competent nuclei, and fibril elongation (Elbaum-Garfinkle and Rhoades 2012; Nakatani-Webster and Nath 2017; Wickramasinghe et al. 2019). Digestion of polyanionic cofactors following the formation of fibrils causes them to dissociate, indicating that they also play a role in stabilizing mature fibrils (Fichou et al. 2018). The microtubule-binding repeat region is highly positively charged, and polyanions counter this charge to enable tau self-association. The role of polyanionic cofactors *in vivo* is unclear, and further experimental work is necessary to identify disease-associated polyanions. However, given their presence in cells and efficiency at inducing aggregation *in vitro*, it is likely that they also play a role in disease states.

Recently, structures of tau fibrils derived from patients with Alzheimer's Disease, Pick's Disease, and Chronic Traumatic Encephalopathy were solved to near-atomic resolution by cryoEM (Fitzpatrick et al. 2017a; Falcon et al. 2018a, 2019). The structured core resolved by EM consisted primarily of the third and fourth microtubule-binding repeats for all fibrils, but the fibril morphology and tau fold (i.e. the structure of a single tau molecule within the fibril) differed significantly between patients with different tauopathies. Although the tau fold was consistent in all extracted fibrils from the same patient, many patient brains contained fibrils with two distinct morphologies in which the relative orientation of tau protofilaments differed. CryoEM structures have been solved for fibrils derived from five Alzheimer's Disease and three Chronic Traumatic Encephalopathy patients, and in each case the tau fold is consistent for all patients with the same disease but differs between diseases (Falcon et al. 2018b, 2019). This suggests that the tau fold within fibrils plays a role in distinguishing the different tauopathies. Recent work has shown that

tau spreads via a prion-like mechanism, and that there are multiple distinct prion "strains" of tau that each encode unique gross morphologies (Sanders et al. 2014; Sharma et al. 2018). This supports the possibility that different tauopathies are caused by different prion-like strains of tau which each encode disease-specific fibril morphologies.

While fibril formation correlates well with disease progression, increasing evidence suggests that the primary toxic species is a pre-fibrillar oligomeric state of tau. In tauopathy-model mice expressing human tau with the disease-associated mutation P301L, memory function can recover by stopping the expression of transgenic tau, despite the fact that fibrillar tau species persist in the brain under these conditions. This suggests that the toxic species is something that occurs on-pathway to fibril formation rather than the fibrils themselves (SantaCruz et al. 2005). Oligomeric tau species correlate better with memory loss in tauopathy model mice than fibrils (Berger et al. 2007), and mice injected with tau oligomers had greater memory deficits, neuronal damage, and mitochondrial and synaptic dysfunction relative to mice injected with monomeric or fibrillar tau (Lasagna-Reeves et al. 2011). Recombinant tau preparations with higher oligomer content were shown to induce more leakage in artificial membranes than preparations with higher fibril content, and oligomeric content correlated with tau toxicity to neuronal cells (Flach et al. 2012). Tau oligomers were also shown to inhibit axonal transport (Ward et al. 2012). Overall, these results indicate that tau oligomers likely don't have a single specific mechanism of action but rather are highly toxic to multiple cellular processes.

1.3 CHAPERONE INTERACTIONS WITH TAU

Many chaperones have been shown to interact with tau, including members of the Hsp90, Hsp70, Hsp40, and small heat shock protein (sHSP) families. When studied *in vitro*, most chaperones have inhibitory effects on tau amyloid formation, although the nature and potency of

these effects vary between chaperones (Mok et al. 2018). Multiple chaperones with ATPase activity have been shown to act as chaperones toward tau in the absence of ATP, indicating that they have anti-aggregation activity that is distinct from their canonical ATP-dependent activity (Kundel et al. 2018; Zhang et al. 2019). Studies conducted in vivo have mixed results. Most show that chaperones play protective effects, although others indicate that some chaperones may exacerbate tau toxicity. For example, Hsp90 and FKBP51 can act together to promote tau aggregation and toxicity (Oroz et al. 2018). In most of the cases studied to date, chaperones bind the aggregation-prone regions of tau, although the affinity for tau varies between chaperones (Mok et al. 2018; Karagöz et al. 2014; Jinwal et al. 2013; Zhang et al. 2019). Overall, studies indicate that chaperones generally target the aggregation-prone regions of tau to inhibit its aggregation, but the effects of this inhibitory activity in living systems are highly dependent on the chaperone being studied and may depend on co-chaperones and additional cellular factors. Additional work is necessary to determine how chaperones function to protect against tau aggregation in a cellular context, how different chaperones and co-chaperones work together within larger networks, and what roles different chaperones play within the cell.

The work in this dissertation focuses on interactions between tau and the chaperones Hsc70 and HspB1. Both are known to directly interact with tau and alter its pathology *in vivo*, but they belong to distinct families and provide a useful comparison in studying the ways in which different chaperones may interact with tau. Hsc70 (gene name *HSPA8*) is a constitutively-expressed member of the Hsp70 family that is abundant in neurons. Canonically, it functions as a "refoldase" which uses ATP hydrolysis to drive the refolding of misfolded proteins, in concert with co-chaperones from the Hsp40 and Hsp110 families (Stricher et al. 2013). However, ATP-independent anti-aggregation activity has also been documented (Chaari et al. 2016).

Overexpression of Hsc70 in HEK cells slowed the clearance of overexpressed tau protein. By contrast, Hsp72, another member of the Hsp70 family, has the opposite effect and accelerates tau clearance due to its enhanced interactions with ubiquitination machinery, providing a clear example of how different chaperones from the same family can have profoundly different effects (Jinwal et al. 2013). A small-molecule binder of Hsc70 reversed its effect of slowing tau clearance and was able to rescue deficits in long-term potentiation in brain slices from a tauopathy model mouse (Abisambra et al. 2013). Hsc70 was also shown to promote tau association with microtubules and modulate the extracellular release of tau (Fontaine et al. 2015, 2016). Together, these results indicate that Hsc70 plays important roles in modulating tau activity *in vivo* but do not address the specific effects that Hsc70 has on the process of tau amyloid formation.

HspB1 (also known as Hsp27) is a member of the sHSP family, which are ATP-independent chaperones that act to delay protein aggregation but lack enzymatic activity. HspB1 co-localizes with tau fibrils in tauopathy brains (Nemes et al. 2004). It was shown to interact with tau from Alzheimer's brain lysate in pull-down assays, implying a direct interaction between the two proteins (Shimura et al. 2004). Delivery of HspB1 decreased hyperphosphorylated tau relative to non-phosphorylated tau and attenuated toxicity in HCN2A cells, and overexpression rescued deficits in long-term potentiation in a tauopathy model mouse brain (Shimura et al. 2004; Abisambra et al. 2010). These results indicate that HspB1 plays an ameliorative role in tau pathology. However, molecular details of the interaction between the two proteins are lacking, in part due to experimental difficulties in studying sHSP structure and function, discussed in detail below.

1.4 HspB1 biology, structure, and function

HspB1 is one of ten human sHSPs, which differ in their expression pattern and tissue distribution. HspB1 is ubiquitously expressed throughout the body, and its expression is upregulated by the transcription factor HSF-1 in response to stress conditions (Janowska et al. 2019). Its activity is regulated by phosphorylation in response to stress. Mutations in the HSPB1 gene have been linked to various neuropathies, including Charcot-Marie Tooth Disease and Distal Hereditary Motor Neuropathy, indicating that it plays important roles in neurons (Nefedova et al. 2015; Datskevich et al. 2012). As discussed in section 1.3, it directly interacts with tau and plays an ameliorative role in tauopathies.

All small heat shock proteins contain a conserved alpha-crystallin domain (ACD), which has a β-sandwich fold and is flanked by variable disordered regions, termed the N-terminal region (NTR) and C-terminal region (CTR) (Figure 1.2A). The ACD forms an antiparallel homodimer through interactions between the β6+7 strands of two protomers (Figure 1.2C). The NTR and CTR both interact with the ACD, and these interactions drive many human sHSPs including HspB1 to form polydisperse oligomeric ensembles (Figure. 1.2D). HspB1 oligomers can contain up to ~30 subunits and are highly dynamic in solution, with subunits continually exchanging between oligomers. The oligomeric distribution of HspB1 changes in response to cellular conditions. For example, phosphorylation decreases the average size of HspB1 oligomers, while low pH increases it (Rogalla et al. 1999; Clouser and Klevit 2017).

The CTR of HspB1 contains mostly hydrophilic residues and is thought to serve in part as a solubility tag. It contains the motif ^{181}IPV^{183}, which binds a hydrophobic groove on the outer edge of the ACD dimer termed the β4-β8 groove (Hochberg et al. 2014; Freilich et al. 2018). In many human sHSPs, this groove has been documented to bind so-called IXI motifs, which consist

of two hydrophobic residues, typically isoleucine or valine, separated by a single residue (Delbecq et al. 2012). These hydrophobic residues bind two hydrophobic pockets within the groove in a knob-and-hole type manner. Binding to the β4-β8 groove was shown to be important in driving subunit recruitment in the formation of oligomers (Delbecq et al. 2015)

The NTR of HspB1 makes up almost half the protein and contains the three phosphorylation sites (Ser15, Ser78, and Ser82), highlighting its importance in HspB1 function and regulation (Figure 1.2B). It is enriched in hydrophobic residues, particularly tryptophan, which tend to be underrepresented in intrinsically disordered regions. Nevertheless, it is highly dynamic and has been resistant to structural characterization, making it the least-understood domain of sHSPs. Recent crystal structures of human sHSPs have begun to shed light on ACD-NTR interactions. A crystal structure of HspB6 in complex with the protein 14-3-3 revealed that the motif ^{5}VPV^{7} near the beginning of the NTR was bound in the β4-β8 groove, indicating that this groove can bind hydrophobic motifs that occur in the NTR in addition to the CTR. The same crystal structure also showed that the NTR sequence ^{27}RLFDQRFG^{34} was bound in a groove at the ACD dimer interface between the two β3 strands and above the β6+7 strands (Sluchanko et al. 2017). Similar NTR-ACD interactions were observed in a crystal structure of an HspB2/HspB3 heterotetramer, indicating that these two types of NTR-ACD interactions occur in multiple human sHSPs (Clark et al. 2018). The sequence that binds at the dimer interface groove is the only region of the NTR that is well-conserved among human sHSPs, indicating that this interaction may be a common feature. Additionally, many sHSPs contain IXI-like motifs in their NTRs that could feasibly bind the β4-β8 groove. Despite the limited experimental evidence, it is likely that these types of interactions occur in other human sHSPs as well.

Recent work has also shown that the NTR residues adjacent to the ACD can form a transient β strand antiparallel to β3 near the dimer interface groove, termed β2. This strand was observed in a crystal structure of the HspB1 ACD but was not detected in a solution NMR structure (Hochberg et al. 2014; Rajagopal et al. 2015a). A recent study using NMR showed that β2 strand formation is transient in solution in a construct consisting of the ACD plus a segment of the NTR beginning at residue 77 (Collier et al. 2019). Given the presence of two phosphorylation sited near this region (residues 78 and 82), it is feasible that phosphorylation could regulate the transient formation of this strand. Further work is necessary to determine how (and whether) phosphorylation regulates these interactions and how it exerts its effects on oligomeric propensity and chaperone activity.

The oligomeric polydispersity, structural heterogeneity, and disordered nature of human sHSPs have all frustrated attempts to characterize their structure and function. Numerous sHSP client proteins have been documented, but our mechanistic understanding of how sHSPs act on these proteins remains limited. Important open questions include which regions of sHSPs are involved in binding and chaperone activity, which sequence elements in clients enable sHSP recognition, what types of client-sHSP complexes may be formed, and how do sHSP oligomerization and subunit exchange dynamics relate to chaperone activity? Such questions are likely interrelated, as client binding involves complicated interplay between the local structure of a client binding site, the tertiary structure of sHSP protomers, the oligomeric state and type of sHSP-client complex formed, and the dynamics of subunit exchange between complexes. Each of these characteristics likely influences the others, complicating efforts to dissect the individual contributions of each component of chaperone activity. Furthermore, sHSPs are highly sensitive to environmental conditions such as temperature and pH, so results obtained from different groups

are not always in agreement. Nevertheless, certain themes have emerged from years of study. Overall, it seems that the mechanism of sHSP activity is highly dependent on the specific sHSP-client pair, so chaperone activity may not be fully described by a single unified model. Both the NTR and ACD have been implicated in client binding and chaperone activity, although the relative contributions of these two domains vary depending on the sHSP and the client. Hydrophobic regions have been identified that bind sHSPs, but no clear patterns have emerged beyond general hydrophobic nature (Janowska et al. 2019).

The amyloid-forming clients tau, amyloid-β, α-synuclein, and huntingtin all interact with and are chaperoned by sHSPs. Tau, amyloid-β, and α-synuclein have all been shown to bind the β4-β8 groove of HspB5, and the ACD has been shown to be sufficient for chaperone activity when the flanking domains are removed (Liu et al. 2018; Hochberg et al. 2014; Mainz et al. 2015). Nevertheless, the mutation S135Q, which blocks binding to the β4-β8 groove of HspB5, enhanced HspB5 chaperone activity against amyloid-β, suggesting that the mechanism of HspB5 chaperone activity may be more complex than simple binding to this groove (Mainz et al. 2015). HspB1 also has been shown to act as a chaperone against α-synuclein. Complex formation by HspB1 and monomeric α-synuclein was not detectable by size-exclusion chromatography or analytical ultracentrifugation, indicating that the interaction between them is highly transient (Cox et al. 2016). HspB1 binds fully-formed α-synuclein fibrils, but the ACD alone does not, indicating that this binding is dependent on either the NTR or CTR (Cox et al. 2018). HspB7 has chaperone activity toward huntingtin, and this chaperone activity is dependent on its NTR. HspB1 is unable to chaperone huntingtin, but a chimeric protein containing the NTR of HspB7 attached to the ACD of HspB1 was an effective chaperone, indicating that the HspB7-specific NTR is responsible for the chaperone activity (Wu et al. 2019). Overall, these results demonstrate that the activity of

human sHSPs against amyloid-forming clients is dependent on both the client and sHSP. While both the NTR and ACD play roles in chaperone activity, the only residue-level binding studies have been conducted using the isolated ACD. Additional work is necessary to better understand how clients interact with the NTR and how NTR-ACD interactions can modulate activity.

1.5 Overview of thesis scope

There were two primary goals for this work. The first was to further our understanding of how chaperones interact with tau in order to better understand the strategies cells use to combat tauopathies. The second was to elucidate the structural basis of HspB1 chaperone function to further our understanding of sHSP mechanisms and the ways in which their disordered regions relate to function.

Chapter two discusses the effects that Hsc70 and HspB1 have on tau aggregation. Although both are inhibitory, the two chaperones alter the kinetics of tau aggregation in different ways and target different stages of the aggregation process. This sheds light on the ways in which chaperones from different families may play complementary roles within the cell, even as they target the same client protein.

Chapter three characterizes interactions between the disordered NTR of HspB1 and the folded ACD. It builds upon structural work by a previous graduate student in the Klevit lab, Amanda Clouser, and identifies multiple specific types of ACD-NTR interactions. An understanding of the interactions between these two domains of HspB1 in the absence of tau enables further study of the structural consequences of tau binding and the structural mechanism of chaperone activity toward tau.

Chapter four characterizes the structural basis for HspB1 chaperone activity against tau and the roles of the three domains of HspB1. It shows that HspB1 is capable of binding tau in both the

NTR and the ACD, but only interactions with the NTR result in productive chaperone activity. It also identifies two mutant variants with enhanced chaperone activity toward tau, which both perturb NTR-ACD interactions identified in Chapter 2. This furthers our understanding of sHSP function and the mechanism of HspB1 activity.

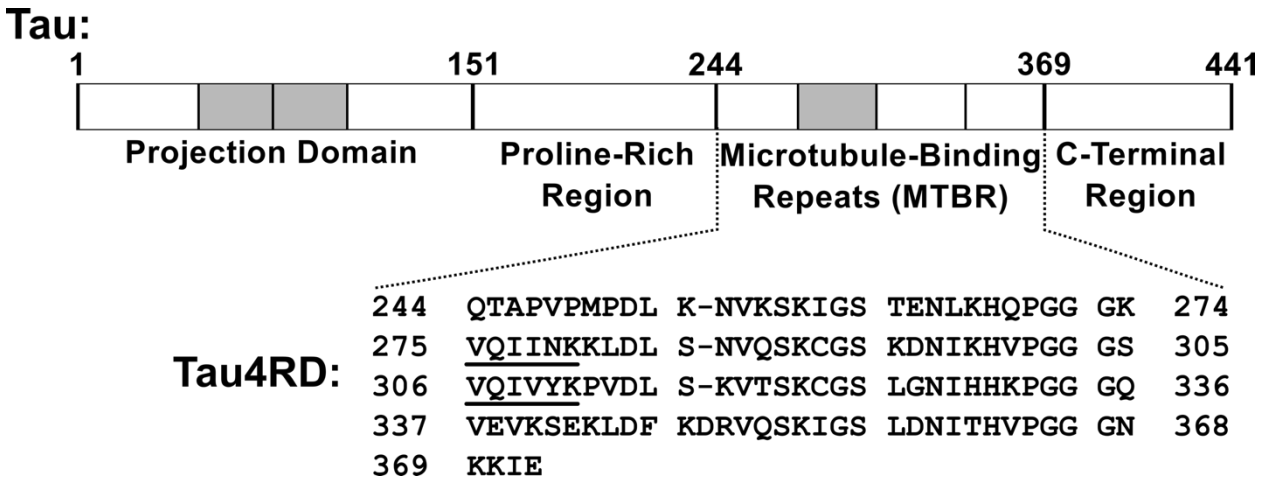

Figure 1.1. Domain architecture of tau.

Tau has four domains: the projection domain, proline-rich region, microtubule-binding repeats, and C-terminal region. Shaded areas represent regions that are alternatively spliced and not present in all tau isoforms. Tau4RD is a shortened construct consisting primarily of the microtubule-binding repeat region of tau. It contains two motifs known to drive the aggregation of tau (underlined) and has faster aggregation kinetics than full-length tau.

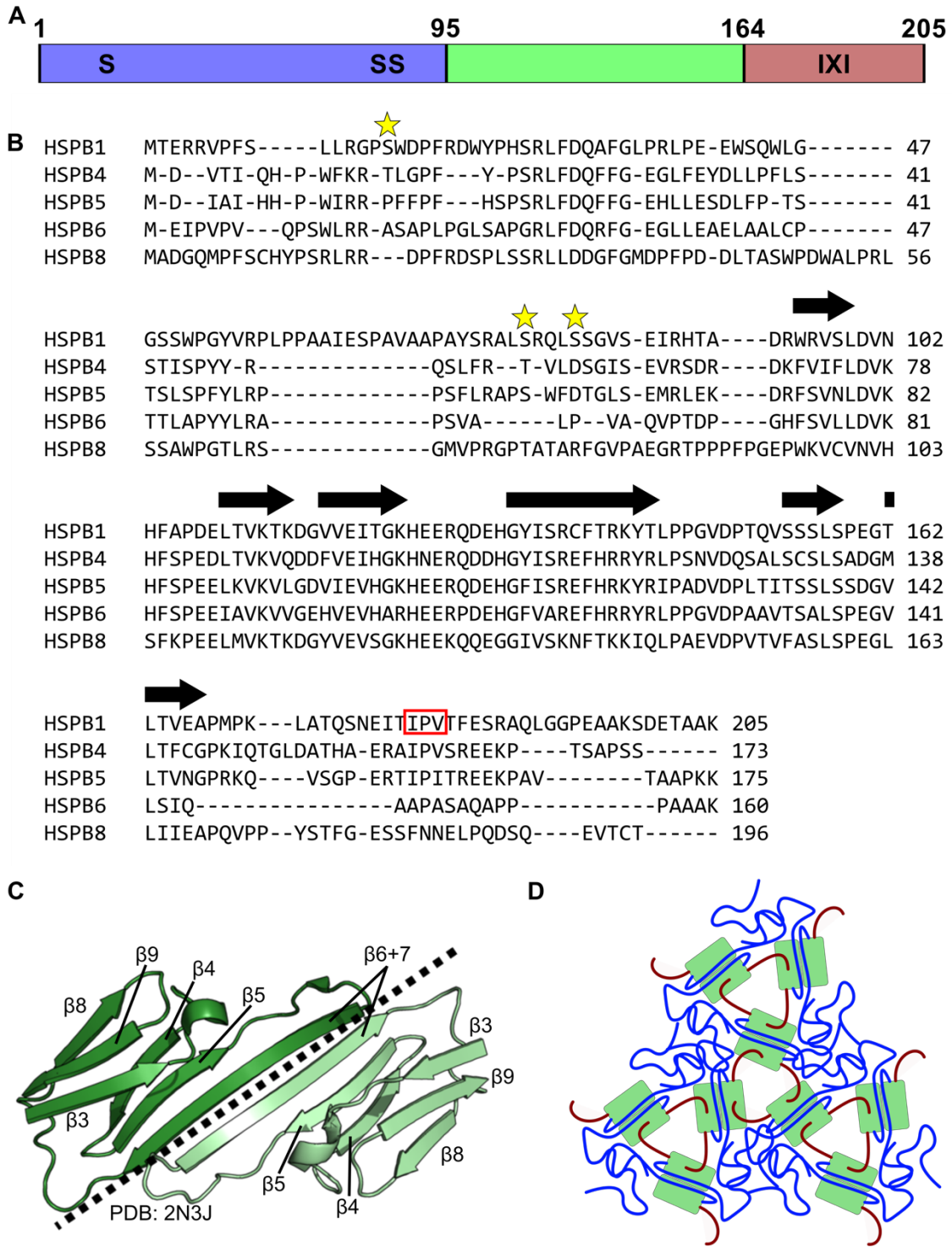

Figure 1.2. HspB1 domain architecture and structure.

(A) HspB1 has three domains: a long, disordered N-terminal region (NTR, blue), a core structured alpha-crystallin domain (ACD, green), and a short disordered C-terminal region (CTR, red). The NTR contains three serine phosphorylation sites, and the CTR contains an IXI motif

that docks into the ACD. (B) sequence alignment of HspB1 with other human sHSPs. Yellow stars denote phosphorylation sites, black arrows denote β strands in the ACD, and the red box denotes the IPV motif that binds the ACD. (C) Solution NMR structure of the ACD, which has a β-sandwich fold and dimerizes along the β6+7 strand. (D) Cartoon of an HspB1 oligomer. HspB1 assembles into large oligomers through interactions between the three domains.

Chapter 2. HSPB1 AND HSC70 CHAPERONES ENGAGE DISTINCT TAU SPECIES AND HAVE DIFFERENT INHIBITORY EFFECTS ON AMYLOID FORMATION

[Reproduced with permission from Baughman HER, Clouser AF, Klevit RE, Nath A. (2018) "HspB1 and Hsc70 chaperones engage distinct tau species and have different inhibitory effects on amyloid formation" *Journal of Biological Chemistry* **293:** 2687-2700.]

Abstract:

The microtubule-associated protein tau forms insoluble, amyloid-type aggregates in various dementias, most notably Alzheimer's disease. Cellular chaperone proteins play important roles in maintaining protein solubility and preventing aggregation in the crowded cellular environment. While tau is known to interact with numerous chaperones, it remains unclear how these chaperones function mechanistically to prevent tau aggregation and how chaperones from different classes compare in terms of mechanism. Here, we focused on the small heat shock protein HspB1 and the constitutive chaperone Hsc70 (also known as HspA8), and report how each chaperone interacts with tau to prevent its fibril formation. Using fluorescence and NMR spectroscopy, we show that the two chaperones inhibit tau fibril formation by distinct mechanisms. HspB1 delayed tau fibril formation by weakly interacting with early species in the aggregation process, while Hsc70 was highly efficient at preventing tau fibril elongation possibly by capping the ends of tau fibrils. Both chaperones recognized aggregation-prone motifs within the microtubule-binding repeat region of tau. However, HspB1 binding remained transient in both aggregation-promoting and non-aggregating conditions, whereas Hsc70 binding was significantly tighter under aggregation-

promoting conditions. These differences highlight the fact that chaperones from different families play distinct but complementary roles in the prevention of pathological protein aggregation.

2.1 INTRODUCTION

Tau is an intrinsically disordered microtubule-associated protein involved in numerous neurodegenerative diseases collectively termed tauopathies. Tau is highly expressed in neurons and plays roles in microtubule stability, axonal transport, and neurite outgrowth (Drubin and Kirschner 1986; Stamer et al. 2002; Dawson et al. 2001). Tauopathies are characterized by the deposition of tau in insoluble amyloid-type fibrillar aggregates (Goedert et al. 1989), and based on disease-associated tau mutations, this aggregation appears to play a causative role in at least some of these neurodegenerative diseases (Wolfe 2009). Although the mechanism of tau toxicity is subject to some debate, increasing evidence suggests that a pre-fibrillar oligomeric state of tau is the primary toxic species responsible for neurodegeneration (Lasagna-Reeves et al. 2011; SantaCruz et al. 2005), similar to models proposed for many other amyloid-forming proteins. According to this model, tau dissociates from microtubules and forms oligomers with the potential to disrupt cellular membranes and impair synaptic and mitochondrial function before ultimately forming relatively inert amyloid fibrils in what may or may not be a protective mechanism to remove toxic oligomers (Flach et al. 2012; Lasagna-Reeves et al. 2011; SantaCruz et al. 2005). How cells control the relative populations of tau monomers, oligomers, and fibrils, and protect against associated toxicity, remains poorly understood.

Fibril formation is primarily driven by the microtubule-binding repeat (MTBR) region of tau, which consists of three or four 31-32 residue pseudo-repeats (Fig. 2.1) involved in microtubule binding (von Bergen et al. 2000; Mukrasch et al. 2005). The tau gene is alternatively spliced, with

the ratio of three-repeat to four-repeat isoforms varying based on normal aging (Goedert et al. 1989) or in disease states (D'Souza et al. 1999). Two six-residue motifs at the start of the second and third repeats, ^{275}VQIINK^{280} and ^{306}VQIVYK^{311} (also called PHF6* and PHF6) are believed to be the primary drivers of aggregation (Von Bergen et al. 2001; Daebel et al. 2012; von Bergen et al. 2000). A recent cryo-electron microscopy study of AD patient-derived fibrils revealed that residues 306-378 form a highly-structured core in two distinct fibril morphologies from a single patient's brain (Fitzpatrick et al. 2017b). These core residues consist of the third and fourth repeats, as well as 10 additional C-terminal residues. Whether such morphologies are common among all AD patients or whether alternate fibril morphologies exist in AD or in other tauopathies remains an open question.

While the precise mechanism of tau fibril formation is unclear, it appears that tau monomers oligomerize and form elongation-competent species which then elongate to form mature fibrils, with the formation of elongation-competent species the rate-determining step (Shammas et al. 2015; Nakatani-Webster and Nath 2017; Carlson et al. 2007). Each stage of the fibril formation process is likely targeted by multiple cellular players, and a better understanding of how the cell works to counteract this process could inform future pharmacological strategies.

The cellular chaperone network is responsible for maintaining protein solubility, promoting proper folding, and preventing aberrant aggregation. Age-linked protein aggregation diseases, including Alzheimer's Disease (AD) and other tauopathies, may represent an eventual saturation of the chaperone machinery's ability to prevent aggregation (Hartl et al. 2011). Individuals carrying disease-associated mutations in the tau gene that enhance aggregation propensity only develop symptoms later in life (Wszolek et al. 2006), suggesting that neuronal cells have the machinery to maintain aggregation-prone tau in a soluble form for years. Interactions between tau

and a number of chaperones have been documented, indicating that multiple players within the chaperone network are involved in this process (Karagöz et al. 2014; Voss et al. 2012; Jinwal et al. 2013; Fontaine et al. 2015; Abisambra et al. 2010; Xu et al. 2013). However, the mechanisms by which these chaperones interact with tau and their effects on tau fibril formation remain unclear. A better biochemical and mechanistic understanding of how chaperone proteins interact with tau will provide insight into the cellular defense mechanism against tauopathies. This work focuses on the chaperones HspB1 and Hsc70, which both interact with tau in ways that are likely relevant to disease pathology (discussed below). These chaperones belong to distinct families, and their juxtaposition provides an example of how different components of the chaperone network may complement each other in the prevention of pathological tau fibril formation.

HspB1 is a member of the small heat shock proteins (sHSPs), a family of ATP-independent chaperones that act as "holdases" to prevent protein aggregation but lack enzymatic activity (Treweek et al. 2015). Like many members of the sHSP family, HspB1 forms large, polydisperse, highly dynamic oligomers ranging in size from dimers to 30-mers (Jovcevski et al. 2015), governed by a network of interactions between the α-crystallin domain (ACD), N-terminal region (NTR), and C-terminal region (CTR) (Lelj-Garolla and Mauk 2012; Hochberg et al. 2014). Due in part to experimental limitations in dealing with dynamic, polydisperse systems, little is known about how HspB1 recognizes clients and functions as a holdase. HspB1 co-localizes with tau fibrils in tauopathy brains and is pulled down by phosphorylated tau (Nemes 2004; Shimura et al. 2004), suggesting an important interaction between HspB1 and tau in disease states. A tauopathy mouse model exhibits deficits in long-term potentiation that are rescued by HspB1 overexpression (Abisambra et al. 2010). This indicates that HspB1 can alter the physiological outcome of aberrant tau aggregation, but the underlying mechanism remains unclear.

Hsc70 is a constitutively-expressed member of the Hsp70 family of chaperones, which are "refoldases" that use the energy of ATP hydrolysis to help misfolded proteins refold to their native states. It contains an N-terminal nucleotide binding domain and a C-terminal substrate binding domain, and interacts with Hsp40 family co-chaperones and nucleotide exchange factors to accomplish protein refolding and ATP hydrolysis (Stricher et al. 2013). However, ATP-independent activity has also been reported in Hsp70-family chaperones (Chaari et al. 2016; Rao et al. 2010; Aprile et al. 2017). Hsc70 binds to the two aggregation-prone motifs in tau and has been proposed as a pharmacological target (Abisambra et al. 2013; Jinwal et al. 2013; Fontaine et al. 2015). Its overexpression leads to an increase in the concentration of tau in cell culture models, while an Hsc70 inhibitor causes a decrease in tau concentration in cell cultures and rescues long-term potentiation deficits in tauopathy model mouse brain slices (Jinwal et al. 2013; Abisambra et al. 2013). Hsc70 may also play roles in enhancing tau's association with microtubules (Fontaine et al. 2015) and in modulating the extracellular release of tau (Imhaus and Duménil 2014). While it is unclear how Hsc70 affects tau fibril formation, it has been shown to block the formation of fibrils by another amyloid-prone protein, α-synuclein, and even disaggregate pre-formed α-synuclein fibrils when combined with co-chaperones from the Hsp40 and Hsp110 families (Gao et al. 2015b; Chaari et al. 2016). Its paralog, Hsp70, has been shown to inhibit tau fibril formation by interacting with tau oligomers (Patterson et al. 2011; Voss et al. 2012). It remains to be determined if these activities are generally applicable to interactions between members of the Hsp70 family and amyloid-prone proteins and which, if any, apply to the interaction between Hsc70 and tau.

Here we compare the effects of Hsc70 and HspB1 on tau self-assembly to explore how different components of the cellular chaperone network interact with tau and impact fibril

formation. Using fluorescence spectroscopy, electron microscopy (EM), and time-dependent NMR spectroscopy, we study how each chaperone alters the kinetics of tau aggregation and how this is achieved mechanistically. We also compare the binding and recognition of tau by each chaperone under stable and aggregation-promoting conditions using NMR and fluorescence correlation spectroscopy (FCS). These experiments reveal that Hsc70 and HspB1 have profoundly different mechanisms of inhibition, suggesting that they have evolved complementary functions within the context of the larger chaperone network. This would enable the cell to avoid redundancy while targeting distinct stages of the tau fibril formation process with different chaperones.

2.2 RESULTS

2.2.1 *Hsc70 and HspB1 inhibit tau fibril formation in distinct ways.*

We focus primarily on a tau construct containing the four microtubule-binding repeats (tau4RD, also referred to in the literature as K18). This sequence, consisting of residues 244-372, forms the core of tau fibrils (Daebel et al. 2012) and contains the two 6-residue motifs that are highly aggregation prone in isolation and in the context of full-length protein (von Bergen et al. 2000). Tau4RD aggregates more readily *in vitro* than full-length tau and is more amenable to study by NMR spectroscopy. As with other amyloidogenic proteins, environmental factors such as temperature, ionic strength, shaking, the amount and nature of aggregation-inducers such as heparin, and even the type of reaction vessel can dramatically affect tau4RD aggregation. We therefore explicitly note these experimental parameters where relevant.

We also used selected constructs (Fig. 2.1, middle panel) to tune the activity and oligomeric state of HspB1 to explore the effects of well-known modifications on its activity and to enable a

broader range of spectroscopic techniques. Wild-type HspB1 forms large and polydisperse oligomers, driven by at least three types of interactions: ACD-ACD, ACD-CTR, and NTR-NTR (Fig. 2.2) (Lelj-Garolla and Mauk 2012; Hochberg et al. 2014). Mutation of three serine residues in the NTR (S15, S78, and S82) to Asp mimics stress-induced phosphorylation and alters NTR-NTR interactions, yielding a construct termed HspB1D3 that forms much smaller oligomers than HspB1WT (Rogalla et al. 1999; Jovcevski et al. 2015). Further mutation of the IXI motif in the CTR to GXG, residues ^{179}ITIPV^{183} in HspB1 to GTGPG, disfavors interactions between the ACD and the CTR, similar to the effects of high temperature (Delbecq et al. 2012; Baldwin et al. 2012). We combined the D3 and GXG mutations to generate a construct, denoted HspB1dimer, that forms a well-defined, monodisperse ~45kDa dimer (Fig. 2.2 B, C) and retains the local secondary structure of the ACD (Fig. 2.2 D). Crucially, HspB1dimer displays much lower background Thioflavin T (ThT) fluorescence than either HspB1D3 or HspB1WT (Fig. 2.2 E). ThT is a popular reporter of amyloid formation but is neither perfectly specific nor selective for amyloid structure (Biancalana and Koide 2010). Indeed, ThT fluoresces strongly in the presence of (presumably non-amyloid) HspB1 oligomers but not dimers. HspB1dimer therefore enables mechanistic experiments based on ThT fluorescence that are impossible with HspB1WT or HspB1D3.

In a ThT-monitored assay, tau4RD shows the sigmoidal fluorescence kinetics expected of unseeded amyloid formation, with an initial lag phase leading into a rapid elongation phase followed by an asymptotic approach to a plateau. HspB1dimer causes a delay in the onset of tau4RD aggregation and in the transition midpoint (t_{50}) in a dose-dependent manner without substantially altering the magnitude of the final ThT fluorescence signal (Fig. 2.3 A). Hsc70 is a much more potent, substoichiometric inhibitor of this process, measurably decreasing the final plateau intensity in a dose-dependent manner even when present at a molar ratio as low as 1:100

(Fig. 2.3 B). However, in contrast to HspB1dimer, Hsc70 does not substantially alter the t_{50} of the tau aggregation reactions.

Hsc70's activity towards tau4RD appears to be nucleotide-independent. In the presence of 1 mM ATP, Hsc70 has a similar effect on tau4RD aggregation, decreasing the plateau intensity without substantially altering the t_{50} (Fig 2.4 A). While it is somewhat less potent under these conditions, it retains substoichiometric activity and likely acts through a similar mechanism.

We verified the ability of HspB1 and Hsc70 to inhibit the aggregation of the longest full-length tau isoform, tau2N4R, to confirm that the chaperone activities we observe are generalizable to interactions with cellular tau. The tau4RD construct lacks six residues (373-378) that were recently shown to form part of the ordered core of AD patient-derived fibrils, (Fitzpatrick et al. 2017b) potentially raising questions about the relevance of this well-studied construct. As with tau4RD, we found that HspB1 predominantly affects the lag phase of tau2N4R aggregation, whereas Hsc70 predominantly affects the plateau (Fig. 2.4 B, C). This indicates that the interactions of these chaperones with tau4RD and tau2N4R are mechanistically similar and that chaperone/tau4RD studies can shed light on chaperone interactions with full-length tau isoforms. We focus on the widely-studied tau4RD construct for the remainder of our studies, as the slower aggregation kinetics and larger molecular weight of tau2N4R make mechanistic and spectroscopic studies challenging.

Negative stain EM of the end products of these reactions (Fig. 2.3 C) shows that tau4RD forms long fibrils in the absence of chaperone, or in the presence of HspB1dimer. This indicates that HspB1dimer only delays fibril formation rather than preventing it. In contrast, Hsc70-containing reactions yield increasing amounts of small oligomeric species (as compared to long fibrils), indicating that Hsc70 holds much of the tau4RD in an oligomeric state and can prevent elongation

of these species into mature fibrils. This confirms that the reduction in ThT fluorescence in reactions containing Hsc70 does indeed correspond to a decrease in the amount of fibrillar material, as opposed to morphological differences that could alter ThT fluorescence. Together, these results demonstrate that, although both chaperones have inhibitory effects on tau aggregation, they are very different in mechanism and outcome.

2.2.2 *HspB1 and Hsc70 have distinct mechanisms of inhibition.*

To better understand the mechanisms by which each chaperone alters tau4RD aggregation, we used one-dimensional NMR spectroscopy to study the interactions of HspB1 and Hsc70 with prefibrillar, ThT-negative species. Large, slowly tumbling species have a weaker signal than smaller species, so the intensity of an NMR spectrum is dependent upon the oligomeric state of protein in solution. We expect monomeric tau4RD to have a strong signal, small oligomers to have a weak signal, and large oligomeric and fibrillar tau4RD to be essentially invisible. A high intensity resonance in the methyl region at 0.77 ppm provides a good read-out for the intensity of the protein signal that is well-separated from buffer components or heparin (Fig. 2.6 A). We used ^{13}C-labeled tau4RD and unlabeled chaperones and collected ^{13}C-edited spectra to observe tau4RD specifically (Fig. 2.6 B-C). Loss of peak intensity over time reports on the disappearance of soluble, monomeric tau4RD and on binding to heparin and chaperones. We normalized all data relative to the intensity of the first spectrum after the addition of heparin, which is slightly lower than that of free tau4RD. Under these conditions, tau4RD again displays sigmoidal aggregation kinetics, with a final intensity < 20% of the first heparin-bound spectrum (Fig 2.5 A,B). Note that these experiments used a different sample concentration and reaction vessel than the ThT experiments and are not shaken, making direct comparison between the two types of experiments impossible. However, an evaluation of the effects of HspB1 and Hsc70 is still informative.

HspB1dimer slows the intensity loss of tau4RD in a dose-dependent manner (Figure 2.5 A). In the presence of one molar equivalent HspB1dimer, ~70% of the original intensity of tau4RD is lost after 18 hours, and in the presence of four molar equivalents only about one third of the intensity is lost. Notably, in unedited spectra, which contain signal from both tau4RD and HspB1dimer, this intensity loss is more gradual than in the ^{13}C-edited spectra that contain signal from only tau4RD (Figure 2.6 D). This means that HspB1dimer is losing signal intensity at a slower rate than tau4RD, remaining predominantly soluble while tau4RD forms large, NMR-invisible species.

Hsc70 is much more potent and has distinct effects (Fig. 2.5 B): in the presence of just 1 μM Hsc70 (1/50 molar equivalents), tau4RD intensity decreases by only ~50%, confirming the highly effective sub-stoichiometric nature of its inhibition. In the presence of one molar equivalent Hsc70, the tau4RD intensity drops quickly in the 1-2 hours following the addition of heparin, then plateaus at ~70% of the initial intensity. We believe that this drop in intensity is due to binding by Hsc70 rather than fibril formation, as the formation of a larger complex with Hsc70 would also result in a loss of NMR signal intensity for tau4RD. Indeed, when the product of this reaction is pelleted and the supernatant and pellet fractions are analyzed by SDS-PAGE, nearly all of the protein remains in the supernatant, indicating that it remains soluble over the course of the 18 hour experiment (Fig. 2.5 C). This is in contrast to reactions containing tau4RD or tau4RD + HspB1dimer, in which most of the tau4RD is in the pellet. Additionally, unedited 1D spectra lose intensity more quickly than ^{13}C-edited spectra, indicating that Hsc70 is losing intensity at an even higher proportion than tau4RD during this process, likely due to binding. Therefore, we conclude that Hsc70 binds aggregation-prone tau4RD early in the aggregation reaction and is able to maintain its solubility over the course of 18 hours. By contrast, HspB1 does not form a tight

complex with tau4RD during aggregation but instead interacts with it transiently and is less effective at maintaining its solubility than Hsc70.

To better understand the mechanisms of inhibition, we added each chaperone to tau fibril formation reactions at varying timepoints after initiating fibril formation with heparin. HspB1dimer was able to delay fibril formation when it was added at the beginning of a reaction or during the lag phase but had no effect on fibril formation when it was added after the start of the elongation phase (Fig. 2.5 D). This indicates that HspB1 acts early in the fibril formation process and interacts with pre-fibrillar species. By contrast, Hsc70 is an effective inhibitor regardless of when it is added during the course of a fibril formation reaction. It has the same effect on fibril formation when it is added at the beginning of a reaction or during the lag phase. When added during the elongation phase, it blocks any subsequent increase in ThT fluorescence and thus halts further fibril formation (Fig. 2.5 E). Taken together with the 1D NMR results, this reveals important differences in how the two chaperones function mechanistically. HspB1 acts early to delay aggregation but is ineffective at blocking elongation of pre-existing fibrils, whereas Hsc70 is effective during all stages of the aggregation process, forming a tight initial complex with aggregation-prone tau and blocking elongation of existing tau fibrils.

2.2.3 *HspB1 and Hsc70 both recognize aggregation-prone regions of tau4RD, but with differences in affinity.*

2D NMR spectroscopy was used to obtain a better structural understanding of tau-chaperone interactions. Despite initial challenges due to the poor chemical shift dispersion of the disordered tau spectrum, recent advances have enabled the complete backbone resonance assignment of the tau4RD and tau2N4R spectra (Smet et al. 2004; Mukrasch et al. 2009; Narayanan et al. 2010; Barre and Eliezer 2013; Mukrasch et al. 2005). Previously-published assignments (Barre and Eliezer

2013) were transferred to our ^{15}N-HSQC spectrum of tau4RD, using HNCACB and CBCA(CO)NH spectra for reference and to resolve ambiguities. Our spectrum was highly similar to that previously published, with a few exceptions in the histidine- and lysine-rich regions at the end of each microtubule-binding repeat. These peaks shifted with slight changes in pH or with EDTA (data not shown), suggesting that these peaks are highly sensitive to pH and to the presence of metals in water, and that the observed discrepancies are likely due to small differences in buffer conditions.

The binding sites of each chaperone were mapped onto the sequence of tau4RD by recording spectra of ^{15}N-labeled tau4RD in the presence of unlabeled chaperone proteins. HspB1dimer causes significant broadening in peaks corresponding to the ^{306}VQIVYK^{311} motif, and it causes less pronounced broadening in ^{275}VQIINK^{280} peaks (Fig. 2.7 A). Hsc70 causes significant broadening in peaks corresponding to both aggregation-prone motifs (Fig. 2.7 B), the same regions affected in full-length tau (Jinwal et al. 2013). This indicates that the two chaperones recognize similar regions in tau under non-aggregation-promoting conditions. Notably, the region of tau4RD recognized by HspB1dimer contains the sequence V-X-I, which is similar to the well-known I-X-I recognition motif for sHSP binding. Valine can be tolerated in place of isoleucine in such sequences (Delbecq et al. 2012), so we predict that HspB1 binds this region of tau in the β4-β8 groove of the ACD.

Since a variety of factors can affect NMR peak width, we turned to fluorescence correlation spectroscopy (FCS) as an orthogonal, direct probe of binding affinity. FCS can measure changes in hydrodynamic radius (R_h) of a fluorescently labeled protein in the presence of binding partners. We used site-directed mutagenesis to selectively label tau4RD with AlexaFluor 488 (A488) at residue 2, and measured R_h of the resulting tau4RD~A488 construct in the presence of increasing

concentrations of chaperones (Fig. 2.8). HspB1dimer had a minor effect on tau4RD~A488 R_h, increasing it only by ~25% when present at 500 μM. This subtle change in R_h increased without saturation over HspB1dimer concentrations. The small apparent change in R_h and lack of a plateau could be due to a relatively compact tau4RD:HspB1dimer complex and/or one or more weak binding modes. It is worth noting that HspB1dimer contains two putative binding sites, one within each protomer, and NMR results suggest that it can bind to two distinct sites in tau4RD with different affinity (Fig. 2.7 B). These factors make it impossible to definitively determine a K_D for the tau4RD:HspB1dimer interaction by FCS. By contrast, Hsc70 caused a saturable ~1.7-fold increase in R_h, suggesting the formation of an Hsc70:tau4RD~A488 complex with an apparent K_D of 99 ± 28 μM.

2.2.4 *Hsc70 binding is enhanced under aggregation-promoting conditions.*

Since the interactions between these chaperones and tau are most relevant under aggregation-promoting conditions, we used NMR to explore how the aggregation-inducer heparin modulates tau-chaperone interactions. Heparin causes peaks in the tau4RD ^{15}N-HSQC spectrum to shift dramatically, most notably those in the region corresponding to the aggregation-prone motif ^{275}VQIINK^{280} (Fig. 2.9 A, B), in agreement with previous reports (Mukrasch et al. 2005; Zhao et al. 2017). Under the conditions used here, binding is nearly saturated and the peaks represent a heparin-bound state of tau (Fig. 2.10 A). When HspB1dimer is added along with heparin, the peaks still shift as they do in the presence of heparin alone and still broaden as they do in the presence of HspB1dimer alone. However, these effects are purely additive: there does not appear to be any additional change beyond what we see when adding HspB1dimer or heparin to tau4RD separately (Fig. 2.9 C). By contrast, when Hsc70 is added in the presence of heparin, significantly more broadening is observed than in the heparin-free Hsc70-bound spectrum (Fig. 2.9 D, E; 2.10 B).

This is presumably due to the formation of a three-component complex in which Hsc70 has enhanced affinity for heparin-bound tau. The difference between HspB1dimer and Hsc70 is well illustrated by the peaks corresponding to ^{306}VQIVYK^{311}. These peaks are broadened to a similar degree by either chaperone in the absence of heparin, but in the presence of heparin are significantly broader with Hsc70 than with HspB1dimer (Fig. 2.9 E). These observations suggest Hsc70 binds more tightly to aggregation-prone heparin-bound tau4RD, while HspB1dimer displays no such selectivity. This agrees well with 1D NMR results, which show that Hsc70 causes a rapid loss of intensity from the tau4RD spectrum following the addition of heparin, whereas HspB1dimer does not detectably affect the earliest timepoints relative to the tau4RD alone curve (Fig. 2.5 A-B). Hsc70's preference for aggregation-prone states may explain why it is so much more potent an aggregation inhibitor than HspB1dimer.

2.2.5 *HspB1WT and HspB1D3 behave similarly to HspB1dimer.*

Finally, we studied the interactions of tau4RD with HspB1WT and HspB1D3. While HspB1dimer is more experimentally tractable due to its defined, monodisperse dimeric state, HspB1WT and HspB1D3 are more physiologically relevant and can still be studied using a subset of the techniques available to us. By 1D NMR, HspB1D3 and HspB1WT inhibit tau4RD aggregation similarly to HspB1dimer (Fig. 2.6; 2.11 A, B), transiently interacting with tau4RD and slowing the loss of monomer signal in a dose-dependent manner. Interestingly, it seems that HspB1dimer is less effective than WT or D3 at an equimolar ratio (50 μM chaperone) but more effective in 4-fold excess (200 μM chaperone). The oligomeric states of HspB1D3 and WT likely vary over this concentration range, a phenomenon that alters their chaperone activity in complicated ways (Rogalla et al. 1999; Jovcevski et al. 2015).

HspB1WT did not significantly perturb the ^{15}N-HSQC spectrum of tau4RD, even in four-fold excess, indicating that its binding is very weak and difficult to detect. HspB1D3 caused some broadening in the spectrum of tau4RD, particularly in peaks corresponding to ^{306}VQIVYK^{311}, but less strongly than HspB1dimer, suggesting intermediate affinity (Fig. 2.11 C-F). Changes in binding affinity between HspB1WT, HspB1D3, and HspB1dimer could be due to differences in the oligomeric state of these constructs, structural changes due to the D3 mutations that enhance affinity for tau4RD, and/or increased availability of the HspB1 β4-β8 groove due to the GXG mutations. Notably, these differences in affinity do not appear to correlate with inhibition of tau4RD fibril formation in 1D NMR experiments, and additional work is needed to elucidate how inhibition of tau fibril formation relates to HspB1 structure and oligomeric state. Nevertheless, it is clear that HspB1 interacts with tau in a way that is similar across constructs and mechanistically distinct from the interactions between Hsc70 and tau.

2.3 DISCUSSION

Molecular chaperones play important roles in maintaining protein solubility and preventing pathological aggregation. The several families of molecular chaperones each with multiple isoforms comprise an intricate functional network in the cell. The disparate mechanisms by which individual chaperones function are not fully understood. We have characterized the interactions between the amyloid-prone protein tau and two molecular chaperones from different families: HspB1, a ubiquitously-expressed sHSP, and Hsc70, a constitutively expressed member of the Hsp70 family. This work shows that the two chaperones interact with distinct tau species and have profoundly different effects on the kinetics of tau aggregation, suggesting that they play complementary roles within the context of the cellular chaperone network.

HspB1 binds tau fairly weakly, and this binding is not enhanced under aggregation-promoting conditions. Rather, HspB1 interacts transiently with early species of tau in a manner that delays but does not prevent fibril formation (Fig. 2.12). Such transient interactions have been observed in many sHSP/client pairings and may be a common mechanism of sHSP "holdase" activity (Cox et al. 2016; Rajagopal et al. 2015b). Little is known about how HspB1 interacts with client proteins structurally, in large part due to experimental limitations in dealing with dynamic, polydisperse systems. The client binding sites of HspB1 have not been mapped to the residue level, to our knowledge, although studies indicate an important role of the NTR in binding at least some clients (McDonald et al. 2012). Two binding sites have been mapped on another ubiquitously expressed human sHSP, HspB5: one in the NTR and one in the ACD (Mainz et al. 2015). We hypothesize that HspB1 binds the V-X-I motif in tau in the β4-β8 groove of the ACD, in accord with previous work on HspB5/client binding (Mainz et al. 2015; Delbecq et al. 2012) and HspB1 ACD/CTR interactions (Hochberg et al. 2014). We find no correlation between the oligomeric state of HspB1 and its chaperone activity toward tau. While the oligomeric state does correlate with binding affinity in this work, it is unclear which factors cause this: the D3 and GXG mutations could alter affinity or chaperone activity independently of their effects on oligomer size.

Hsc70 also has fairly low affinity for tau under non-aggregating conditions, with a K_D around 100 μM. However, this binding is enhanced in the presence of the aggregation-inducer heparin, enabling Hsc70 to form a tight complex with aggregation-prone tau. It is a highly potent inhibitor and is effective even when present at a 1:50 molar ratio, and it can arrest fibril formation when it is added to an aggregation reaction at any time point. Hsc70 is fully capable of binding monomeric tau4RD, but its substoichiometric potency in fibril formation reactions and ability to block elongation even late in a reaction suggest that it can also interact with larger oligomeric or fibrillar

species. Our data are consistent with a model wherein Hsc70 caps the ends of fibrils and elongation-competent oligomers and prevents elongation of these species (Fig. 2.12). Notably, Hsp70 also has been shown to interact with tau oligomers (Patterson et al. 2011), suggesting that this may be a common mode of action for members of the Hsp70 family. Hsp70 family chaperones have also been reported to display similarly ATP-independent, substoichiometric inhibition of α-synuclein amyloid formation, again by interacting with both monomeric and fibrillar states (Chaari et al. 2016; Aprile et al. 2017). It should be noted that our experiments studied the activity of Hsc70 in the absence of co-chaperones from the Hsp40 family or nucleotide-exchange factors. How these co-chaperones engage with Hsc70 and tau remains to be seen. Another open question is whether Hsc70's activity would be beneficial to the cell by preventing fibril formation or detrimental by causing the accumulation of toxic oligomeric species.

Recent cryoEM structures of AD patient-derived tau fibrils have provided valuable new insight into at least two tau fibril morphologies found *in vivo* (Fitzpatrick et al. 2017b). Proteolysis assays indicate that patient-derived fibrils from different tauopathies have distinct morphologies (Taniguchi-Watanabe et al. 2016). An understanding of the diversity of tau fibril morphologies thus remains an important open question. Notably, the Fitzpatrick *et al.* cryoEM structures indicate that residues 373–378 form part of the fibril core in both morphologies, but these residues are absent from the tau4RD construct used in this paper and many others. It is unclear whether or how these residues affect aggregation mechanism, as compared to canonical aggregation drivers such as ^{306}VQIVYK^{311} (von Bergen et al. 2000). We therefore compared chaperone effects on fibril formation by tau4RD and full-length tau2N4R.

HspB1 and Hsc70 have similar effects on the fibril formation kinetics of tau4RD and tau2N4R, indicating that they interact with the full-length protein in a manner similar to the shorter construct

that lacks residues 373-378. NMR studies of Hsc70 binding to tau2N4R show that Hsc70 causes slight broadening in peaks corresponding to residues 375-380 of tau2N4R, though this broadening is not as strong as that of the ^{275}VQIINK^{280} and ^{306}VQIVYK^{311} motifs (Jinwal et al. 2013; Fontaine et al. 2015). Because we found similar Hsc70 chaperone activity against tau4RD, which does not contain these residues, and tau2N4R, which does, we believe that this interaction does not significantly alter Hsc70's mechanism of action. Because no structural studies involving full-length tau and HspB1 have been conducted, it remains to be seen whether HspB1 interacts with regions of full-length tau in addition to those observed here using the tau4RD construct. HspB1dimer was a somewhat more potent inhibitor of tau2N4R fibril formation than of tau4RD fibril formation. Whether this is due to slower aggregation kinetics of tau2N4R, altered binding of HspB1 to tau2N4R, or a different factor is unknown.

The disparate effects of HspB1 and Hsc70 on tau fibril formation point to interesting ways different members of the cellular chaperone network complement each other in the prevention of protein aggregation. The sHSPs have been described as "first responders" to cell stress events (Basha et al. 2012), a descriptor that fits the activity of HspB1 described here well. It is easy to imagine a scenario in which HspB1 interacts with tau during early stages of fibril formation, delaying the formation of toxic oligomers, and Hsc70 interacts with oligomers and later species in the fibril formation process. HspB1 is phosphorylated and upregulated in response to stress, whereas Hsc70 is constitutively expressed. The load of aggregation-prone proteins increases during stress events, and enhanced activity of HspB1 during these events could relieve some of the pressure on Hsc70 by delaying their aggregation until Hsc70 is better able to handle the increased workload. Few studies have examined the interactions between human Hsc70 and HspB1, although recent work suggests the two proteins may be physically linked through

interactions with the nucleotide-exchange factor BAG3 (Rauch et al. 2017). There is evidence that *E. coli* sHSPs work with the *E. coli* Hsp70 homolog, DnaK, in preventing protein aggregation (Veinger et al. 1998; Żwirowski et al. 2017). Additional work is needed to elucidate how HspB1 and Hsc70 function in the context of the full human chaperone network and how this relates to pathological protein aggregation in diseases such as tauopathies. However, our work points to distinct but complementary roles Hsc70 and HspB1 could play in the prevention of tau fibril formation by engaging distinct species along the amyloid formation pathway.

2.4 Experimental Procedures

2.4.1 *Protein expression and purification:*

A plasmid containing the His-tagged tau4RD gene with a TEV-cleavage site was a gift from the Rhoades lab at the University of Pennsylvania. A pMCSG7 vector containing His-tagged Hsc70 (*HSPA8)* with a TEV cleavage site was a gift from the Southworth lab at the University of Michigan. Untagged HspB1 constructs were expressed in pET23a (WT) and pET151D (D3 and dimer) vectors. All recombinant proteins were expressed and purified from *Escherichia coli* strain BL-21 (DE3). Unlabeled tau4RD and HspB1 were expressed in 1L cultures in Luria-Bertani (LB) media, and unlabeled Hsc70 was expressed in Terrific Broth. Isotopically labeled tau4RD was expressed in 1L MOPS minimal media supplemented with ^{13}C glucose, ^{15}N ammonium chloride, or both. All were incubated at 37ºC until reaching an optical density of 0.6. Tau MTBR expression was induced with 0.4 mM IPTG and grown overnight at 16ºC. HspB1 expression was induced with 1 mM IPTG and grown at 22ºC, and Hsc70 expression was induced with 0.2 mM IPTG and grown at 28ºC.

Hsc70 was purified from 1L cell pellets resuspended in 30 mL pH 8.0 50 mM Tris buffer with 500 mM NaCl and 10 mM imidazole. PMSF, 1x Halt protease inhibitor cocktail (Thermo Scientific), DNase, and RNase were added, and sample was lysed using a French press, then pelleted by centrifugation at 4100 RPM for one hour. Supernatant was filtered with a 0.45 μm syringe filter, then passed over a 5 mL Ni^{2+} affinity column (GE Healthcare). His-tagged Hsc70 was eluted with buffer containing 250 mM imidazole, then dialyzed overnight back into buffer containing 10 mM imidazole in the presence of ~ 1 μM TEV protease (expressed from Addgene plasmid #8830, a gift from David Waugh) to cleave the His-tag. Dialyzed sample was run over a Ni^{2+} column to separate cleaved protein from uncleaved protein, cleaved His-tag, and TEV protease. The flow-through was concentrated with a 10,000MWCO Amicon concentrator, then buffer-exchanged into pH 8.0 25 mM Tris buffer with 1 mM EDTA. Sample was loaded onto a 5 mL HiTrap Q HP column (GE Healthcare) and eluted in a 25 mL gradient to buffer containing 500 mM NaCl. Purity was assessed by SDS-PAGE, and pooled fractions were concentrated to 2-3 mL. Sample was passed over a Superdex 200 10/300 GL column (GE Healthcare) in 500 μL batches. Fractions were analyzed by SDS PAGE, pooled based on purity, concentrated, flash-frozen in liquid nitrogen and stored at -80ºC. Tau4RD constructs were purified as described previously (Nakatani-Webster and Nath 2017) in a protocol very similar to Hsc70, but which omits the anion-exchange chromatography step. HspB1 was purified as described previously (Clouser and Klevit 2017).

2.4.2 *Analytical SEC:*

All samples were prepared in pH 7.5 buffer containing 50 mM sodium phosphate, 100 mM sodium chloride, and 0.5 mM EDTA and allowed to equilibrate at room temperature for at least 3 hours. For SEC, 100μL samples of 50 μM HspB1 were run over a Superose 6 10/300 mm column

(GE Healthcare) equilibrated in the identical buffer as the samples, at room temperature. For SEC-MALS, 25μL samples of 100 μM HspB1 were equilibrated at room temperature for at least 3 hours prior to being placed in a 4°C autosampler. Samples were run over a Superose 6 Increase 3.2/300 mm column at room temperature, equilibrated in the identical buffer. Chromatograms were collected on a GE AKTA Pure coupled to a Wyatt miniDAWN TREOS and Optilab T-rEX differential refractive index detector. Molar mass was calculated from the Raleigh ratio based on multi-angle (static) light scattering and protein concentration from the change in refractive index (dn/dc = 0.185). Analysis was performed using Wyatt ASTRA VI software, and curves were calibrated with apoferritin.

2.4.3 *Circular Dichroism:*

CD spectra of HspB1 and its mutants were collected on a Jasco J-1500 CD spectrometer. Samples contained 10μM of protein in 25 mM sodium phosphate buffer with 50 mM sodium chloride and 0.25 mM EDTA at pH 7.5. Samples were equilibrated at room temperature for at least 3 hours prior to measurement and measured in a 0.1 cm cuvette. Measurements were taken at 20°C from 260-190 nm in continuous scanning mode with a scanning rate of 50 nm/min, data integration time of 2 seconds, and bandwidth of 1 nm. Data presented are an average of 3 scans and data are truncated at a wavelength resulting in a high-tension value at or above the recommended 800V cutoff.

2.4.4 *ThT fluorescence spectra:*

Samples were prepared containing 5 or 20 μM HspB1 in 50 mM sodium phosphate buffer (pH 7.5) containing 100 mM sodium chloride and 0.5 mM EDTA. ThT was added to a concentration

of 75 μM and samples were covered in foil and incubated at room temperature for 3 hours. Samples were incubated at 37ºC immediately prior to fluorescence measurements, which were also recorded at 37ºC. Using a Horiba Fluorolog 3 fluorimeter, samples were excited at 440 nm (1.2 nm slit width) and emission spectra from 450 to 550 nm (5 nm slit width) were collected.

2.4.5 *ThT kinetic assays:*

Tau4RD, ThT, and chaperone were added to wells in a 96-well black flat-bottom non-binding plate (Corning) in buffer containing 30 mM sodium phosphate, 20 mM sodium chloride, 5 mM dithiothreitol, and 0.5 mM EDTA at pH 7.4. Immediately before beginning the reads, 100 μL heparin (MP Biomedicals, average MW 3,000 Da) solution was added to each well, bringing the total volume to 200 μL and the concentrations to 3.5 μM tau4RD, 6 μM heparin, and 75 μM ThT. Six replicates were included for each experimental condition. Experiments done in the presence of ATP also included 1 mM ATP, 1 mM $MgCl_2$, and 1 mM KCl. Solutions containing heparin and tau4RD + ThT were filtered with a 0.22 μm syringe filter immediately prior to addition to the plate. Solutions containing chaperone were centrifuged at 21.1 g for 10 minutes prior to addition. The plate was covered with clear polyolefin sealing tape (Thermo Scientific) to prevent evaporation and placed in a Biotek Synergy HTX multi-mode plate reader. Samples were held at 37ºC and fluorescence was measured every 2.5 minutes using 440 nm and 485 nm filters for excitation and emission, respectively. Immediately before each fluorescence read, plate was shaken linearly at 1096 cpm for one minute. Delayed addition experiments were programmed to pause at appropriate timepoints to enable addition of 10 μL chaperone solution or buffer to the appropriate wells. All other conditions were the same. Experiments with full-length tau were conducted under similar conditions, but used 5 μM tau2N4R, were shaken continuously, and were read at 10 minute intervals.

2.4.6 *Electron microscopy:*

300 mesh carbon-coated copper grids (Electron Microscopy Services) were glow-discharged and spotted with 3 μL of the end products of tau4RD ThT assays. Samples adsorbed for 60 seconds, then were blotted by filter paper, rinsed with filtered milliQ water and blotted twice, and floated on a drop of NanoW stain (NanoProbes) for 60 seconds. Stain was blotted with filter paper, and grids were allowed to dry on filter paper then stored in a container at room temperature. Grids were visualized on a Morgagni electron microscope with a 100kV beam.

2.4.7 *1D NMR assays:*

50 μM samples of ^{13}C-labeled tau4RD were prepared with or without chaperone in pH 7.4 buffer containing 25 mM sodium phosphate, 10 mM sodium chloride, 5 mM dithiothreitol, 0.5 mM EDTA, and 10% D_2O. Initial unedited 1D watergate and ^{13}C-edited spectra were collected on a 500 MHz Bruker magnet at 37ºC. ^{13}C-edited 1D spectra are the first slice of a ^{13}C-HSQC. The sample was then removed, heparin was added to a final concentration of 120 μM, and a series of alternating unedited and ^{13}C-edited spectra were collected over the course of 18 hours. At the end of the experiment, sample was removed from the NMR tube, and a 100 μL aliquot was centrifuged at 21.1x g for 60 minutes. Supernatant was removed and 100 μL buffer was added to wash the pellet. Sample was centrifuged at 21.1x g for 15 minutes, supernatant was removed, and pellet was resuspended in 100 μL buffer. Samples from the total reaction, the supernatant, and the pellet were analyzed by SDS-PAGE. NMR spectra were processed using NMR pipe. For each spectrum, the intensity of a peak in the methyl region at 0.77 ppm in the unedited and 0.89 ppm in the edited spectra was measured. The intensity of this peak was normalized to the intensity of the same peak

in the first spectrum following heparin addition, and relative intensities were plotted as a function of time.

2.4.8 *Fluorescence correlation spectroscopy:*

A construct of tau4RD with both native cysteines mutated to serine and an additional cysteine incorporated as the second residue was created using the Phusion Site-Directed Mutagenesis kit (Thermo Scientific). Alexa Fluor 488 C5 maleimide (Life Technologies) was conjugated to this cysteine residue by incubating 100 μM purified protein with ~3-fold excess dye at room temperature for 2 hours. Labeled protein was separated from unlabeled protein and free dye on a BDS Hypersil C18 column run with a water/acetonitrile gradient in the presence of 0.05%TFA on a Dionex Ultimate 3000 HPLC. Fractions containing labeled protein were collected, and solvent was evaporated. Dried labeled protein was stored at -20ºC and resuspended in buffer prior to use. Aliquots of resuspended protein were flash-frozen in liquid nitrogen and stored at -80ºC until immediately prior to use. 50 μL samples containing chaperone protein and 2 mg/mL BSA were prepared in pH 7.4 buffer containing 25 mM sodium phosphate, 100 mM sodium chloride, 2 mM dithiothreitol, and 0.5 mM EDTA. For Hsc70 binding experiments, 1 μL labeled tau4RD was added to the sample 5 minutes prior to recording FCS measurements. For HspB1dimer binding experiments, tau4RD was added and samples were incubated at room temperature for 3-5 hours prior to FCS measurements. The diffusion of each sample was measured on a Zeiss Axio Observer D1 confocal microscope equipped with a Picoquant PDL 828 Sepia II pulsed laser driver, HydraHarp 400 detection electronics and a Picoquant τ-SPAD single photon counting module. Laser excitation was at 485 nm, and emitted light was collected through a 488 nm dichroic mirror and 535/70 emission filter. Seven consecutive 1-minute measurements were recorded and autocorrelation curves for each measurement were calculated using SymphoTime 64 software.

Each curve was fit using GraphPad Prism to the following equation for free diffusion, where N is average number of particles in the focal volume, τ_D is the diffusion time of each particle, and s (the ratio of the radial to axial dimension of the focal volume) fixed to 0.2 based on calibration measurements:

$$G(\tau) = \frac{1}{N\left(1 + \tau/\tau_D\right)\sqrt{1 + s^2\tau/\tau_D}}$$

Each curve was normalized to the value of N determined by this fitting, and the seven curves for each condition were averaged. Since $R_h \propto \tau_D$, all diffusion times were normalized to that of free tau4RD, and the relative fold-change was fit to the following 1-site model:

$$R_h^{norm} = 1 + \frac{\Delta R_{h,\infty}^{norm}[hsp]}{K_D + [hsp]}$$

where R_h^{norm} is the normalized R_h at a given chaperone concentration, $\Delta R_{h,\infty}^{norm}$ is the maximal fold-change in R_h, $[hsp]$ is the concentration of chaperone, and K_D is the dissociation constant.

2.4.9 *2D NMR spectroscopy:*

NMR samples contained 100 or 200 μM labeled tau4RD protein in pH 7.4 buffer containing 25 mM sodium phosphate, 100 mM sodium chloride, 2 mM DTT, and 0.5 mM EDTA. Spectra were collected at 10ºC on a Bruker Avance III 800 MHz magnet equipped with a triple-resonance, z-gradient cryoprobe. HNCACB and CBCA(CO)NH spectra were used to transfer published assignments (Barre and Eliezer 2013) to the ^{15}N TROSY HSQC spectrum of tau4RD. Data were processed using NMRpipe and analyzed with NMRViewJ. Peak broadening was quantified by dividing the intensity of each peak in the bound spectrum by the intensity of the corresponding peak in the unbound spectrum. Chemical shift perturbations were quantified with the following

equation, where ΔHN is the amide proton chemical shift difference and ΔN is the ^{15}N backbone amide chemical shift difference:

$$CSP = \sqrt{(\Delta HN)^2 + (\Delta N/5)^2}$$

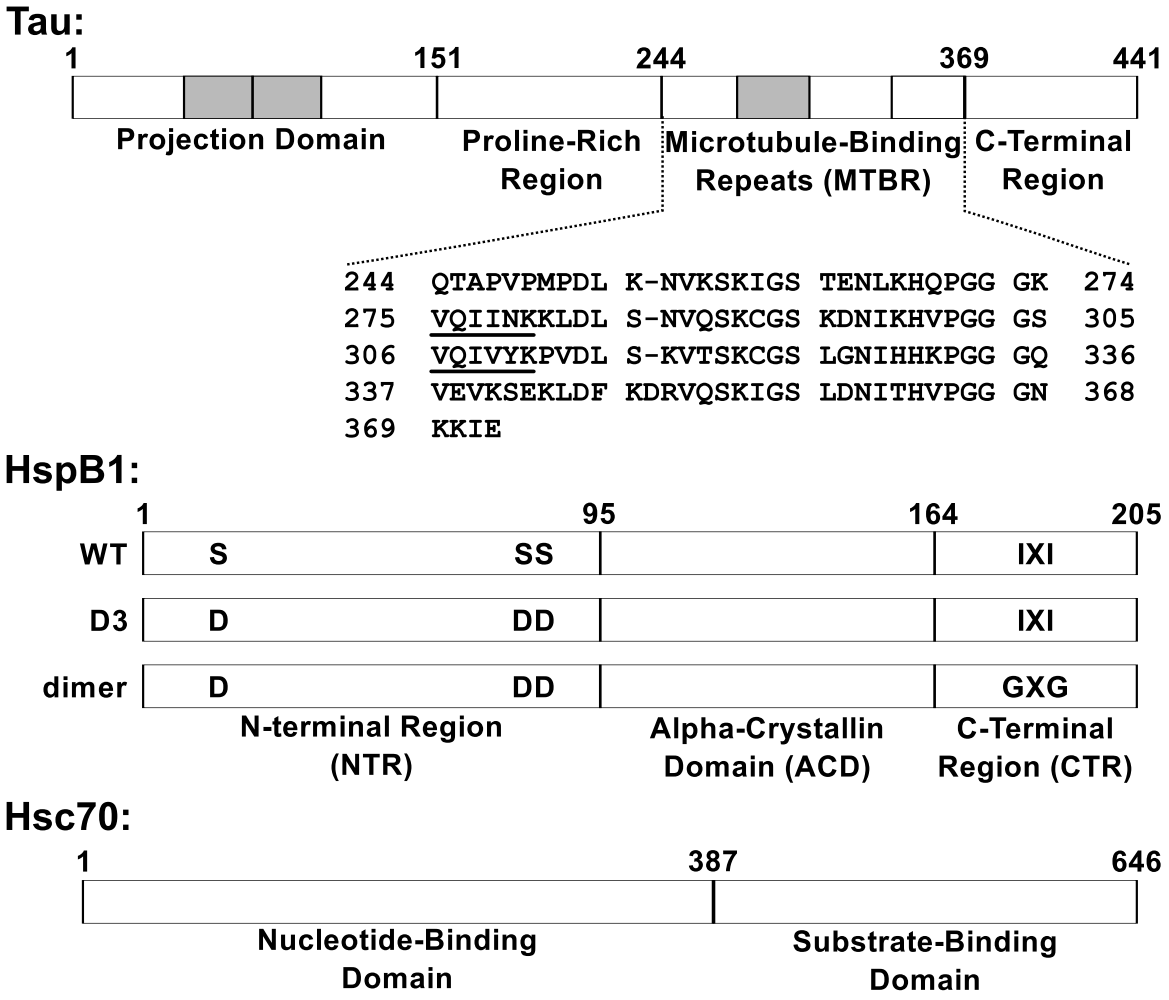

Figure 2.1. Domain organization of tau, HspB1, and Hsc70

(Top) Full-length tau2N4R is natively unstructured, and consists of four domains. The tau4RD construct used in this work contains residues 244-372, which includes the four microtubule-binding repeats. The sequences ^{275}VQIINK^{280} and ^{306}VQIVYK^{311} at the beginning of the second and third repeats drive tau fibril formation. Shaded areas denote regions that can be alternatively spliced.

(Middle) HspB1 contains three domains. The core ACD has a β-sandwich fold and forms a stable dimer. The CTR is intrinsically disordered and contains an IXI motif that interacts with the ACD in the context of large oligomers. The NTR is partially disordered and involved in oligomerization, and it contains three serine residues that are phosphorylated in response to cellular stress. The "D3" and "dimer" constructs, described in the text, affect the oligomerization state of HspB1.

(Bottom) Hsc70 contains two domains: an N-terminal nucleotide binding domain with ATPase activity and a C-terminal substrate binding domain that interacts with client proteins.

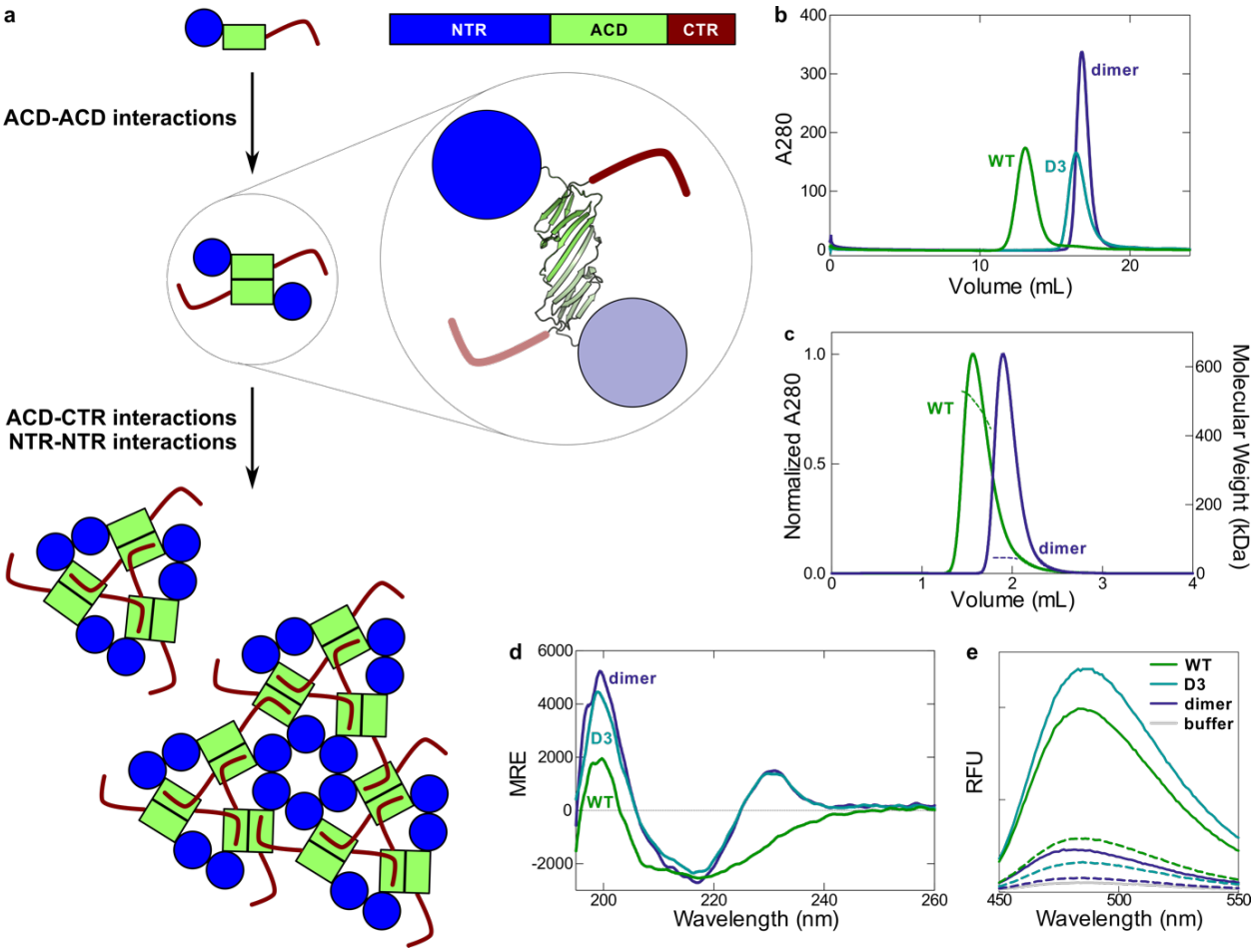

Figure 2.2.. Characterization of HspB1dimer

(A) Oligomerization schematic of HspB1. Dimerization is driven by the core ACD (green; PDB ID: 2N3J). Each protomer has a β-sandwich fold and dimerizes along the β6+7 strand (53). Higher-order oligomerization is caused by interactions between the β4-β8 groove of the ACD and the sequence ^{179}ITIPV^{183} in the C-terminal region, as well as interactions between N-terminal regions from different subunits.

(B) Size-exclusion chromatograms of HspB1 constructs (50μM initial concentration) run on a 24 mL analytical Superose 6 column. HspB1WT (green) elutes early as a broad peak, indicating a polydisperse population of high molecular weight oligomers. HspB1D3 (teal) elutes later but remains broad, indicating a polydisperse population of smaller oligomers. HspB1dimer elutes last and has a highly symmetric, sharp peak, indicating a more monodisperse sample.

(C) SEC-MALS chromatograms comparing HspB1WT (green) to HspB1dimer (blue) run over a 2.4 mL Superose 6 column. HspB1WT elutes earlier and consists of a range of molecular weight species (dotted green line). HspB1dimer elutes later and contains a single molecular-weight species corresponding to a monodisperse dimer (dotted blue line).

(D) Far-UV circular dichroism spectra recorded on 10 μM samples of HspB1 constructs. HspB1D3 and HspB1dimer are similar in secondary structure and distinct from HspB1WT.

(E) ThT fluorescence emission spectra of HspB1 constructs. Solid lines contain 20 μM pro- tein, and dashed lines contain 5 μM protein.

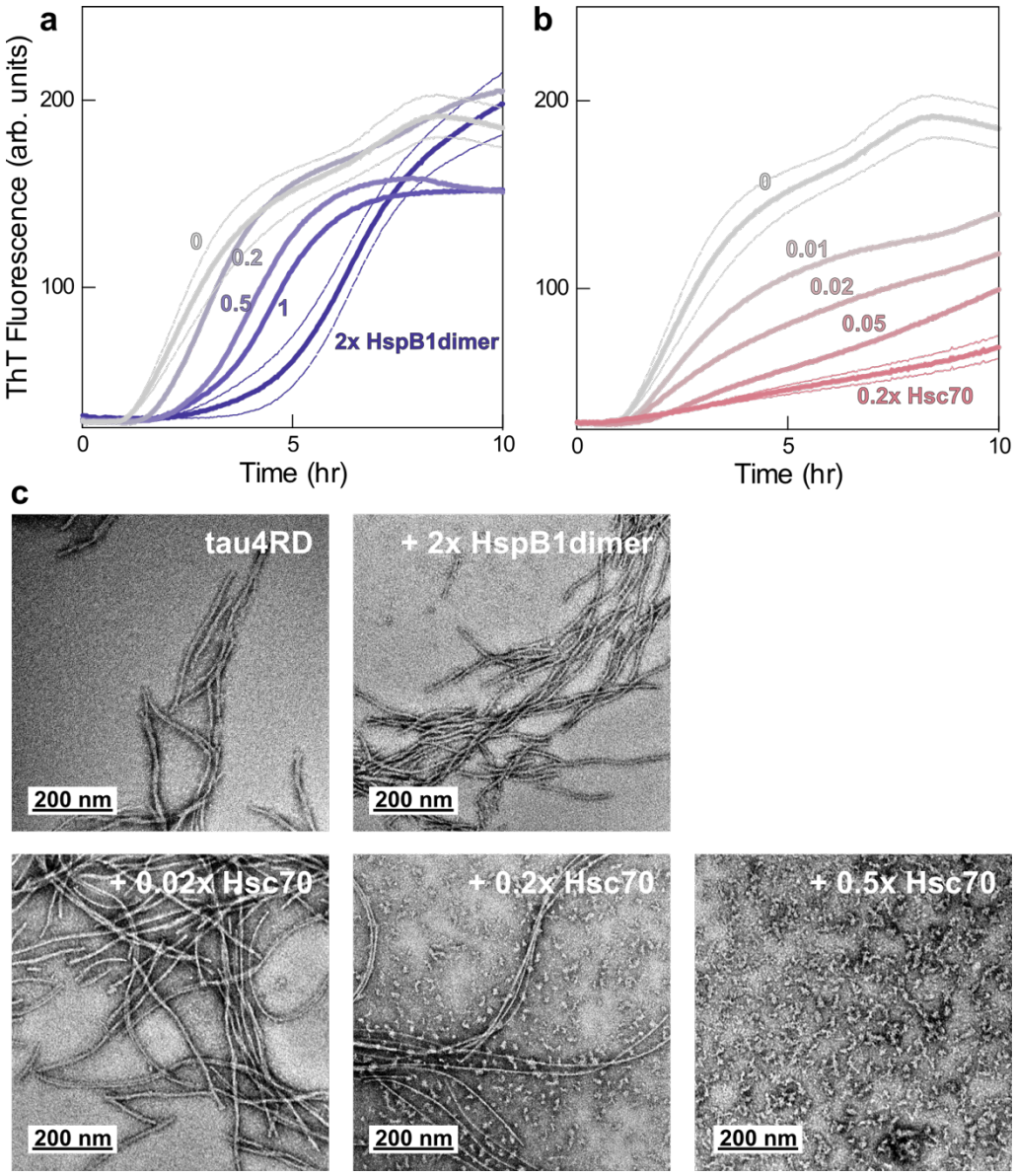

Figure 2.3. Effects of Hsc70 and HspB1 on tau4RD fibril formation

(A) ThT fluorescence traces over the course of a representative fibril formation reaction. Tau4RD (3.5 μM) fibrillizes over the course of 10 hours following the addition of the aggregation-inducer heparin (6 μM, average MW 3 kDa) and follows expected unseeded amyloid formation kinetics. HspB1dimer delays the onset of tau4RD fibril formation in a dose-dependent manner but does not alter the final ThT fluorescence signal. Each trace is the average of 6 replicates in a 96-well plate. For clarity, error bands (SEM) are shown only for the highest and lowest chaperone concentrations.

(B) Hsc70 is a highly potent substoichiometric inhibitor and decreases the extent of fibril formation in a dose-dependent manner.

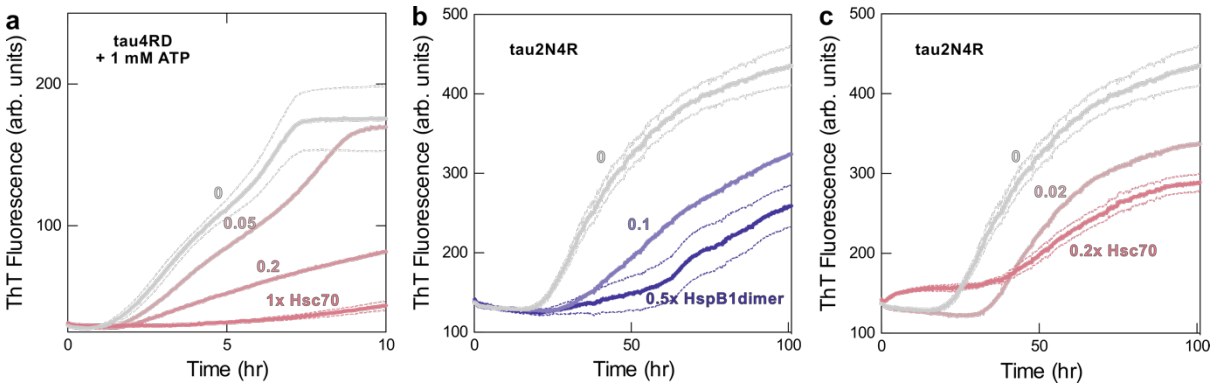

Figure 2.4. Effects of tau sequence and ATP on chaperone activity

(A) ThT fluorescence traces over the course of a tau4RD fibril formation reaction in the presence of 1 mM ATP. Hsc70 has a similar effect on tau4RD fibril formation kinetics under these conditions, but is a slightly less potent inhibitor.

(B) ThT fluorescence traces over the course of a full-length tau fibril formation reaction. Tau2N4R (5 μM) fibrillizes over the course of four days following the addition of 6 μM heparin. As with tau4RD, HspB1dimer delays the onset of fibril formation in a dose-dependent manner. Note the expanded timescale of the *x*-axis relative to Panel A, due to the slower kinetics of full-length tau.

(C) Hsc70 remains a highly potent substoichiometric inhibitor capable of lowering the plateau intensity of tau2N4R fibril formation. Note the expanded timescale of the *x*-axis relative to Panel A, due to the slower kinetics of full-length tau.

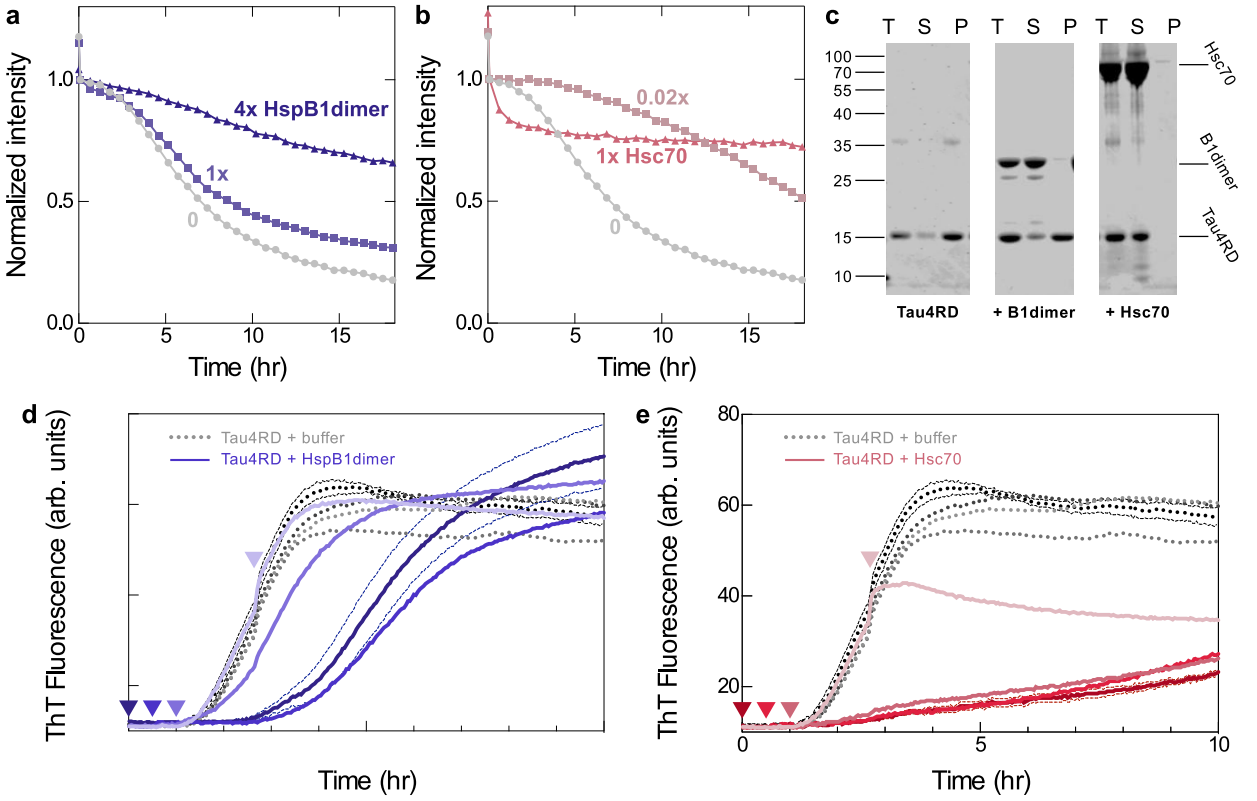

Figure 2.5. Mechanisms of chaperone inhibition

(A) Intensity from 1D NMR spectra monitoring the disappearance of small, soluble tau4RD species during aggregation. In the absence of chaperone (grey circles), 50 μM tau4RD loses some intensity following the addition of 120 μM heparin (drop between first and second data points), then loses intensity in a sigmoidal manner as it becomes incorporated in NMR-invisible fibrils. HspB1dimer slows this intensity loss in a dose-dependent manner (blue squares and triangles).

(B) Hsc70 is inhibitory even at a 1:50 molar ratio, making it a highly potent substoichiometric inhibitor. At a 1:1 ratio it causes a rapid decrease in intensity, likely due to enhanced binding in the presence of heparin, followed by a plateau.

(C) SDS-PAGE analysis of end-products of 1D NMR experiments. End products were centrifuged, and total end products (T), supernatant (S), and pellet (P) were run on a gel. In the absence of chaperone and in the presence of 1 molar equivalent HspB1dimer, most of the tau4RD ends up in the insoluble fraction. In the presence of 1 molar equivalent Hsc70, almost all of the tau4RD remains soluble. This indicates that the rapid intensity loss in the presence of Hsc70 is due to binding rather than aggregation.

(D) ThT fluorescence traces over the course of a tau4RD fibril formation reaction. HspB1dimer (1 molar equivalent) was added to 3.5 μM tau4RD either at the beginning of the reaction (dark blue) or 0.5, 1, or 2.5 hours after the reaction had been initiated by the addition of 6 μM heparin (lighter blues). HspB1dimer was still effective at delaying aggregation when added during the lag phase of the reaction but was no longer effective when added during the elongation phase of the reaction. Adding buffer instead of chaperone at any time point did not alter aggregation kinetics (grey curves). Curves are averages of 6 replicates. For clarity, error bands (SEM) are shown only for the 0 hour experiments.

(E) Hsc70 (0.05 molar equivalents) was added to 3.5 μM tau4RD either at the beginning of the reaction (dark red) or 0.5, 1, or 2 hours after the reaction had been started by the addition of 6 μM heparin (lighter reds). Addition of Hsc70 during the lag phase did not alter its effect on the aggregation kinetics, and addition during the elongation phase prevented any further increase in ThT fluorescence. Adding buffer instead of chaperone at any time point did not alter aggregation kinetics (grey curves). Curves are averages of 4 or 6 replicates.

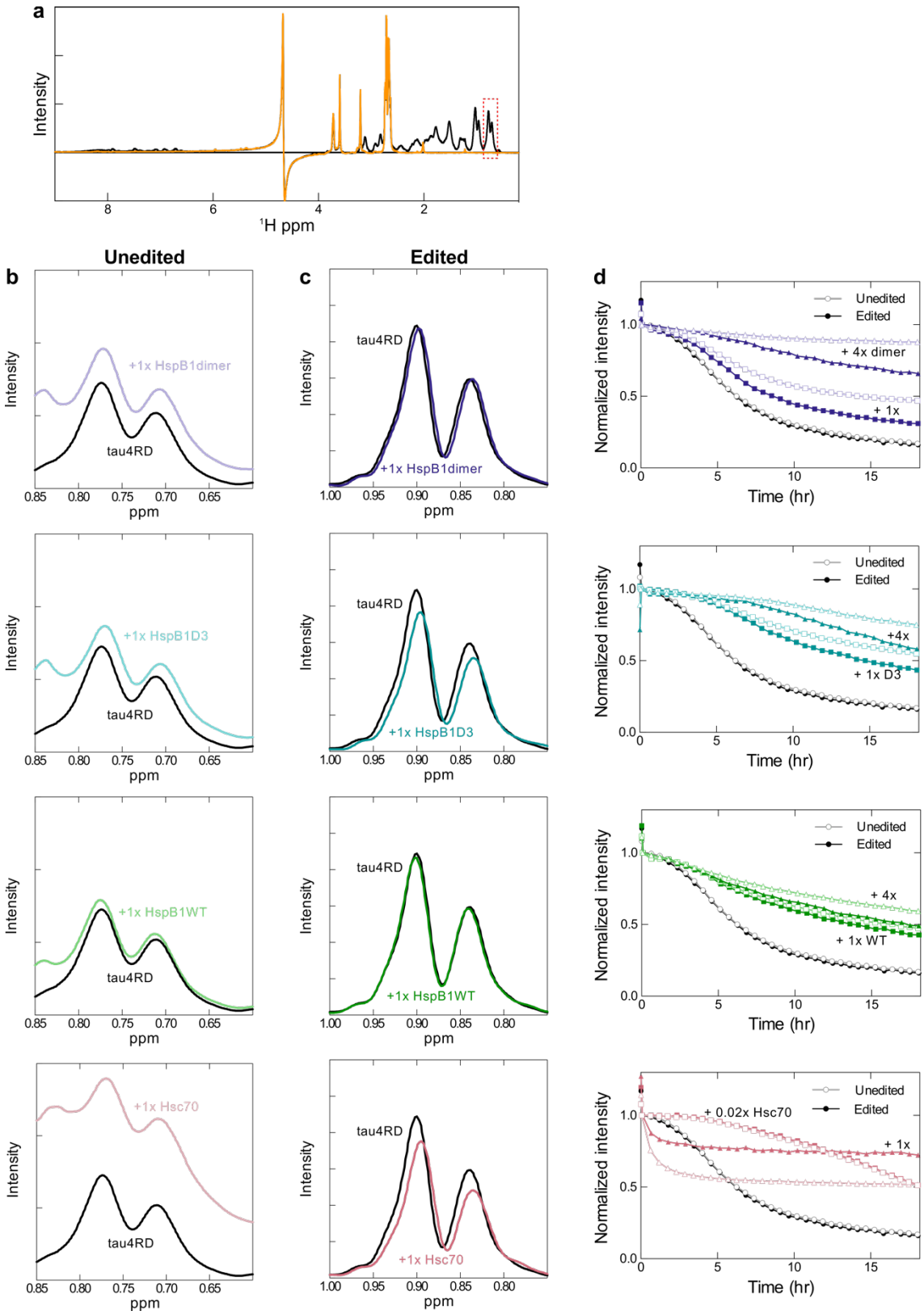

Figure 2.6. 1D NMR data from ^{13}C-edited and unedited ^{1}H NMR spectra

(A) Unedited ^{1}H NMR spectra of 50 μM tau4RD (black) and 240 μM heparin (orange) in buffer. The peak used to quantify relative tau4RD intensity at 0.77 ppm (red dashed box) is well-separated from signal arising from heparin and buffer components.

(B) Region of the unedited ^{1}H NMR spectrum of tau4RD (50 μM) containing the peak used to quantify relative intensity (black). The addition of 50 μM chaperone protein increases the signal in this region (colors).

(C) Region of the ^{13}C-edited spectrum of 50 μM tau4RD alone (black) and in the presence of 50 μM unlabeled chaperone protein (colors). The chaperones do not contribute to the signal in these spectra, but some constructs cause broadening of the tau4RD signal.

(D) Quantification of intensity loss of ^{13}C-edited and unedited ^{1}H spectra over time. Tau4RD loses intensity at the same rate in both types of spectra in the absence of chaperone (black and gray circles). In experiments containing Hsc70, unedited spectra lose intensity at a faster rate than ^{13}C-edited spectra, indicating that Hsc70 loses intensity at a rate faster than tau4RD. In experiments containing HspB1, unedited spectra lose intensity at a slower rate than ^{13}C-edited spectra, indicating that HspB1 does not lose intensity as quickly as tau4RD.

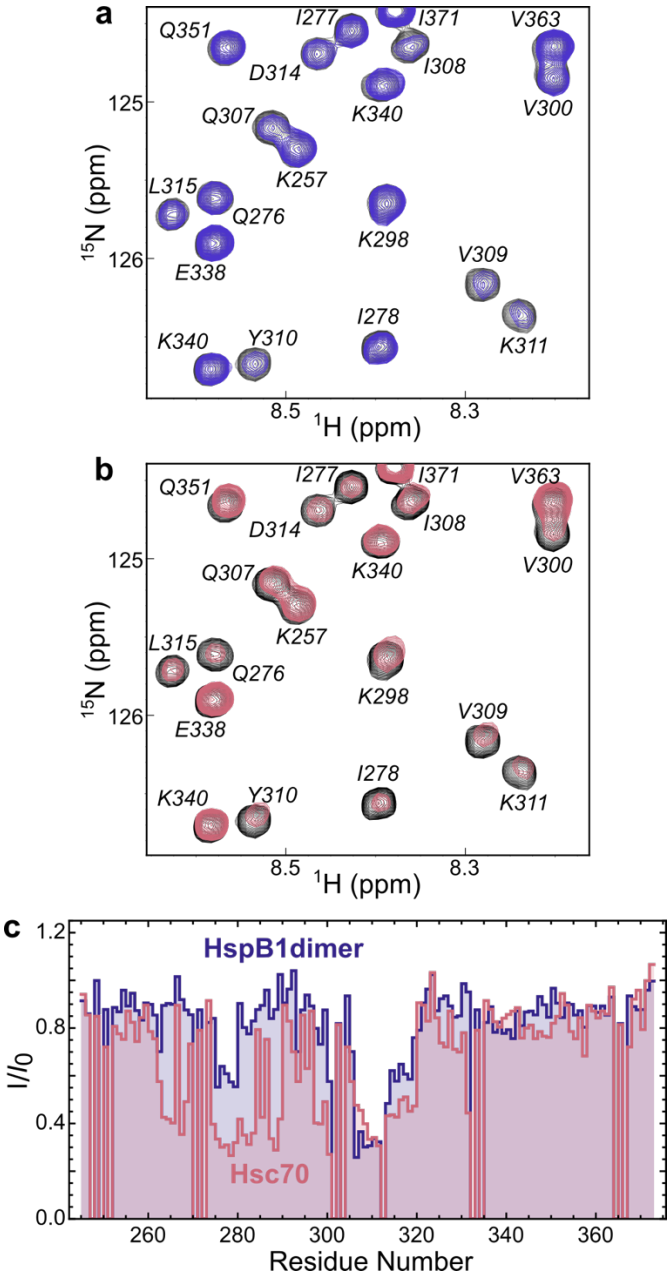

Figure 2.7. Chaperone binding sites

(A) ^{15}N-HSQC TROSY of ^{15}N-labeled tau4RD alone (black) and in the presence of 2 molar equivalents HspB1dimer (blue).

(B) ^{15}N-HSQC TROSY of ^{15}N-labeled tau4RD alone (black) and in the presence of 2 molar equivalents Hsc70 (red).

(C) Peak broadening from (A) and (B), quantified by dividing the intensity of a peak in the bound spectrum (I) by the intensity of the same peak in the unbound spectrum (I_0). Broadening due to HspB1dimer maps primarily to the aggregation-prone motif in the third repeat of tau4RD (^{306}VQIVYK^{311}), while broadening due to Hsc70 maps to the aggregation-prone motifs at the start of both the second and third repeats of tau4RD (^{275}VQIINK^{280} and ^{306}VQIVYK^{311}).

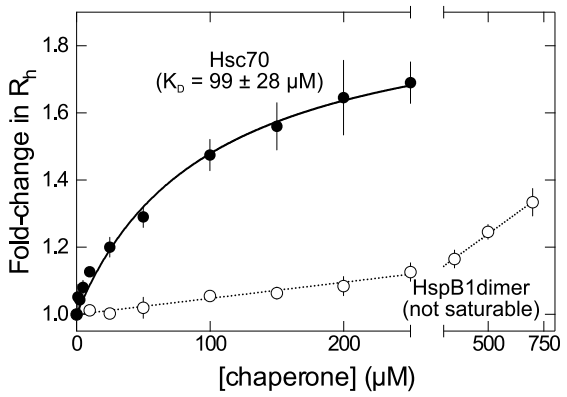

Figure 2.8. Chaperone binding affinities

FCS-derived changes in hydrodynamic radius of tau4RD~A488, measured in the presence of increasing concentrations of Hsc70 (solid circles) or HspB1dimer (empty circles). The Hsc70 data are well-fit by a one-site binding model with $K_D = 99 \pm 28$ μM, while HspB1dimer does not appear to saturate up to a chaperone concentration of 750 μM.

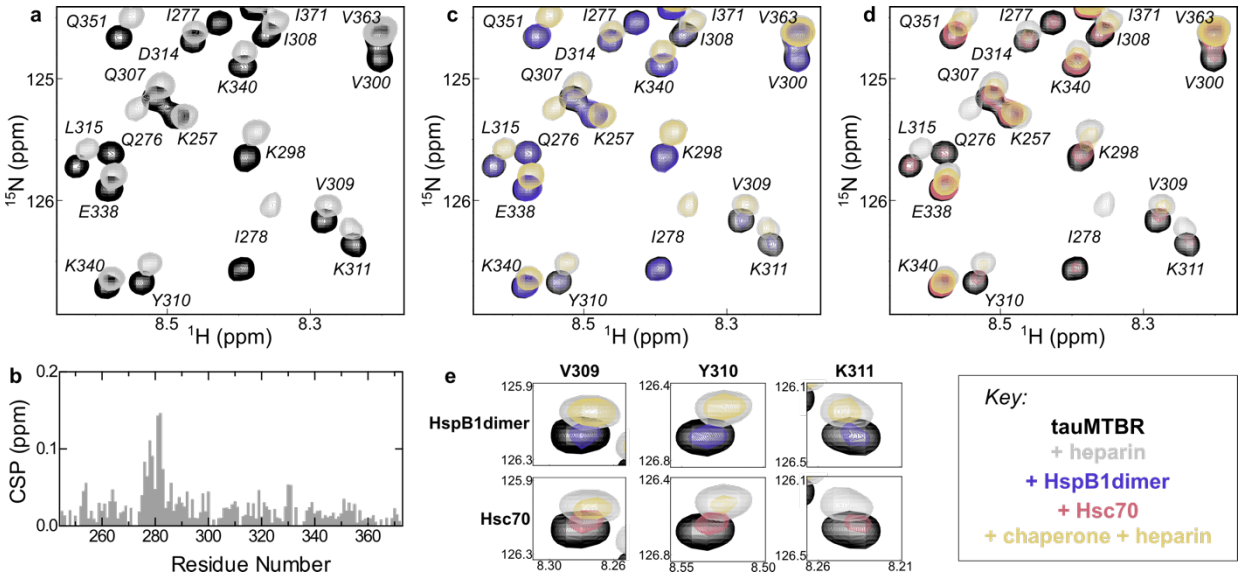

Figure 2.9. Effects of heparin on chaperone binding

(A) ^{15}N-HSQC TROSY of ^{15}N-labeled tau4RD alone (black) and in the presence of 2.4 molar equivalents heparin (gray).

(B) Chemical shift perturbations (CSPs) of each peak in (A) plotted as a function of residue number. Highest CSPs map to the aggregation-prone motif at the start of the second repeat of tau4RD, ^{275}VQIINK^{280}.

(C) ^{15}N-HSQC TROSY of ^{15}N-labeled tau4RD alone (black), in the presence of 2.4 molar equivalents heparin (gray), in the presence of 2 molar equivalents HspB1dimer (blue), and in the presence of both 2.4 equivalents heparin and 2 equivalents HspB1dimer (yellow). HspB1dimer binding is largely unchanged by the presence of heparin.

(D) ^{15}N-HSQC TROSY of ^{15}N-labeled tau4RD alone (black), in the presence of 2.4 molar equivalents heparin (gray), in the presence of 2 molar equivalents Hsc70 (red), and in the presence of both 2.4 equivalents heparin and 2 equivalents Hsc70 (yellow). Hsc70 binding is enhanced by the presence of heparin, as indicated by the enhanced broadening in the yellow spectrum relative to the red.

(E) Comparison of residues V309, Y310, and K311 in the HspB1dimer-bound and Hsc70-bound spectra in the presence of heparin. Although HspB1dimer and Hsc70 cause a similar amount of broadening in these peaks in the absence of heparin, in the presence of heparin Hsc70 causes significantly more broadening in these peaks than HspB1dimer, indicating that heparin enhances Hsc70 binding in a way that it does not for HspB1dimer.

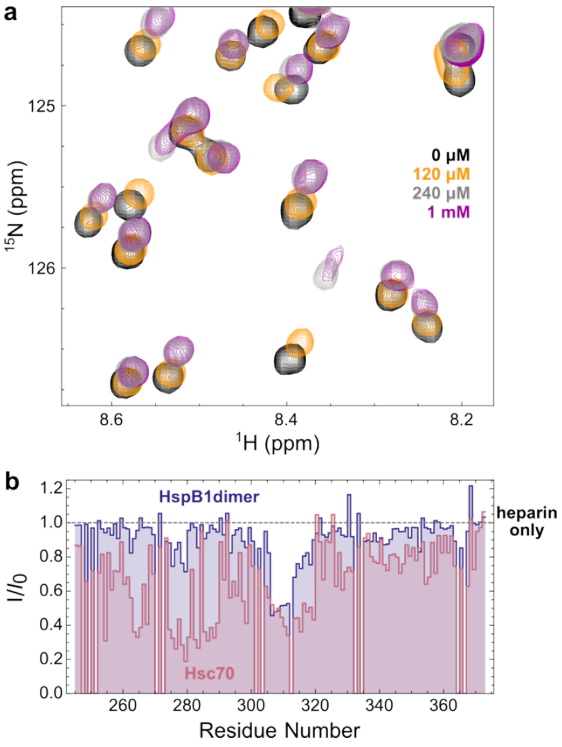

Figure 2.10. Characterization of chaperone binding to heparin-bound tau

(A) ^{15}N-HSQC spectra of tau4RD in the presence of heparin. Under the conditions used in Fig. 2.9 (grey, 100 μM tau4RD + 240 μM heparin), heparin binding is near saturation, as peaks nearly overlap with a fully-saturated spectrum (purple, 200 μM tau4RD + 1 mM heparin). At a lower heparin concentration (orange, 100 μM tau4RD + 120 μM heparin), peaks shift relative to unbound tau4RD (black, 100 μM tau4RD) but less than they do in the saturated spectra.

(B) Quantification of tau4RD peak broadening due to chaperone binding in the presence of heparin, relative to the heparin-only spectrum. Hsc70 (red) causes significantly more broadening in the presence of heparin than HspB1 (blue), indicating that it has enhanced affinity for aggrega- tion-prone tau4RD.

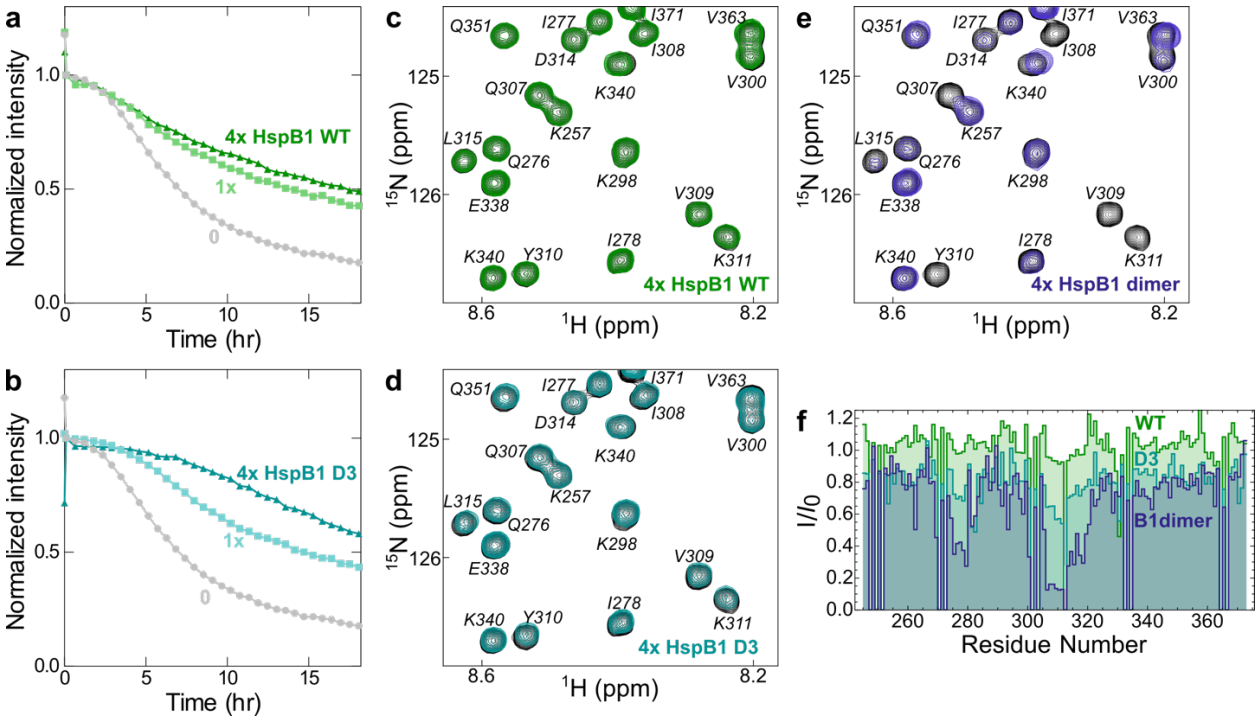

Figure 2.11. Effects of HspB1WT and HspB1D3 on tau4RD

(A) Intensity from 1D NMR spectra monitoring the disappearance of small, soluble tau4RD species during aggregation in the presence of HspB1WT. HspB1WT (green squares and triangles) slows this intensity loss in a manner similar to HspB1dimer (Fig. 2.5A).

(B) Intensity from 1D NMR spectra monitoring tau4RD aggregation in the presence of HspB1D3 (teal squares and triangles). HspB1D3 slows intensity loss in a manner similar to HspB1dimer and WT.

(C) ^{15}N-HSQC TROSY of ^{15}N-labeled tau4RD alone (black) and in the presence of 4 molar equivalents HspB1WT (green). There is very little significant broadening in the spectrum with HspB1WT, suggesting that binding is very weak.

(D) ^{15}N-HSQC TROSY of ^{15}N-labeled tau4RD alone (black) and in the presence of 4 molar equivalents HspB1D3 (teal). There is slight broadening in peaks corresponding to ^{306}VQIVYK^{311}, indicating some binding.

(E) ^{15}N-HSQC TROSY of ^{15}N-labeled tau4RD alone (black) and in the presence of 4 molar equivalents HspB1dimer (blue). Peak broadening is much more substantial, indicating that HspB1WT and D3 both bind more weakly than HspB1dimer.

(F) Quantification of tau 4RD peak intensity loss due to HspB1WT, HspB1D3, and HspB1dimer binding.

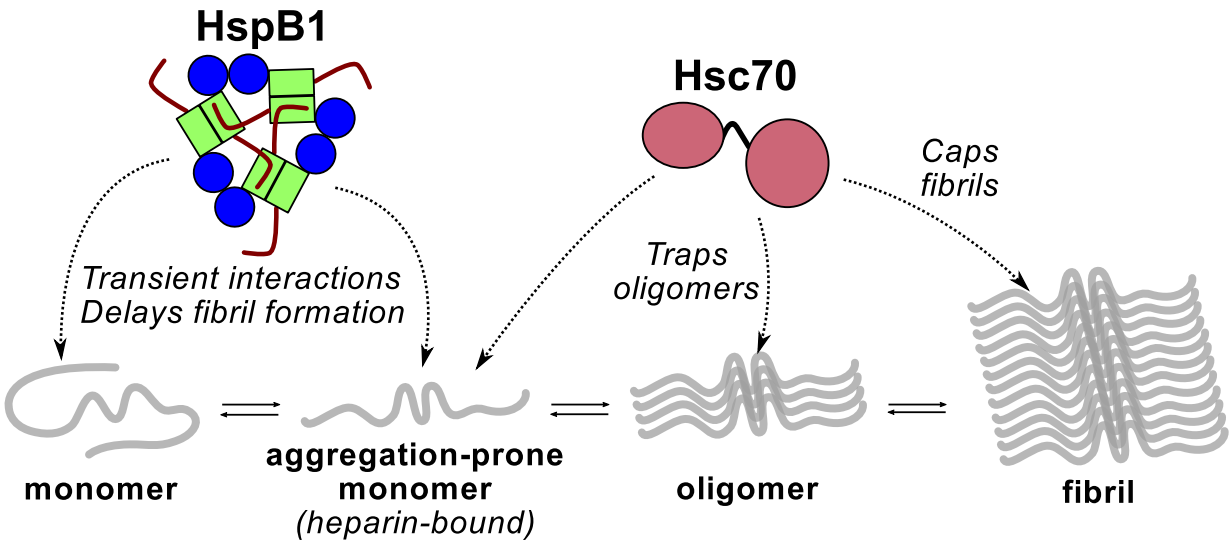

Figure 2.12. Model of chaperone effects on tau aggregation

HspB1 and Hsc70 interact with different species along the tau amyloid formation pathway. HspB1 interacts with early species and delays the formation of tau oligomers and fibrils (1D NMR and ThT results). Hsc70 has enhanced affinity for aggregation-prone, heparin-bound tau (1D and 2D NMR results), can hold tau in an oligomeric state (EM results) and can prevent fibril elongation (ThT results).

Chapter 3. INTERPLAY OF DISORDERED AND ORDERED REGIONS IN A HUMAN SMALL HEAT SHOCK PROTEIN YIELDS AN ENSEMBLE OF "QUASI-ORDERED" STATES

[Adapted from Clouser, Baughman, Basanta, Guttman, Nath, and Klevit (2019) "Interplay of disordered and ordered regions in a human small heat shock protein yields an ensemble of 'quasi-ordered' states" (under review)]

Abstract:

Small heat shock proteins (sHSPs) are nature's "first responders" to cellular stress; their ubiquitous presence and rapid activation via phosphorylation make them readily available to interact with affected proteins and help prevent their aggregation. However, relatively little is known about the structure of sHSPs, especially regarding the disordered regions and their relationship to the well-defined structural cores. In the human sHSP HSPB1, the disordered N-terminal region (NTR) makes up nearly 50% of the sequence, yet there is essentially no structural information available for this domain. Building on NMR and hydrogen-deuterium exchange mass spectrometry (HDXMS) work from a previous graduate student, Amanda Clouser, we investigated interactions between the NTR and the alpha-crystallin domain (ACD) of HSPB1. We used solution NMR to elucidate extensive interactions between regions of the NTR and grooves on the ACD. Many of these interactions were highly specific and were used to build a structural model of dimeric HSPB1 involving extensive NTR-ACD interactions. The combined results support a model in which multiple grooves of an ACD dimer can interact with discrete regions of the NTR or be unoccupied. The resulting myriad combinations yields an ensemble of "quasi-ordered" NTR states and helps explain the conformational heterogeneity observed in large, polydisperse oligomers and even

monodisperse dimers. We also investigated the mechanisms by which alterations such as phosphorylation and disease-associated mutations alter NTR-ACD contacts and alter the distribution of accessible states.

3.1 INTRODUCTION

Small heat shock proteins (sHSPs) are a class of molecular chaperones that help maintain cellular proteostasis. Unlike other heat shock proteins, sHSPs are ATP-independent and are believed to interact with exposed hydrophobic regions of partly unfolded or misfolded proteins to help prevent irreversible aggregation. However, our understanding of sHSP structure and function lags behind that of other classes of chaperones. Several properties make mammalian sHSPs particularly challenging for structural characterization. First and foremost, many sHSPs form large homo- and/or hetero-oligomers, and many of these exist as broad distributions of differently sized oligomeric species. Furthermore, subunits exchange rapidly among oligomers, making it difficult to capture a single oligomeric state, or even a narrow distribution of states. Second, up to 50% of the sequence of sHSPs is unresolved in the few structures of full-length sHSPs available and is believed to be intrinsically disordered. Third, there is often local conformational heterogeneity even within ordered regions of the protein. Finally, the transient and promiscuous nature of interactions between sHSPs and client proteins makes it challenging to capture a sHSP/client complex of the sort that has fueled structural-mechanistic understanding of other chaperones.

sHSPs consist of three regions that also define different types of inter-protomer interactions in homo-oligomers (Figure 3.1 A). Most current structural information on human sHSPs is based on the structures of their defining feature, the central α-crystallin domain (ACD) (Rajagopal et al. 2015b, 2015a; Hochberg et al. 2014; Baranova et al. 2011; Bagnéris et al. 2009). Both sequentially

and structurally conserved among the human paralogs, ACDs form an IgG-like β-sandwich fold of six or seven strands (Fig. 3.1b). ACDs dimerize by anti-parallel alignment of their β6+7 strands to form a long β-sheet dimer interface (ACD-ACD interaction). The flanking regions on either side of the ACD are far less conserved among paralogs and are predominantly disordered. The C-terminal region (CTR) is a relatively short extension that contains many charged residues and is inherently disordered. Most human sHSPs known to exist as large oligomers contain a three-residue motif of alternating Ile or Val residues known as the "IXI" motif near the beginning of their CTR. IXI motifs can bind in a "knob-and-hole" fashion into a groove formed between the top and bottom sheets of the ACD β-sandwich (the "β4/β8 groove", Fig. 3.1b) (Delbecq et al. 2012). Finally, the N-terminal region (NTR) is a relatively long extension (50-100 residues in vertebrates) that is presumed to be disordered based on secondary structure prediction and the lack of density in electron microscopy (EM) and X-ray crystallography-based structures of sHSPs.

Relative to typical disordered regions, the NTR is enriched in hydrophobic and aromatic residues. Short regions of order have been observed in the NTR by solid-state nuclear magnetic resonance (NMR) of HPSB5 (Jehle et al. 2011), in a crystal structure of HSPB6 in complex with a client protein (Sluchanko et al. 2017), and in a crystal structure of an HSPB2/HSPB3 heterotetramer (Clark et al. 2018). Given the lack of conservation in the NTRs among paralogs (Figure 3.1 C), whether there are similarities among the structural features of NTRs of other sHSPs remains an open question.

HSPB1 is among the most ubiquitously expressed of the ten human sHSPs. It is implicated in multiple biological roles in diverse cellular pathways, diseases, and tissues (Janowska et al. 2019). HSPB1 is phosphorylated within minutes after cells are subjected to stress (heat, oxidative stress) by stress-related kinases at three conserved serines in the NTR (Fig. 3.1a and c) (Larsen et

al. 1997). Biochemical investigations have demonstrated that phosphorylated HSPB1 and HSPB1 carrying phosphomimetic mutations form oligomers that are much smaller than the distribution formed by unmodified HSPB1 and tend to have increased holdase activity (Shashidharamurthy et al. 2005; Hayes et al. 2009; Jovcevski et al. 2015). Several inherited mutations in HSPB1 are reported to be associated with the severe neurological disorders Charcot-Marie-Tooth disease and distal hereditary motor neuropathy. Most disease-associated mutations appear to be autosomal dominant and are harbored in all three regions of the protein, with overrepresentation in the NTR and in residues near the dimer interface of the ACD (Datskevich et al. 2012; Nefedova et al. 2015). There is a striking paucity of structural information on HSPB1 beyond the ACD, for which there are now several atomic-level structures solved (Hochberg et al. 2014; Rajagopal et al. 2015a; Collier et al. 2019). Little is known about the structural mechanism for dissociation into smaller oligomers upon phosphorylation or the structural effects of disease-associated mutations.

Here, we present structural analysis of the NTR of HspB1, using a hybrid approach of NMR spectroscopy and structural modeling, which builds on prior work using NMR and hydrogen-deuterium exchange mass spectrometry (HDXMS) (Clouser 2018). Our work sheds light on the structural consequences of stress-induced phosphorylation and disease-associated mutations in HSPB1. We defined sub-regions of the NTR based in part on their HDXMS behaviors, as illustrated in Figure 3.1 C. NMR experiments using peptides containing the NTR sub-regions and spin labels placed in each region revealed that, although the NTR is predominantly disordered, there are nevertheless specific interactions between the NTR and ACD in the context of full-length HSPB1. Structural modeling demonstrates that it is possible to build physically realistic models of the NTR and ACD of HSPB1 with multiple different types of interactions. Altogether, our results show that even in a monodisperse dimeric form of HSPB1, there is

substantial conformational heterogeneity, with multiple, specific contacts between regions of the NTR and the ACD. These contacts are altered in phosphorylated and disease-associated mutated states, shedding light on the mechanisms by which perturbations such as phosphorylation and mutation can influence sHSP structure and function.

3.2 RESULTS

3.2.1 *The NTR makes extensive contact with the ACD*

The dimeric HSPB1 construct presented in Chapter 2 is amenable to study by solution NMR, enabling the first residue-level analysis of HSPB1. $HSPB1_{dimer}$ is generated by three phosphorylation-mimicking substitutions in the NTR (S15D, S78D, and S82D) and substitution of the CTR IXI motif to "GXG" (179-ITIPV-183 to GTGPG) (Figure 3.1 A). A construct in which the CTR is truncated to the same position as the end of our ACD-only construct (residue 176) is also dimeric in the phosphomimic context (termed "NTR-ACD"). The NMR spectrum of an HSPB1 construct that lacks both its NTR and CTR ("B1-ACD") and forms a well-structured dimer has been assigned (Rajagopal et al. 2015a). The simplest model for $HSPB1_{dimer}$ would be a structured ACD dimer with flexible, disordered NTRs and CTRs that behave independently of the other domains. Such a species would give rise to an NMR spectrum that would resemble that of the isolated ACD plus resonances that correspond to "random coil" positions. However, few peaks overlap perfectly in overlays of (^{15}N, ^{1}H)-HSQC spectra of B1-ACD and either $HSPB1_{dimer}$ or NTR-ACD (Fig. 3.2 A) (Clouser 2018), Therefore, the model in which the ACD behaves independently of its flanking domains is inaccurate, demanding investigation of interactions between domains. The NMR spectrum of NTR-ACD overlays well with that of full-length $HSPB1_{dimer}$ (Clouser 2018). The high spectral similarity confirms that the CTR lacking its IXI

motif does not interact detectably with the rest of the protein in the otherwise phosphomimetic context and the differences between the $HSPB1_{dimer}$ and B1-ACD spectra are due to the presence of the NTR.

The largest perturbations in ACD peaks are for residues in the β3, β4, and β8 strands and loop (L3/4), which exhibit large CSPs relative to their position in the ACD-only spectrum (Fig. 3.2 B). These structural elements compose two grooves on the ACD dimer: the β4-β8 groove on the outer edges and the β3/β3 or "dimer interface" groove at the center (Fig. 3.1 B). The large perturbations in these regions indicate that they are probable sites for interaction between the NTR and the ACD.

To investigate sources of the perturbations in ACD peaks in the NTR-ACD context, we examined NMR spectra of a mixture of ^{15}N-B1-ACD and excess unlabeled NTR-ACD. Under reducing conditions (to inhibit disulfide bond formation at the dimer interface), mixed dimers composed of one ^{15}N-B1-ACD subunit and one NTR-ACD subunit can form. This allowed us to observe perturbations in an ACD due to the NTR of its dimeric binding partner. New peaks are observed in the spectrum of the mixture that align with peaks in the NTR-ACD spectrum (Fig. 3.2 A). Peaks that exhibit this doubling behavior in the spectrum of mixed dimers nearly all correspond to residues in the β4/β8 groove and its flanking loops- predominantly the same residues whose peaks exhibit the largest CSPs compared to their position in the ACD-only spectrum (Figure 3.2 B, C). The congruence of certain peaks in the mixed-dimer spectrum with those in the NTR-ACD spectrum provides unambiguous evidence that their resonance positions arise from an interaction involving the NTR of the other subunit within a dimer. The identity of these peaks reveals that a site of interaction is the β4/β8 groove and its flanking loops. Additionally, many other peaks in the mixed-dimer spectrum lose intensity, shift, and/or change shape as compared to the B1-ACD

spectrum. Peaks that undergo such changes correspond to residues near the dimer interface, in the β3 strand and preceding residues, and at the end of the β9 strand and start of the CTR (Fig 3.2 C). Overall, the extent of perturbations observed in this mixing experiment reveals wide scale NTR-ACD contact, particularly at the dimer interface and β4-β8 grooves, and establishes that NTR/ACD interactions can occur between subunits within a dimer.

3.2.2 *Distinct regions of the NTR bind different ACD interfaces.*

To identify specific NTR regions that interact with the ACD, we subdivided the NTR sequence into six regions, referred to here as the distal region, aromatic region, conserved motif, tryptophan-rich region, insertion, and boundary region (Fig. 3.1 C). We tested the ability of peptides from each region to bind to B1-ACD by NMR. Peptides from the distal, aromatic, conserved motif, and boundary regions all caused distinct changes (either chemical shift perturbations, loss of peak intensity, or both) in the ^{15}N-HSQC of the ACD, implying specific interactions of these regions with the ACD. No perturbations were observed for the Trp-rich peptide, providing confidence that the effects observed for other peptides are specific.

We also performed paramagnetic relaxation enhancement (PRE) experiments to detect interactions between the NTR and the ACD within the context of the NTR-ACD construct. PRE from a spin label broadens resonances of residues proximal to the label. The sole native cysteine at position 137 was substituted with serine and multiple constructs were created in which a single cysteine residue was introduced at sites within the NTR to which the spin label MTSL was conjugated. Spin label positions were selected to probe each NTR region, as shown in Figure 3.1 C. Before performing NMR experiments, each Cys mutant was assessed for alterations in secondary structure (by CD) and oligomeric properties (by SEC). Only variants that retain

HSPB1$_{dimer}$-like properties were investigated further. ^{15}N and spin label were incorporated into these species and HSQC spectra of labeled dimers were collected with the active spin label and with the MSTL quenched by ascorbate. Quenched spectra were compared to the NTR-ACD spectrum to confirm that MTSL conjugation did not significantly perturb the constructs. PREs were quantified as ratios of peak intensity in the two spectra. A range of behaviors were observed, depending on the spin label position: 1) strong, discrete effects, 2) smaller but still localized effects, or 3) widespread general effects. The results from the PRE experiments agree well with the peptide-binding studies, confirming that the interactions observed in the peptide-binding studies are recapitulated in the full-length protein (as summarized in Figure 3.3). Results from individual peptides and spin-labels are described below and are provided in Figures 3.4 and 3.5.

Addition of the distal peptide (residues 1-13) to ^{15}N-B1-ACD caused distinct chemical shift perturbations (CSPs) in the ^{15}N-HSQC spectrum that map to the β4-β8 groove (Fig. 3.4 A, C). Importantly, the perturbed peaks fall on a trajectory between their positions in the spectra of B1-ACD and NTR-ACD (Fig. 3.4 A). This is strong evidence that the large perturbations observed for these peaks in the NTR-ACD spectrum (relative to B1-ACD) are due to binding of the NTR distal region to the β4-β8 groove. The peptide binding is not saturated in the NMR experiments, thereby producing smaller CSPs relative to the NTR-ACD spectrum. The results also add clarity to the ^{15}N-B1-ACD/NTR-ACD mixing experiment described above (Fig. 3.2). The peaks that appear in positions that correspond to those observed in the NTR-ACD spectrum are due to distal region binding to the β4-β8 groove of the other subunit of the dimer in a "domain swap" relationship. We cannot rule out the possibility of a similar intra-chain interaction, but if it occurs it must be essentially identical to the inter-chain one observed in the mixed dimer.

The spectrum of NTR-ACD with MTSL at position 2 has strong peak intensity loss in two distinct sequence regions that correspond to loops L7/8 and L4/5, both of which lie near one entrance to the β4-β8 groove (Fig. 3.3, 3.5 A). Other peaks in the spectrum are largely unaffected by the spin label. This remarkably discrete PRE effect from a spin label at the extreme N-terminus of HSPB1 indicates that when the region is near the ACD, it inhabits a highly localized position. Furthermore, the PREs are consistent with only one of the two possible orientations of distal region binding in the groove, namely aligned parallel to the β8 strand and antiparallel to β4 strand. This is the opposite orientation from that observed for the CTR IxI/ β4-β8 groove binding observed in a crystal structure of HSPB1-ACD (Hochberg et al. 2014, PDB 4MJH). Distal region binding to the β4-β8 groove has been observed in crystals of HSPB6 and an HSPB2/3 complex, but those sHSPs contain canonical I/V-X-I/V motifs in their NTR (Sluchanko et al. 2017; Clark et al. 2018). HSPB1 does not contain such a motif in its distal region; we propose instead that alternating hydrophobic residues in the HSPB1 segment ^{6}VPFSLL^{11} bind, supporting the idea that other hydrophobic amino acids can participate in β4-β8 binding. Our results thus identify a novel interaction and indicate that motifs from both the NTR and CTR of HSPB1 can bind in the β4-β8 groove but are oriented in opposite directions within the groove.

Peptide binding and PRE results indicate that the conserved motif binds at the ACD dimer interface groove, composed of strands β3 and β6/7 from each subunit, and that the aromatic region spans between the β4-β8 groove and the dimer interface, connecting the distal region to the conserved motif (Fig. 3.3). The aromatic peptide (residues 12-27) caused distinct chemical shift perturbations in peaks corresponding to one side of the ACD, primarily loops L3/4 and L5/6, as well as some residues in β6+7 (Fig. 3.4 B, D). This is consistent with the orientation inferred for the distal region (Fig. 3.5 A), and shows that as the NTR exits the β4-β8 groove, it contacts the

side of the ACD via loops L3/4 and L5/6. The aromatic region contains one of the three HSPB1 phosphorylation sites (Ser15), so we also tested binding by a version of the aromatic peptide containing phospho-serine at site 15. For the most part, the CSPs are absent or markedly reduced (Fig. 3.4 B, 3.6 A), indicating that phosphorylation of Ser15 may serve to release the aromatic region from the ACD. We note that both L3/4 and L5/6 are enriched in negatively-charged amino acids (D^{100}VNHFAPDE and H^{124}EERQDEHG, respectively), suggesting an electrostatic mechanism by which phosphorylation at Ser15 regulates HspB1 structure and activity.

Conserved motif binding at the ACD dimer interface is indicated by intensity loss in peaks corresponding to residues in β3, β6+7, and loop L3/4 upon addition of the conserved peptide (residues 25-37) to ^{15}N-B1-ACD (Fig. 3.4 E). A spin label at the end of the aromatic region/beginning of the conserved motif (position 26) causes subtle peak intensity loss localized to loops L3/4 and L8/9 leading out of the interface groove, as would be expected if the conserved motif is bound in the groove and the aromatic region runs along one side of the ACD between the β4-β8 groove and the dimer interface groove (Fig. 3.5 B). Conserved motif binding at the dimer interface groove has been observed in HSPB6 and in HSPB2/3 hetero-tetramer crystal structures (Sluchanko et al. 2017; Clark et al. 2018). Given the high conservation of this motif and of residues that compose the dimer interface, it is unsurprising that a similar relationship exists in HSPB1.

Although the Trp-rich peptide (residues 37-53) showed no detectable interactions with B1-ACD (Fig. 3.4 F), we were able to obtain some insights regarding its behavior. While attempting to introduce spin labels, we found the Trp-rich region to be highly sensitive to mutagenesis and were unable to probe its interactions with the NTR through PRE experiments. Cys substitutions of S43 and V55 within the NTR-ACD construct yielded species larger than dimers and not amenable to NMR. An S50C NTR-ACD construct was dimeric but conjugation of MTSL at this position

produced larger species. While the altered oligomeric propensity rendered these mutants unsuitable for PRE experiments, the ability of changes in this region to override the dimer-promoting mutations implicates it in regulating HSPB1 oligomerization.

The insertion region was probed by a spin label at position 65, near the center of the region. Intermediate intensity loss was observed in most ACD peaks, with some stronger effects in β9. The widespread but modest PREs suggest that the insert region does not make sustained contact with any specific region of the ACD but rather "hovers" over all faces of the ACD (Fig. 3.5 C). The region was omitted from peptide binding experiments due to its hydrophobicity and insolubility in aqueous buffer.

Finally, the boundary region appears to interact at the dimer interface groove, as evidenced both by peptide binding and PRE results (Fig 3.4 G; 3.5 D, E). Addition of the boundary region peptide (residues 74-91) to ^{15}N-ACD caused intensity loss and CSPs in peaks corresponding to residues near the dimer interface (Fig. 3.4 G). We were able to incorporate spin labels at two boundary region positions: residues 83 and 91 flank the predicted β2 strand (residues 86-88 in PDB 4MJH). The spin label at position 91 (S91-SL) caused distinct intensity loss in peaks from loops L5/6 and L7/8 and from residues at the beginning of β3 and end of β9 (Fig. 3.5 E). The highly localized PREs on one side of the ACD are congruent with residues 91's position four residues from the beginning of the β3 strand. In contrast, the spin label at position 83 caused wide-spread intensity loss in peaks corresponding to the dimer interface and the opposite side of the ACD (Fig 3.5 D). In this case, the ACD residues that are *not* affected by the spin-label are more informative: the data clearly show that position 83 does not approach loops L4/5, L7/8, and L9/CTR, all of which are localized to one side of the ACD dimer (the side affected by S91-SL). Together these observations provide strong evidence that the boundary region spans the dimer

interface groove in an antiparallel direction to strand β3, consistent with formation of a β2 strand. Whether this interaction is mutually exclusive with binding of the conserved motif to the dimer interface or can occur simultaneously cannot be deciphered from these experiments.

A boundary-region peptide that contains phospho-serine residues at positions 78 and 82 caused nearly identical perturbations to the non-phosphorylated peptide (Fig. 3.6 B), indicating that phosphorylation neither directly disrupts nor enhances the interaction between the boundary region and the dimer interface groove. However, the PRE results from S83-SL indicate that this region approaches residues that are perturbed by the aromatic peptide (Fig. 3.4 D), suggesting that the boundary region phosphorylation sites may be close in space to the S15 phosphorylation site, despite being over 60 residues apart in sequence.

To leverage new insights regarding local structure in the NTR and interactions with the ACD, we sought to assess how reported disease-associated mutations in the HSPB1 NTR affect NTR-ACD interactions. We chose two NTR disease mutants whose effects on oligomer size (larger than WT) and chaperone function have been previously characterized: G34R and P39L mutants in the conserved and Trp-rich regions, respectively (Muranova et al. 2015). To identify localized effects of the mutations, we performed ACD-peptide binding experiments with mutant peptides. Glycine at position 34 is conserved among orthologs and paralogs; its mutation to Arg is expected to reduce flexibility of the backbone and/or alter the region's interactions. At the start of the Trp-rich region, Pro39 is conserved among orthologs but not among paralogs. As presented above, the conserved region peptide (residues 25-37) causes peak broadening in dimer interface groove residues (i.e., β3 and β6/7) in the HSPB1 ^{15}N-B1-ACD spectrum. An otherwise identical peptide that contains the G34R substitution yields greatly reduced perturbations (Fig. 3.6 C), indicating that the large, charged Arg sidechain disrupts the ability of the conserved region to

interact with the dimer interface groove. As mentioned above, we did not detect evidence of binding for the Trp-rich region peptide to ^{15}N-ACD. We obtained similar results for a peptide that contains the P39L substitution, indicating that the mutation does not lead to a gain of binding function (Fig. 3.6 D). Altogether, the results highlight a variety of alterations that occur in the HSPB1 NTR under situations such as phosphorylation or disease mutation. While some alterations (Ser15 phosphorylation, G34R mutation) directly impact local NTR-ACD contacts, others likely have more indirect effects (Ser78 and Ser82 phosphorylation, P39L mutation), potentially through interactions with other regions of the NTR that lead to global changes in HSPB1 structure and oligomerization.

3.2.3 *Conformational heterogeneity is observed throughout the NTR*

In addition to assignments of HSQC peaks corresponding to ACD residues, Amanda Clouser was able to assign a number of peaks to residues in the Trp-rich, insertion, and boundary regions of the NTR (Clouser 2018). Assignments of NTR peaks provided information regarding proximities of NTR regions to each other from PRE experimentss (Fig. 3.5 F). The spin label at insert region residue 65 yields strong PREs across the assigned NTR peaks, validating their assignments to this region of sequence. The position 2 spin label does not yield PREs in assigned NTR residues or in weak unassigned peaks, indicating that the distal region's locations do not overlap with those of the Trp-rich or insert regions. A position 26 spin label at the beginning of the conserved region gives modest-to-strong PREs to the Trp-rich and boundary regions but weak PREs to the insert region. The position 83 spin label gave strong PREs to the boundary and insert regions, and the position 91 spin label gave moderate PREs to the same regions. Together, this provides evidence for extensive interactions between the regions of the NTR. In particular, the conserved and Trp-rich regions seem to be in close contact with each other, as are the insertion

and boundary regions. Only the distal region does not appear to make extensive contact with other parts of the NTR. The data support a model in which the NTR exists in a compact state with extensive NTR/ACD and NTR/NTR contacts as well as some residual structure, rather than a more flexible, extended conformation seen for many IDRs.

3.2.4 *Modeling inter-region interactions in HSPB1$_{dimer}$*

The results presented above indicate that the HSPB1 NTR contains distinct regions that reside in specific locations relative to the well-defined ACD dimer and that, in many cases make direct contact with the ACD. We sought to combine the information garnered from the peptide-binding, PRE, and HDX experiments into a set of structural models. Our goals for this modeling process were two-fold. First, the models aid in visualization of the NTR-ACD interactions described above. Second, the modeling process allows us to determine which combinations of NTR-ACD interactions are able to generate physically realistic structural models, and thus whether any combination of NTR-ACD interactions may not be physically possible. These structures are intended neither as a complete sampling of HSPB1 conformational space nor as atomic-level models of specific interactions.

We produced a homology model by combining the crystal structure of the HSPB1 ACD (4MJH) with peptides from the crystal structure of the HSPB2/3 hetero-tetramer in Pymol. The starting model included all of the possible NTR-ACD interactions identified above: two copies of the β2 strand, a distal motif bound in each β4/β8 groove, and a copy of the conserved motif bound in the dimer interface groove. Clashes between the HSPB1 ACD structure and the peptides from the HSPB2/3 crystal structure were eliminated, and missing loops were modeled in using PyRosetta. In total, there are four possible ways to connect the fragments in the homology model: either copy of the distal motif in the β4-β8 grooves could be connected to the conserved motif at

the dimer interface, and the conserved motif could be connected to either copy of the β2 strand (Fig. 3.7 A). In total, we created four ensembles of 100 structural models, which each sampled a different way of connecting the NTR peptide fragments in our initial homology model (Fig. 3.7 B-E). We found that it was possible to develop realistic structural models containing all types of NTR-ACD interactions identified above, as well as all possible loop connectivities. The dimer interface groove is able to accommodate two copies of the β2 strand in addition to the conserved motif, and both β4/β8 grooves are able to bind a copy of the distal motif. These peptide fragments can be connected to each other in all four conceivable ways.

If the conserved motif is connected to the distal motif oriented in the opposite direction, the aromatic region forms a loop along the side of the ACD containing loops 3/4, 5/6, and 8/9 to connect these regions (Fig. 3.7 B, C). Given our peptide-binding NMR results for the aromatic region, we believe that this configuration is favored, particularly in the non-phosphorylated state. Nevertheless, it is also physically possible for the aromatic region to connect the conserved motif to the distal region in the opposite groove, in which case it spans across the top of the ACD β-sandwich, contacting the β8, β9, and β3 strands (Fig. 3.7 D, E). While we do not observe experimental evidence for this interaction, we cannot rule it out, particularly in the phosphorylated state in which the aromatic region has low affinity for the ACD. In either case, the conserved motif can then be connected to either one of the β2 strands, while the distal motif not connected to the bound conserved motif can be connected to the other. These connections consist of ~50-75 residues and contain part of the boundary region, the insertion region, the Trp-rich region, and (for the chain with an unbound conserved motif) the conserved and aromatic regions. Given their length, they can adopt multiple conformations and orientations relative to the ACD. We have omitted these regions from the models shown in Fig. 3.7 for clarity and avoid over-interpretation of the structural

aspects of regions for which we have limited experimental data. Surface representations of these models show that the locations of the NTR sub-regions are in good agreement with the ACD surfaces perturbed in the peptide binding and PRE NMR experiments (comparing Fig. 3.3 with Fig. 3.7 G).

Overall, the results from the modeling suggest that any combination of the NTR-ACD interactions defined in our study is theoretically possible. While we only created models containing the maximum NTR-ACD interactions supported by our experimental data, any of the interacting motifs we have modeled could dissociate from the ACD and adopt a more disordered conformation. The results from our NMR and HDX experiments indicate that most of these NTR regions occupy both ACD-bound and -unbound conformations, so it is likely that multiple combinations of NTR/ACD interactions occur in solution. The peptide fragments depicted in our dimeric models could conceivably be connected to other ACD dimers or monomers within an oligomer (Fig. 3.7 F). The array of possible interactions within sHSP oligomers is depicted in Fig. 3.7 H. Many regions can form intra-chain, intra-dimer, and inter-dimer interactions. The possibility for multiple combinations of interactions and connectivities contributes to the high degree of plasticity and heterogeneity observed for HSPB1 in NMR and HDX experiments.

3.3 DISCUSSION

Despite being among the most ubiquitously expressed of the human small heat shock proteins, there is a paucity of structural information regarding HSPB1. The central ACDs of two subunits of HSPB1 adopt a dimeric β-sandwich structure ((Rajagopal et al. 2015a; Hochberg et al. 2014; Collier et al. 2019)). However, there has been a complete lack of structural information for the remaining ~50% of HSPB1, most of which is represented by the enigmatic NTR. To overcome

the challenges posed by high heterogeneity and polydispersity of large HSPB1 oligomers, we sought to obtain new structural information from a more tractable dimeric form of HSPB1 that retains its chaperone activity. Although this species, $HSPB1_{dimer}$, is monodisperse in solution, it exhibits substantial heterogeneity as judged by both NMR and HDXMS (Clouser 2018).

Our effort to generate a well-behaved dimer of HSPB1 and characterize its NTR both when tethered to its ACD and when presented as short peptides derived from NTR sub-regions was surprisingly revealing. Peptides representing sub-regions of the NTR display specific interactions with the ACD of HSPB1. Furthermore, PRE experiments revealed that the interactions have preferred orientations. In addition to the previously observed interaction of the IXI motif from the CTR with the β4/β8 groove, our results establish four distinct NTR/ACD interactions: 1) distal region with β4/β8 groove, 2) aromatic region with L3/4 and L5/6, 3) conserved region with dimer interface groove, and 4) boundary region with dimer interface groove (Fig. 7H). Altogether, this set of interactions creates a large combinatorial array of possible states within a dimer, and even more states within an oligomer. For example, each HSPB1 dimer contains two β4/β8 grooves and four interacting regions (two copies each of the distal region and the CTR IXI motif). Our data and modeling indicate that a given groove may be empty, bound by an inter-chain distal region, bound by an intra-chain distal region, or bound by a CTR IXI motif (usually from another dimer within an oligomer). A dimer may have zero, one, or two of its grooves filled, presumably with any combination of binders. The HDX results on HSPB1 oligomers indicate that a large proportion (at least half) of the distal regions and the CTRs are bound, meaning the β4/β8 grooves must be predominantly occupied (Clouser 2018). Each HSPB1 dimer has a single dimer interface groove, but its potential interactions with two NTR regions creates a similarly complicated situation: a given dimer interface groove may be empty, bound by a single boundary region, a single conserved

region, two boundary regions, one boundary plus one conserved, or two boundary regions plus a conserved region. Again, in the context of an oligomer, the combinatorial possibilities will be increased if the interactions can occur from neighboring dimer units.

While the NTR of sHSPs has long been known to be intrinsically disordered, it is clear from this work and recent crystal structures that further definition is required to characterize sHSPs NTRs. The only segment of the NTR that exhibits solvent-accessible, random coil-like structure is the insertion sub-region. In recent years, it has come to be appreciated that the term intrinsic disorder can encompass a broad variety of behaviors beyond random coil. Disordered proteins or regions that adopt compact conformations and transiently sample secondary structure have been described as molten globule-like, and disordered regions that interact with binding partners in a dynamic manner have been described as fuzzy (van der Lee et al. 2014; Dyson and Wright 2005). By definition, fuzzy protein-protein interactions cannot be described by a single conformational state (Tompa and Fuxreiter 2008). However, given the high degree of orientational specificity of many NTR-ACD interactions, these interactions cannot be described as fuzzy in the canonical sense, nor as molten globule-like. The only region of the NTR which could be said to interact with the ACD in a fuzzy manner is the insertion region, as a spin label placed in this position causes non-specific PREs in many regions of the ACD, inconsistent with a single conformational state or orientation.

Notably, ordered interactions occur for several NTR sub-regions with the ACD with varying levels of affinity, and some interactions are likely interdependent. The high degree of heterogeneity in HSPB1 dimers and oligomers is generated not by multiple random or fuzzy states but rather by the large number of possible combinations of several specific and orientationally-

defined states. For this reason, we propose the term "quasi-ordered" to describe the NTR of HSPB1, as it makes highly-specific long-lived contacts yet remains dynamic and heterogeneous.

The structural information gleaned from the approaches presented here on HSPB1 add substantially to the small but growing structural insights on human sHSPs. Knob-into-hole binding of CTR IXI motifs and β4/β8 grooves has been well established in numerous sHSPs. This type of interaction has recently been shown for NTR IXI motifs as well (Sluchanko et al. 2017; Clark et al. 2018). Recognition of non-canonical hydrophobic motifs by the β4/β8 groove has been shown previously for the client proteins amyloid-β and α-synuclein and in crystal structures of artificially-truncated sHSP constructs (Mainz et al. 2015; Liu et al. 2018; Weeks et al. 2014; Collier et al. 2019), but never within a full-length sHSP. Our results show that a motif of alternating hydrophobic residues in the HSPB1 distal region competes effectively with a canonical IxI motif in the protein's CTR, expanding the repertoire of potential binding partners.

The eight-residue conserved motif is the only stretch of identifiable sequence conservation in the NTR of human sHSPs. Recently, conserved motifs bound at the dimer interface groove have been observed in the HspB6 and HspB2/3 structures. In the HspB6 structure, the conserved sequence occupies the groove and no β2 strand is present (Sluchanko et al. 2017). In the HspB2/HspB3 structure, the conserved motif of HspB2 and one copy of a β2 strand from the same protomer occupy the groove (Clark et al. 2018). Our modeling shows that it is physically possible for two copies of β2 strand and a conserved motif to be bound simultaneously, at least for HSPB1.

An interaction analogous to the one defined for the aromatic sub-region of HSPB1 has not been previously reported. Our results indicate that the interaction is favored in the absence of Ser15 phosphorylation, which disrupts the interaction. Only two other human sHSPs are enriched in aromatic residues in this region, namely HspB4 and HSPB5. HSPB1, HSPB4, and HSPB5 are also

the only human sHSPs known to form large oligomers, leading us to speculate that the aromatic region/ACD interaction may be a driver of oligomer formation. Notably, HSPB1 and HSPB5 are both phosphorylated in response to stress conditions on serine residues within their aromatic regions. Our results show clearly that serine phosphorylation disrupts the interaction in HSPB1, hinting at a shared structural mechanism by which stress-induced phosphorylation disrupts HSPB1 and HSPB5 oligomers, allowing them to form smaller, more dispersed species (Peschek et al. 2013; Jovcevski et al. 2015).

Intriguingly, PRE results place residue 83 in the same region we observe aromatic peptide binding, indicating that the other two phosphorylation sites of HSPB1 (Ser78 and Ser82) are in proximity to the phosphorylation site in the aromatic region. A recent crystal structure of an HSPB1 construct containing part of the boundary region and the ACD in complex with a peptide containing residues 76-88 phosphorylated at position 82 contained density in this same region. While this density could be attributed to the peptide, it was unclear which residues specifically were involved (Collier et al. 2019). Our results confirm that the two phosphorylation sites in this peptide could reside near this location. Thus, all three sites of stress-induced modification are near each other and close to a conserved ACD surface that is highly enriched in negatively-charged amino acids (i.e., L3/4 and L5/6), providing an environment that can easily be disrupted by additional negative charge. It has been demonstrated that singly- and doubly-phosphorylated HSPB1 species adopt intermediate-sized oligomers, consistent with the arrangement acting as a rheostat that tunes the distribution of oligomeric states in response to cellular stress. While there is clear interplay among the three phosphorylation sites, additional work is necessary to determine the nature of the interactions between the sites in the boundary region and the aromatic region. In particular, the role of boundary region phosphorylation is unclear, as we did not see any difference

in binding by the phosphorylated and non-phosphorylated forms of this peptide. Recent NMR work showed that an elongated ACD construct containing the boundary region with phosphomimetic mutations at regions 78 and 82 formed a transient β2 strand in solution (Collier et al. 2019). However, without a direct comparison to a construct of the same length but without phosphomimetic mutations, the role of phosphorylation in this interaction remains unclear.

In sum, an approach using solution-state NMR, HDXMS, and modeling has succeeded in defining the heretofore intractable NTR of HSPB1. Rather than behaving as a completely intrinsically disordered region, we find it to be quasi-ordered, with six sub-regions that display distinct properties and preferences. The results reveal that, contrary to expectation, the high degree of heterogeneity and polydispersity that is a defining feature of HSPB1 (and other human sHSPs) derives not from fuzzy disorder but rather from an array of combinatorial interactions involving discrete sub-regions. We expect other oligomeric sHSPs are similarly defined and that they can be parsed out using approaches similar to those described here. Finally, it is reasonable to think that there are other examples of quasi-order, with multiple interacting regions in a polypeptide chain, that can likewise be defined at a structural level by these experimental approaches.

3.4 Experimental Procedures

3.4.1 *Protein expression and purification*

Human HSPB1 (accession # P04792) had previously been cloned into pET23a and pET151d vectors (ampicillin resistant). The ACD-only construct had previously been optimized to truncation of the full-length sequence from Gln80 to Ser176. Site-directed mutagenesis using the QuikChange protocol was used to introduce substitution mutations throughout the sequence.

Several protocols for protein expression were used to obtain different isotopically labeled samples. In almost all cases (unless otherwise specified) for full-length HSPB1, BL21(DE3) *E. coli* cells were used and a final concentration of 1.0 mM isopropyl β-D-1-thiogalactopyranoside (IPTG) was added to induce protein expression. For the truncated ACD-only construct, 0.5 mM IPTG was used.

For natural abundance (or non-isotopically labeled) protein, cells were grown in 0.5 L of lysogeny broth (LB) with 100 μg/mL ampicillin. Cells were grown at 37°C in a shaking incubator until OD_{600} ~0.6. IPTG was then added to a final concentration of 1.0 mM and the temperature reduced to 22°C. Protein was expressed in a shaking incubator for ~22 hours. Cells were harvested by centrifugation and resuspension in lysis buffer (50 mM Tris, pH 8.0, 100 mM NaCl, 1 mM ethylenediaminetetraacetic acid [EDTA]).

For ^{15}N-labeled (no deuteration) protein, MOPS minimal media was used. Per 1 L culture, 1 g of $^{15}NH_4Cl$ was used for isotopic labeling. 4 g/L of glucose was used. Growth and expression steps were identical to those used for natural abundance protein.

For $^{2}H^{15}N^{13}C$-labeled (partial deuteration, ~75%) protein, cells were grown in stages to acclimate the cells to deuterated minimal media. For all ^{13}C-labeling, 3 g/L of ^{13}C-glucose was used. One colony was grown in 3 mL of LB for ~5 hours and then centrifuged to pellet the cells. These cells were resuspended and grown in 50 mL of H_2O-based M9 minimal media to an OD_{600} ~0.6. Cells were again pelleted, resuspended, and grown in 100 mL of D_2O-based M9 minimal media to an OD_{600} ~0.6. Cells were then transferred directly to a larger 500mL (total) D_2O-based M9 minimal media and grown to an OD_{600} ~0.6. After induction and reduction of temperature, protein was expressed for ~48 hours.

For $^{2}H^{15}N^{13}C$-labeled (perdeuteration) protein, cells were grown in additional stages to acclimate the cells to deuterated minimal media. 3 g/L of $^{2}H^{13}C$-glucose was used. Stocks for deuterated M9 minimal media were also prepared in D_2O. One colony was grown in 3 mL of LB for ~5 hours and then centrifuged to pellet the cells. These cells were resuspended and grown in 50 mL of H_2O-based M9 minimal media to an OD_{600} ~0.6. Cells were again pelleted, resuspended, and grown in 100mL of D_2O-based M9 minimal (no deuteration) media for 1-2 hours. Cells were again pelleted, resuspended, and grown in 200mL of D_2O-based and ^{2}H-glucose-based M9 minimal media to an OD_{600} ~0.6. Cells were then transferred directly to a larger 1 L (total) D_2O-based and ^{2}H-glucose-based M9 minimal media. Cells were grown to an OD_{600} ~0.6 and induced. After induction and reduction of temperature, protein was expressed for ~48 hours.

Cells containing full-length HSPB1 were lysed by freeze-thaw and incubation with lysozyme and protease inhibitors in lysis buffer on ice for 20 minutes. Generally 0.5 L cultures of cells were lysed in one tube to maximize yield and purity. Deoxycholate was added to the lysed cells and placed on a shaking incubator at 37°C for 15 minutes. DNase, RNase, and magnesium chloride were then added and shaking incubation continued for 15 minutes. Cell lysate was centrifuged at high speed at 4°C. Ammonium sulfate was added to the supernatant to 40% saturation on a slow shaker at room temperature and allowed to equilibrate for 30 minutes. Ammonium sulfate precipitate was centrifuged at high speed at 20°C and the supernatant discarded. Pellets were used immediately or stored at -80°C for up to 1 week.

Ammonium sulfate pellets were resuspended in anion exchange buffer (AEX- 20 mM Tris, 10 mM $MgCl_2$, 30 mM NH_4Cl, pH 7.6) at room temperature. Remaining solids were pelleted briefly at 20°C. Protein was desalted using a G25 column in AEX buffer at room temperature. Precipitated material was pelleted briefly at 20°C. Desalted protein was separated by an anion

exchange DEAE column with a step gradient of AEX buffer with increasing sodium chloride at room temperature. Protein fractions were analyzed for purity by SDS-PAGE, pooled, and concentrated for SEC. Protein was separated on Superdex 200 or 75 columns in 50 mM NaPi, 100 mM NaCl, 0.5 mM EDTA, pH 7.5 buffer. Oligomeric proteins (WT, disease mutants) were separated on a Superdex 200 column, while smaller constructs ($HSPB1_{dimer}$, NTR-ACD) were separated on a Superdex 75 column. SEC separated fractions were analyzed for purity by SDS-PAGE, pooled, and concentrated to the desired concentration. Concentration was determined by 280 nm absorbance (extinction coefficient of 40,450 $M^{-1}cm^{-1}$).

For cysteine-free proteins or proteins containing only the native cysteine at position 137, no reducing agent was added during purification. With the native cysteine present, the resulting protein was generally >95% oxidized at the dimer interface as seen by dimer formation by non-reducing SDS-PAGE. For proteins containing non-native cysteines (for fluorophore or spin labeling), the reducing agent dithiothreitol (DTT) was included at each stage of purification to avoid disulfide formation.

3.4.2 *Nuclear magnetic resonance spectroscopy*

All NMR experiments were carried out on either 600 or 800 MHz Bruker spectrometers equipped with cryoprobes. All samples were prepared in 25 mM sodium phosphate, 100 mM NaCl, 0.5 mM EDTA, pH 7.4 buffer. Spectra were collected at 30°C. Data were processed using NMRPipe. NMRViewJ was used to measure intensities and positions of peaks. The following equation was used to calculate chemical shift perturbations (CSPs) between peaks in two spectra:

$$CSP = \sqrt{(\delta_H)^2 + (\delta_N/5)^2}$$

Spin-label constructs were made with a NTR-ACD/C137S background and cysteines introduced at positions throughout the NTR, one at a time. Samples were prepared in 25 mM sodium phosphate, 100 mM NaCl, 0.5 mM EDTA, pH 7.4 buffer and 5 mM DTT to fully reduce all cysteines. Reducing agent was then removed from protein samples using a desalting column. Immediately after removing reducing agent, 5-fold molar excess (1-oxyl-2,2,5,5-tetramethylpyrroline-3-methyl)-methanethiosulfonate (MTSL) spin label (in DMSO) was added to protein samples and allowed to incubate overnight at 4°C or at room temperature for 2 hours. Excess MTSL was then removed from the labeled protein using a desalting column followed by dialysis. The resulting NMR samples contained 300-400 μM protein. 2D ^{1}H-^{15}N HSQC-TROSY spectra were collected for each spin-labeled mutant protein. The unpaired spin label was then quenched in each sample by addition of ascorbate (5 mM final concentration). Identical spectra were collected for each quenched sample for intensity comparison between quenched and unquenched spectra.

The distal, aromatic, conserved, and boundary region peptides were purchased from Genscript. The N-terminal residue of all but the distal peptide was formylated, and the C-terminal residue of all peptides was amidated. The Trp-rich peptides were purchased from (LifeTein) and were acetylated on the N-terminus and amidated on the C-terminus. The distal, conserved, and boundary peptides were dissolved in NMR buffer prior to use. The aromatic and Trp-rich peptides were dissolved in DMSO to a concentration of 100 or 50 mM, then diluted in buffer to a concentration of 1 mM. All peptides were stored at -80°C. A spectrum of ^{15}N B1-ACD in the presence of 1% DMSO was collected and used as a reference for the aromatic and Trp-rich peptide experiments, although it was highly similar to the ^{15}N B1-ACD spectrum in the absence of DMSO.

3.4.3 *Modeling*

A starting homology model was produced by aligning a crystal structure of the HspB1 ACD (PDB 4MJH) with a crystal structure of an HspB2/HspB3 heterotetramer (PDB 6F2R) and creating a new PDB file with structural elements from both. It contained the HspB1 ACD, including both β2 strands, a copy of the HspB2 motif ^{157}VNEVYISLL^{164} bound in each β4/β8 groove, and a copy of the HspB2 conserved motif ^{23}RLGEQRFG^{30} bound in the dimer interface groove. Residues from the HspB2/HspB3 crystal structure were mutated to the appropriate sequence for HspB1 using Pymol. PyRosetta was used to eliminate clashes and model in missing segments. The function FastRelax was used to relax the starting homology model and eliminate clashes between chains. Fragment insertion using BlueprintBDR was then used to add the initial residues of the distal region and a segment of the 2/3 loop that was not resolved in the crystal structure. Two distinct connectivities involving the aromatic region were modeled using BlueprintBDR. One structure was generated in which the aromatic region connected the distal region bound in the opposite orientation of the conserved region, such that it wrapped around the edge of the ACD and contacted loops 3/4, 5/6 and 8/9. Another was generated in which it connected the conserved region to the other distal region and crossed over strands β8, β9, and β3. Each of these structures was then subject to 100 rounds of Generalized Kinematic Closure to generate two sets of 100 structures that sample the conformational flexibility of the aromatic region. The missing loops connecting the beginning of the NTR to the β2 strands were then modeled in using BlueprintBDR. Again, there were two possible connectivities for each structure: the conserved motif could be connected to either β2 strand, while the distal region not connected to the conserved motif could be connected to the other β2 strand. For each model, both connectivities were sampled, producing four sets with unique topologies that each contained 100

structures. For each step in which additional residues were introduced in the model, FastRelax was used to relax the new segment and the residues adjacent to it. Finally, FastRelax was used to relax all atoms in the final structures.

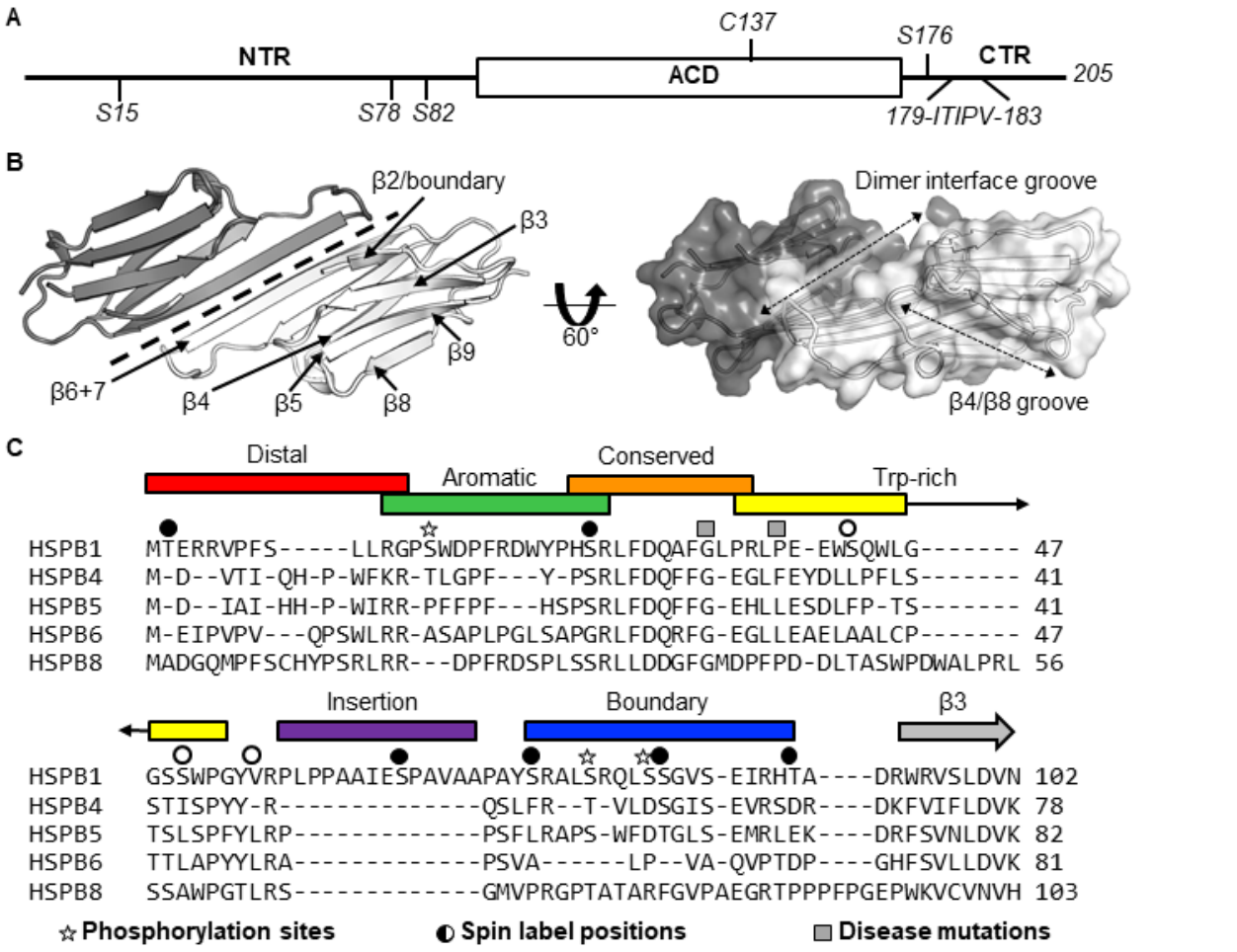

Figure 3.1. sHSP domain architecture and sequence alignment

(a) All sHSPs are defined by a conserved alpha-crystallin domain (ACD), which is flanked by N-terminal and C-terminal regions (NTR and CTR, respectively). HSPB1 contains a single cysteine, located in the ACD, which is mutated to serine in some experiments in this study. Some constructs are truncated after position 176 in the CTR or contain mutations of the IXI motif (ITIPV to GTGPG) (b) ACD homodimer structure (4MJH), with dotted line indicating axis of symmetry along which ACDs interact via beta6+7 strands. Dotted arrows in the right panel indicate the axes of the dimer interface and beta4/beta8 grooves. (c) NTR alignment of better-characterized human sHSPs shows minimal sequence conservation aside from the "conserved" region. The NTR sequence of HSPB1 is divided into 6 sub-regions for this study, which are probed in peptide form aside from the highly hydrophobic insertion region. Sites of interest in this study are indicated- Phosphorylation sites in HSPB1 are mutated to aspartate to mimic phosphorylation. Several sites tolerated mutation to cysteine for spin label attachment (filled circles), but mutation or spin label attachment at three positions in the Trp-rich region perturbed the structure (unfilled circles). Two disease-associated mutations (G34R, P39L) were examined in this study, although other NTR mutations have been reported.

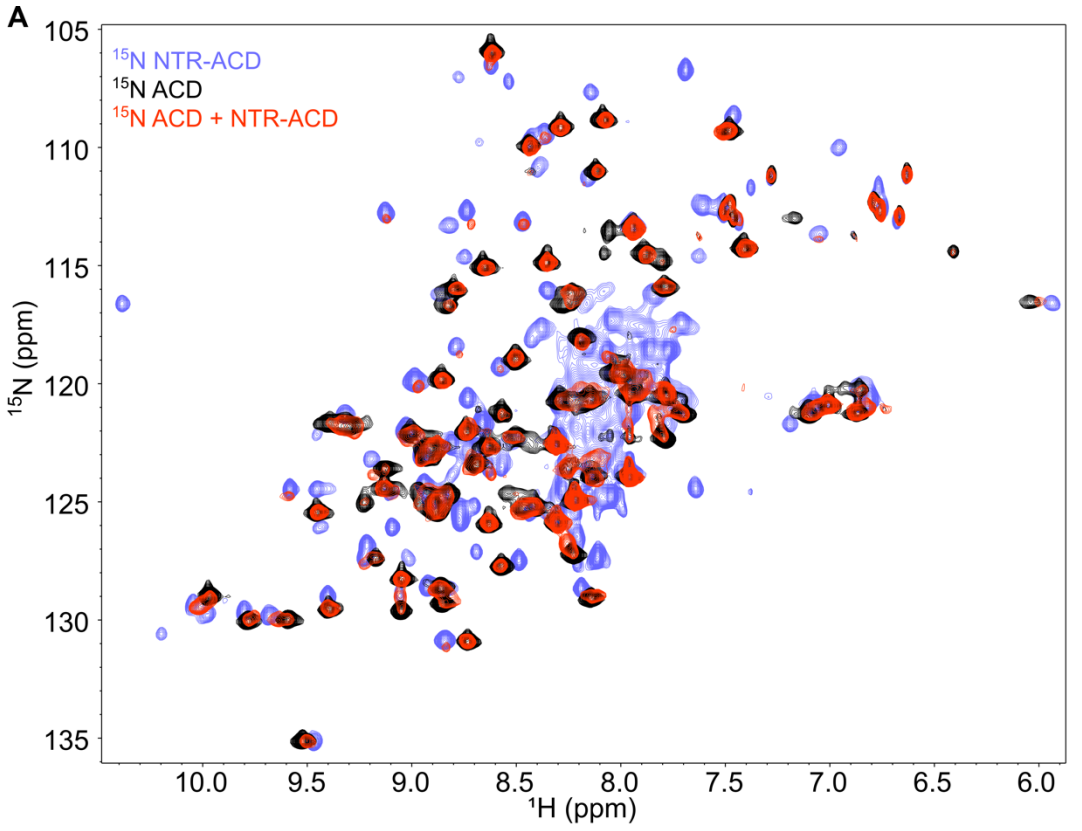
A
15N NTR-ACD
15N ACD
15N ACD + NTR-ACD
15N (ppm)
1H (ppm)
105
110
115
120
125
130
135
10.0
9.5
9.0
8.5
8.0
7.5
7.0
6.5
6.0

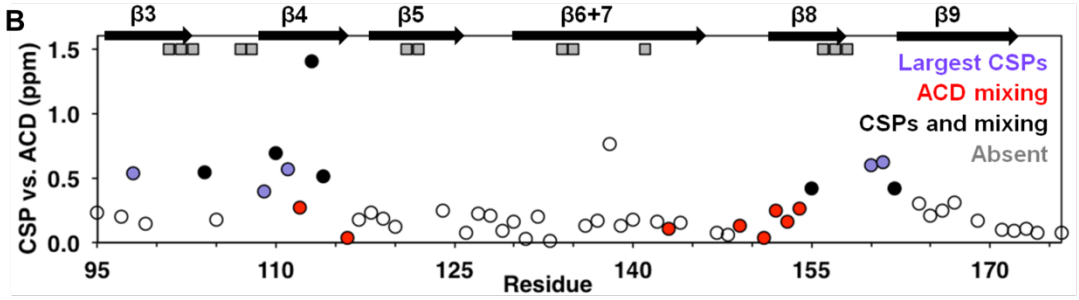
B
β3
β4
β5
β6+7
β8
β9
CSP vs. ACD (ppm)
1.5
1.0
0.5
0.0
95
110
125
140
155
170
Residue
Largest CSPs
ACD mixing
CSPs and mixing
Absent

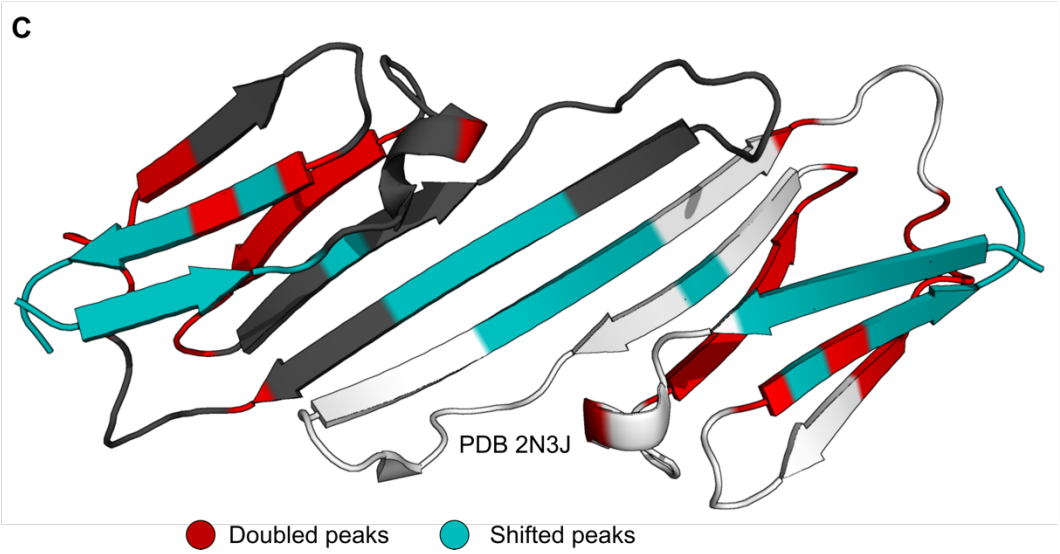
C
PDB 2N3J
Doubled peaks
Shifted peaks

Figure 3.2. NMR of NTR-ACD reveals changes in the ACD caused by the NTR

(A) Comparison of ACD (black), NTR-ACD (blue), and a mixture of 15N-labeled ACD and unlabeled NTR-ACD (red) 1H-15N HSQC-TROSY spectra. (B) CSPs measured for each residue with the following color coding- residues that are most perturbed in NTR-ACD compared to ACD (blue), show NTR-ACD-like chemical shifts in the ACD mixing experiment (red), and show effects for both cases (black). Gray squares correspond to absent residues in NTR-ACD that are presumably in substantially different chemical environments between ACD and NTR-ACD. (C) Perturbed residues in the mixed ^{15}N-B1-ACD/NTR-ACD dimer spectrum plotted onto the solution NMR structure of the ACD. Residues for which a distinct, new peak arises in the same position as the NTR-ACD spectrum are highlighted in red. These mainly cluster around the β4-β groove. Residues for which the peak is perturbed, but there is not a clear, new peak are highlighted in teal. These mostly occur in and around the dimer interface.

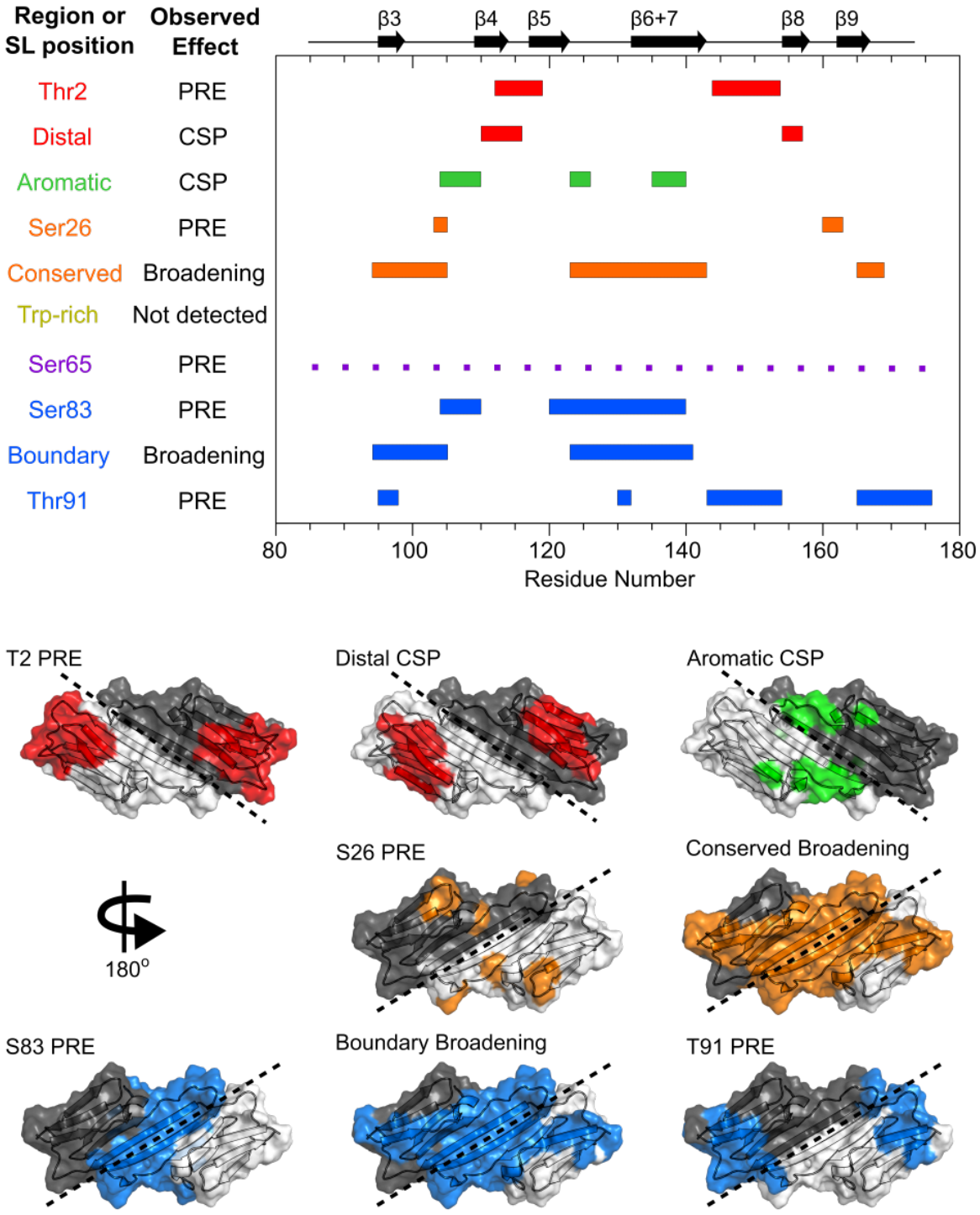

Figure 3.3. Summary of results from peptide-binding and PRE NMR experiments

Regions of the ACD that are perturbed upon peptide binding or lose intensity in the presence of a spin label are highlighted on the primary structure (top) and NMR structure (PDB 2N3J, bottom) of HspB1. The peptide from the Trp-rich region did not cause significant perturbations, and the presence of a spin label at position 65 caused widespread, nonspecific intensity loss, so these were not included in the bottom panel.

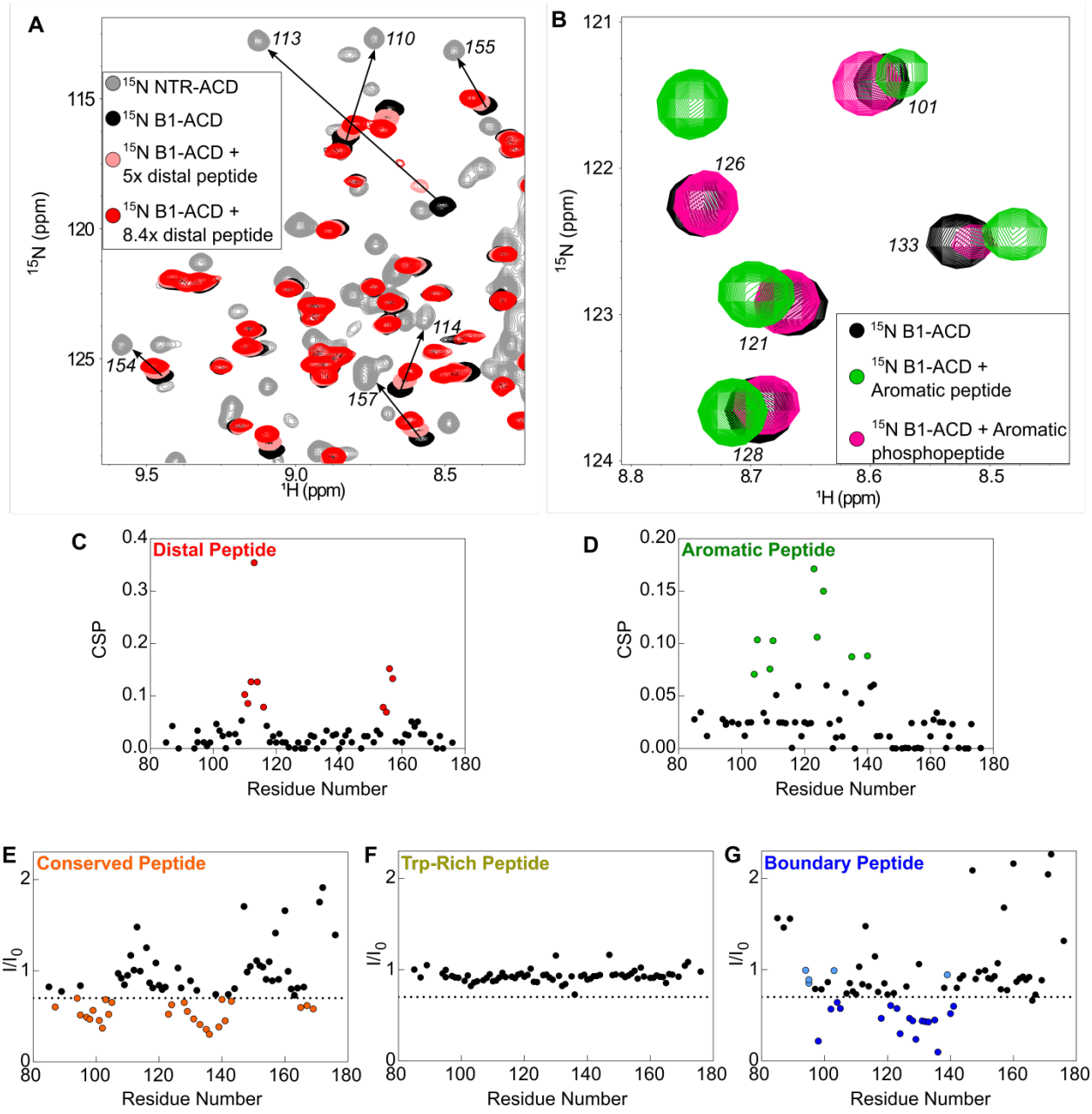

Figure 3.4. Perturbations of ^{15}N-B1-ACD due to NTR peptide binding

The distal peptide, consisting of the first 13 residues of HspB1, causes CSPs in the ^{15}N-HSQC spectrum of B1-ACD (black). The peak shifts (pink: 5 molar equivalents, red: 8.4 molar equivalents) occur along a trajectory toward the peak positions of the same residues in the ^{15}N-HSQC of NTR-ACD (grey) (A). The strongest CSPs map to residues in the β4-β8 groove (C). The aromatic peptide (residues 12-27) also causes CSPs in the spectrum of B1-ACD (green), but these are weakened when the peptide contains phosphoserine at site 15 (pink) (B). The CSPs map to residues in loops 3/4 and 5/6 and strand β6+7 (D). The conserved peptide (residues 25-37) causes intensity loss in peaks in the ^{15}N-HSQC spectrum of HspB1 ACD corresponding to strands β3, β6+7, and β9. Peaks that lose more than 30% of their original intensity are colored in orange (E). The Trp-rich peptide (residues 37-53) does not cause significant CSPs or intensity loss (F). The

boundary peptide (residues 74-91) causes both CSPs and intensity loss. Peaks that lose over 30% of their initial intensity are colored dark blue, and peaks with CSPs >0.05ppm that do not lose 30% of their initial intensity are colored light blue (G).

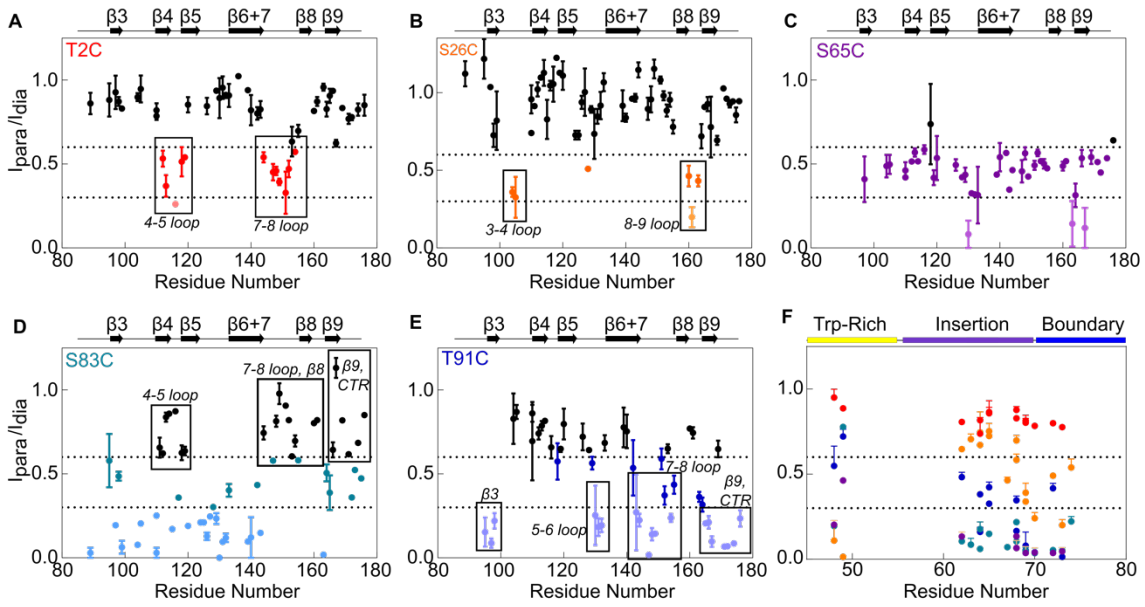

Figure 3.5. PRE NMR reveals contacts between NTR sites and ACD residues

The spin label MTSL was conjugated at five positions in the NTR of ^{15}N-NTR-ACD, and spectra were collected in the presence of the active spin label (paramagnetic) and after it had been quenched by ascorbate (diamagnetic). Error bars represent the range of two independent experiments. Panels A-E show PRE data for peaks corresponding to residues in the ACD for each of the five spin label positions. Peaks that lose more than 40% of their intensity are highlighted in color, and peaks that lose more than 70% are shown in lighter colors. Panel F shows PRE data for peaks corresponding to residues in the NTR for which assignments are available. The colors match the colors in panels A-E.

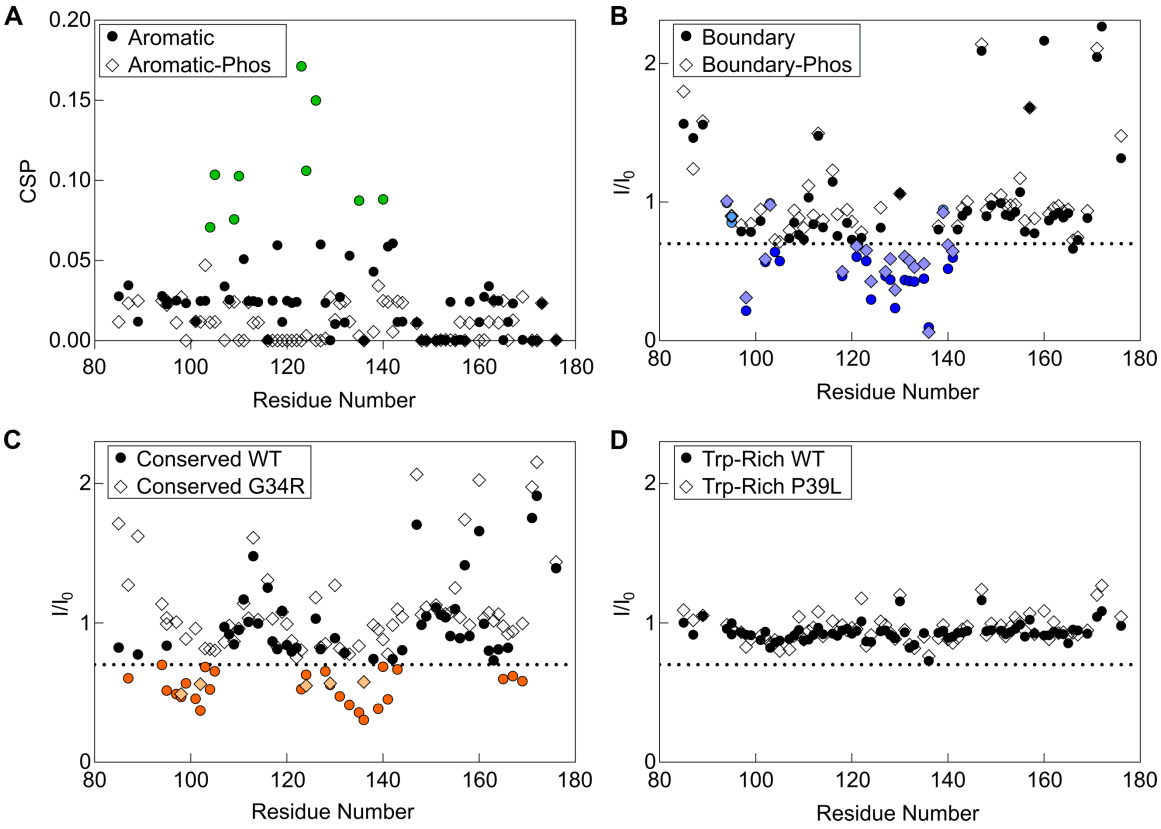

Figure 3.6. Phosphorylation and disease-associated mutations can alter peptide binding

(A) CSPs in the aromatic peptide binding experiment with ^{15}N ACD. A phosphorylated form of the aromatic peptide with phophoserine at position 15 does not cause strong CSPs (diamonds), indicating that phosphorylation disrupts binding of this peptide to the ACD.
(B) NMR intensity loss in boundary region peptide binding experiment with ACD. A peptide with phosphoserine at positions 78 and 82 caused similar perturbations to the non-phosphorylated peptide, indicating that phosphorylation does not have a direct effect on this interaction. Colored points lost >30% intensity, had CSPs over 0.5, or both.
(C) NMR intensity loss in G34R-modified conserved peptide binding experiment with ACD. "WT" conserved peptide intensity ratios are shown as circles, and G34R peptide ratios as diamonds. Affected residues below the dotted line are colored orange. Fewer residues are affected by mutant peptide binding and to a lesser extent. (D) Analogous peptide binding experiment with Trp-rich peptide and P39L-modified peptide. In both cases, no notable intensity losses occur.

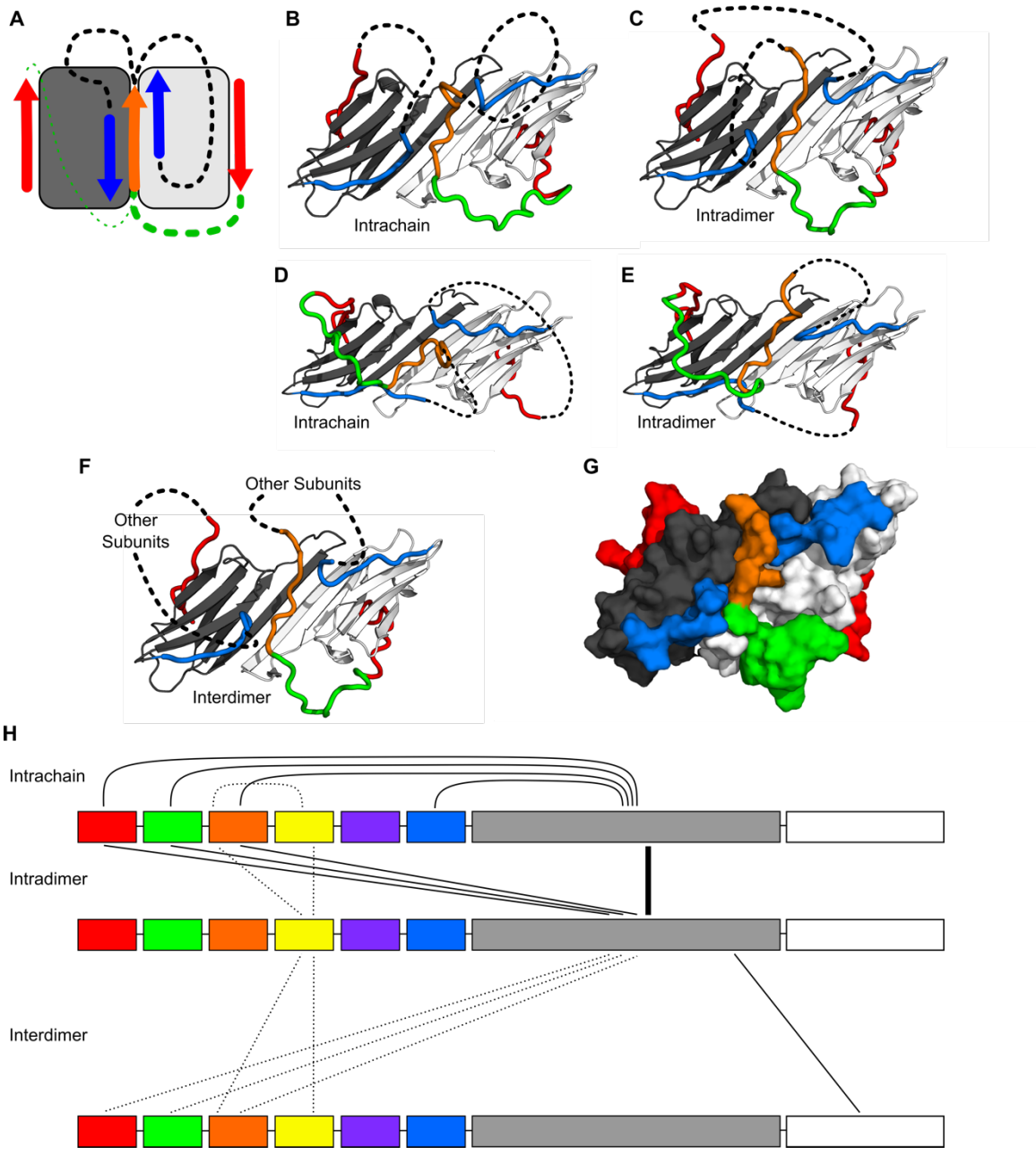

Figure 3.7. Modeling of NTR-ACD interactions reveals basis of conformational heterogeneity

A starting structure of the ACD with two copies of the distal motif (red arrows), on copy of the conserved motif (orange arrow), and two copies of β2 (blue arrows) can have the missing loops modeled with four potential connectivities (A). Either copy of the distal motif can be connected to the conserved motif (green lines), which can then be connected to either copy of β2 (black lines). Based on our NMR results, we believe it more likely that the conserved motif is connected to the distal motif oriented in the opposite direction (thicker green line), placing the aromatic region on the side of the ACD with loops 3/4 and 5/6. Representative models of the four possible

connectivities are shown in panels B, C, D, and E, with B and C being favored over D and E. Depending on how the conserved region is connected to the boundary region, contacts between the distal and aromatic regions and the ACD can occur within a single polypeptide chain (B and D) or between different chains within a dimer (C and E). It is likely that within the context of a higher-order oligomer, the contacts could occur between subunits that are not part of the same ACD dimer building block (F). A surface representation of the model in panel C shows that the regions of the NTR included in our model make extensive contact with the ACD and match the perturbed regions highlighted in Figure 3 well (G). The types of intra- and interchain contacts that are possible within HspB1 dimers and higher-order oligomers are outlined in panel (H). Solid lines represent interactions for which we have evidence from our NMR and modeling data. Dotted lines represent hypothetical interactions for which we do not have direct evidence but which we believe are likely to occur.

Chapter 4. RELEASE OF A DISORDERED DOMAIN ENHANCES HSPB1 CHAPERONE ACTIVITY TOWARD TAU

[Adapted from Baughman, Pham, Adams, Nath, and Klevit (2019) "Release of a disordered domain enhances HspB1 chaperone activity toward tau" (in preparation)]

Abstract

Small heat shock proteins (sHSPs) are a class of ATP-independent molecular chaperones that play vital roles in maintaining protein solubility and preventing aberrant protein aggregation. They form highly dynamic, polydisperse oligomeric ensembles and contain long intrinsically disordered regions. Due to experimental challenges posed by such systems, the field's understanding of the mechanisms of sHSP function is lacking. Here, we characterize interactions between the small heat shock protein HspB1 and the microtubule-associated protein tau, which has been implicated in multiple dementias including Alzheimer's disease. Using NMR spectroscopy, we show that tau is capable of binding sites within both the folded alpha crystallin domain (ACD) and the disordered N-terminal region (NTR) of HspB1. However, only interactions involving the NTR lead to productive chaperone activity, whereas ACD binding is uncorrelated with chaperone function. Furthermore, we identify mutations in HspB1 that disrupt interactions between the ACD and NTR and drastically enhance the chaperone activity of HspB1. This points to mechanisms by which sHSP chaperone activity can be increased, either by native factors within the cell or by therapeutic agents. These results shed light on the mechanisms by which sHSPs achieve their chaperone activity against amyloid-forming clients and how cells defend against pathological tau aggregation.

4.1 INTRODUCTION

Protein aggregation is implicated in numerous human diseases, including neurodegenerative disorders, diabetes, and cataract formation. Small heat shock proteins (sHSPs) are molecular chaperones that play important roles in protein homeostasis by working to prevent aberrant protein aggregation. They interact with numerous aggregation-prone client proteins in an ATP-independent manner. Humans have 10 sHSPs, which differ in their expression and tissue distribution (Janowska et al. 2019). The family is defined by the presence of an alpha-crystallin domain (ACD), which has an immunoglobulin-like β-sandwich fold and is flanked by disordered, highly variable domains termed the N-terminal region (NTR) and C-terminal region (CTR). Interactions between these domains drive the formation of polydisperse ensembles of oligomers, which can range in size from dimers to 40mers (Jovcevski et al. 2015). Subunits continually exchange between oligomers, and the distribution of oligomeric sizes is highly sensitive to conditions such as pH and stress-induced phosphorylation (Rogalla et al. 1999; Rajagopal et al. 2015b).

Due to experimental difficulties of studying highly dynamic, polydisperse, and disordered species, our understanding of sHSP structure and function lags behind our understanding of other classes of chaperones. High-resolution structures of the ACD have been determined for multiple human sHSPs by x-ray crystallography and NMR spectroscopy, but detailed structural information about the disordered domains remains lacking. Recent studies have shed light on NTR-ACD interactions using x-ray crystallography and a combination of NMR and hydrogen-deuterium exchange mass spectrometry (Sluchanko et al. 2017; Clark et al. 2018; Clouser 2018). NMR and x-ray crystallography have been used to characterize the CTR and its interactions with the ACD, and hybrid approaches have been used to develop structural models of sHSP oligomeric

architecture (Alderson et al. 2017; Hochberg et al. 2014; Braun et al. 2011; Jehle et al. 2011).While none of this structural work provides a complete, atomic-level model of a human sHSP, taken together it indicates that the NTR adapts a compact-yet-dynamic state involving extensive interactions with the ACD, while the CTR is mostly flexible in solution. One well-documented interaction between the ACD and the terminal domains involves docking of so-called IXI motifs into a hydrophobic groove on the outer edge of the ACD, termed the β4-β8 groove (Delbecq et al. 2012; Sluchanko et al. 2017; Clark et al. 2018; Hochberg et al. 2014). These motifs consist of hydrophobic residues, typically isoleucine or valine, separated by a single reside and occur in the beginning of the NTR and/or in the CTR of many human sHSPs.

Structural information regarding sHSP-client interactions is also lacking. Both the NTR and the ACD have been shown to interact directly with client proteins, but the relative contributions of these two domains seems to be highly dependent on the sHSP-client pair studied (Janowska et al. 2019). The CTR plays roles in subunit recruitment and regulation of oligomeric state (Delbecq et al. 2015), but is not known to interact directly with clients. The only client-binding site that has been mapped to the residue level is the β4-β8 groove in the ACD, although the NTR has been shown to be necessary for interactions between a number of sHSPs and specific clients. To further our structural understanding of sHSP-client interactions and the mechanisms of sHSP chaperone activity, we investigated interactions between the small heat shock protein HspB1 and the amyloid-forming client tau.

Tau is a neuronal microtubule-associated protein that forms amyloid-type aggregates in a set of neurodegenerative disorders termed tauopathies. These include Alzheimer's Disease, Frontotemporal Dementia, and Chronic Traumatic Encephalopathy. Under disease conditions, tau is found to be hyperphosphorylated, dissociated from microtubules, and deposited in β-rich

amyloid fibrils (Mandelkow and Mandelkow 2011). The morphology of these fibrils appears to vary by disease (Falcon et al. 2018b, 2018a, 2019; Fitzpatrick et al. 2017a). Fibril formation is driven primarily by two aggregation-prone motifs: ^{275}VQIINK^{280} and ^{306}VQIVYK^{311} (von Bergen et al. 2000; Von Bergen et al. 2001). The mechanism of tau toxicity is not fully understood, but it is generally believed that toxicity is primarily driven by oligomeric species that form during the process of fibril formation. Pathological tau aggregates are able to spread between neurons via a prion-like mechanism, the details of which are still being investigated (Sanders et al. 2014).

Overexpression of HspB1 has been to shown to reduce deficits in a tauopathy model mouse and reduce tau-mediated cell death in a neuronal cell line, indicating that it plays an ameliorative role in tauopathies (Abisambra et al. 2010; Shimura et al. 2004). We have previously shown that HspB1 binds the two aggregation-prone motifs in tau and delays its aggregation in vitro (Baughman et al. 2018). However, many open questions remain regarding how HspB1 achieves this chaperone activity. It has been shown that tau binds the β4-β8 groove of the ACD of HspB1, but that the ACD alone lacks chaperone activity and the NTR is necessary for chaperone function (Freilich et al. 2018). From this work, it is unclear how binding to the β4-β8 groove relates to chaperone activity, whether binding of tau to full-length HspB1 differs from binding to the truncated ACD, and how interactions between the NTR and ACD may relate to chaperone function.

We have recently characterized interactions between the NTR and ACD of HspB1 using a combination of NMR and hydrogen-deuterium exchange mass spectrometry (Clouser 2018; Chapter 3). Building on the insights we gained from that work, here we seek to structurally characterize interactions between tau and full-length HspB1. We show that tau binds to sites within both the NTR and the ACD, although only binding to the NTR is necessary for chaperone activity.

Further, we develop mutations that inhibit interactions between the β4-β8 groove and the distal region of the NTR and show that these mutations greatly enhance chaperone activity toward tau. Together, the results indicate that the NTR drives chaperone activity toward tau whereas ACD binding does not seem to play a role. Our ability to enhance HspB1 chaperone activity by altering NTR-ACD interactions suggests possible ways HspB1 activity could be enhanced in cells, which could potentially be exploited to treat tauopathies.

4.2 RESULTS

4.2.1 *The NTR and ACD of HspB1 are involved in tau binding and chaperone activity*

To further our structural understanding of how full-length HspB1 interacts with tau, we used NMR to study the binding of tau to a chaperone-active, full-length construct of HspB1, called $HspB1_{Dimer}$. This construct contains three phosphomimetic mutations in its NTR in addition to "GXG" mutations that eliminate the IPV motif in its CTR, blocking ACD-CTR interactions (Fig. 4.1A). It forms a monodisperse population of dimers in solution, thereby eliminating the heterogeneity inherent in samples containing polydisperse HspB1 oligomers. $HspB1_{Dimer}$ is small enough to study by NMR spectroscopy, and we have been able to assign resonances in the ^{15}N HSQC spectrum to most residues in the ACD and CTR of $HspB1_{Dimer}$, in addition to some regions of the NTR (Clouser 2018).

In the presence of unlabeled tau4RD, many of resonances in the spectrum of $HspB1_{Dimer}$ lose intensity. This intensity loss is widespread throughout resonances assigned to both the ACD and the NTR but not the CTR, indicating that both the NTR and ACD are perturbed upon tau binding (Fig. 4.1B, 4.2A). This intensity loss is not localized to specific regions of either domain,

but rather is widespread throughout the ACD and the regions of the NTR for which assignments are available. This indicates that the interactions between tau and HspB1 are not as simple as binding to a specific site on HspB1 but likely involve a large-scale structural rearrangement, interactions with multiple binding sites, or both. In contrast, tau binding to the isolated ACD of HspB1 has been shown to cause perturbations almost exclusively in the β4-β8 groove (Freilich et al. 2018). The discrepancy between the results obtained using the isolated ACD versus full-length $HspB1_{Dimer}$ indicates that the disordered domains of HspB1 alter the nature of its interactions with tau.

To further elucidate the roles of each of the three domains of HspB1 in its ability to bind tau and delay tau fibril formation, we systematically deleted domains from HspB1. By removing the CTR of $HspB1_{Dimer}$, we created a construct containing the ACD and the NTR with the phosphomimetic mutations, which we termed $HspB1_{NTR\text{-}ACD}$ (Fig. 4.1A). We tested its chaperone activity against tau4RD in a Thioflavin T (ThT)-monitored fibril formation assay. Tau4RD has sigmoidal aggregation kinetics, with a lag phase of approximately one hour, followed by an increase in ThT fluorescence as fibrils form and elongate, then a plateau in fluorescence after 4-5 hours. We found that $HspB1_{NTR\text{-}ACD}$ delayed tau4RD aggregation by about 2 hours, and that its chaperone activity was highly similar to that of $HspB1_{Dimer}$ (Fig. 4.1C). We also tested the ability of $HspB1_{NTR\text{-}ACD}$ to bind tau4RD by NMR. We found that $HspB1_{NTR\text{-}ACD}$ caused intensity loss in the ^{15}N-HSQC of tau4RD in peaks corresponding to the two aggregation-prone motifs in tau, ^{275}VQIINK^{280} and ^{306}VQIVYK^{311} (Fig. 4.1D, 4.2C). This intensity loss was highly similar in pattern and magnitude to the intensity loss caused by $HspB1_{Dimer}$, indicating that these two constructs bind tau in a similar manner. The similarity in binding and chaperone activity between $HspB1_{Dimer}$ and $HspB1_{NTR\text{-}ACD}$ indicates that the CTR of HspB1 bearing the GXG mutations is not

involved in tau binding or chaperone activity. This is consistent with the NMR results from $HspB1_{Dimer}$ that show no change in intensity in CTR peaks upon tau binding.

We also tested the effect of deletion of the NTR in addition to the CTR, leaving only the ACD (Fig. 4.1A). $HspB1_{ACD}$ was unable to delay tau aggregation, proving that the NTR is necessary for HspB1 chaperone activity (Fig. 4.1C). However, $HspB1_{ACD}$ retained the ability to bind the ^{275}VQIINK^{280} and ^{306}VQIVYK^{311} motifs of tau4RD in the absence of the NTR, and in fact caused greater peak intensity loss than either $HspB1_{Dimer}$ or $HspB1_{NTR\text{-}ACD}$ (Fig. 4.1D, 4.2D). $HspB1_{ACD}$ also perturbed residues at the start of the fourth microtubule-binding repeat of tau, which contains the sequence ^{337}VEVKSE^{342}. This region was not perturbed by either of the other HspB1 constructs. The greater degree and extent of peak intensity loss caused by $HspB1_{ACD}$ relative to $HspB1_{NTR\text{-}ACD}$ indicates that the binding of tau to HspB1 is strongly influenced by the presence of the NTR. Because $HspB1_{ACD}$ is lower molecular weight than $HspB1_{Dimer}$ or $HspB1_{NTR\text{-}ACD}$, the increased intensity loss can only be explained by tighter binding. This indicates that the ability to bind tau is not only insufficient for chaperone activity, but in fact the binding affinity is in no way correlated with chaperone activity. The results involving these truncation constructs are in good agreement with results obtained independently by a different group using somewhat different constructs, indicating that these surprising findings are robust and reproducible (Freilich et al. 2018).

4.2.2 *Tau interacts with regions of the both ACD and the NTR*

While the results above implicate both the NTR and the ACD in tau binding, they do not provide information on which regions of these domains are important. We sought to obtain finer-grained structural information through Paramagnetic Relaxation Enhancement (PRE) NMR experiments. Constructs of $HspB1_{NTR\text{-}ACD}$ were created in which the native cysteine was mutated

to serine, and single residues throughout the NTR and ACD were mutated to cysteine to enable conjugation of the spin label MTSL at these sites. MTSL causes intensity loss in peaks in an NMR spectrum corresponding to residues close in space to the spin label. By probing the interaction between these constructs and a construct of ^{15}N-labeled tau4RD in which both native cysteines were mutated to serine, we were able to determine the relative distances between residues in tau4RD and the spin label positions in HspB1. In total, nine spin label positions in HspB1 were tested: residues 2, 26, 65, 74, 83, 91, 151, 154, and 174 (Fig. 4.3A, 4.4A). To ensure that the mutation and MTSL conjugation did not perturb the ability to bind tau, we compared peak intensity loss in the HSQC spectrum of tau4RD due to binding of HspB1 constructs with ascorbate-quenched MTSL to intensity loss due to the binding of $HspB1_{NTR\text{-}ACD}$ without a spin label. Eight of the nine constructs caused a similar degree of broadening compared to $HspB1_{NTR\text{-}ACD}$ (Fig. 4.4B), indicating that MTSL conjugation at these positions did not alter the ability of HspB1 to bind tau. The construct S83C~MTSL caused only subtle intensity loss, indicating that the binding of tau was weakened by the presence of the mutation and spin label at this position (Fig. 4.4B). We tested whether the construct with the mutation S83C but without MTSL conjugated at that site also had perturbed tau binding and found that the mutation alone severely weakened the ability of $HspB1_{NTR\text{-}ACD}$ to bind tau4RD (Fig. 4.4C). The S83C construct was not included in further analysis; however, the ability of this mutation to disrupt HspB1/tau interactions likely indicates an important role for this region of the NTR in tau binding. Notably, Ser83 is flanked by a phosphorylation site (Ser82) and the location of a disease-associated mutation (G84R), supporting the notion that this region is important for HspB1 activity.

The presence of MTSL at position 2 had almost no effect on the ^{15}N-HSQC spectrum of tau4RD, indicating that the beginning of the NTR, which we term the distal region, does not come

into close contact with tau4RD. MTSL at positions 26, 74, 91, and 174 had an intermediate effect, while MTSL at positions 65, 151, and 154 caused the strongest PREs in the spectrum of tau4RD (Fig. 4.3B, 4.4D). This indicates that tau comes in close contact with residues in both the NTR and the ACD. Residues 151 and 154 are both near the β4-β8 groove, while residue 65 is in an insertion region of the NTR that is not conserved in other human sHSPs (Fig. 4.4A). The PREs observed for each of these constructs are similar in magnitude, although the spin label at position 65 causes somewhat more intensity loss in the ^{275}VQIINK^{280} motif while the spin labels at positions 151 and 154 cause more in the ^{306}VQIVYK^{311} motif. From the data, we cannot determine whether the insertion region of the NTR comes into close proximity of the β4-β8 groove upon binding tau, forming a single binding site, or whether tau interacts with the ACD and the NTR independently of each other.

To test whether tau binds to a single site on HspB1 or multiple sites in the NTR and ACD, we conjugated MTSL to position 65 of ^{15}N-labeled HspB1$_{NTR-ACD}$ and tested whether the presence of tau changed the intramolecular PREs observed for this construct. We have previously shown that MTSL at this position causes moderate PREs in peaks corresponding to nearly all residues in the ACD, indicating that this region of the NTR is solvent-exposed and makes transient, non-specific contact with all parts of the ACD (Fig. 4.4E) (Clouser 2018). If tau bound to a single site within HspB1 composed of the β4-β8 groove and the insertion region of the NTR, we would expect that tau binding would enhance the intramolecular PREs observed for residues in and around the β4-β8 groove. However, we do not see any significant change in the PREs for these residues in the presence of unlabeled tau4RD (Fig. 4.3C). This suggests that there are two separate binding sites in HspB1: one in the β4-β8 groove and another in the NTR. The only major change observed

was a weakening of PREs in the β9 strand in the presence of tau4RD, indicating that the insertion region of the NTR makes less contact with this strand upon tau binding.

We also tested whether binding of tau4RD changes the association of the distal region of the NTR with the β4-β8 groove. We have previously shown that the distal region of the NTR binds in the β4-β8 groove, and that MTSL at position 2 causes highly localized PREs in loops 7/8 and 4/5 (Fig. 4.4F). In the presence of tau4RD, these intramolecular PREs are weakened, indicating that tau4RD causes the distal end of the NTR to move away from the ACD (Fig. 4.3D). This is likely caused by competition between tau and this region of the NTR for binding in the β4-β8 groove. It also explains the lack of intermolecular PREs observed in the intermolecular PRE experiments when MTSL is conjugated at position 2 (Fig. 4.3B). If binding of tau and the distal region of the NTR to the β4-β8 groove is mutually exclusive, they would likely never be close in space, and PREs would not be observed. Overall, the results from these PRE experiments demonstrate that tau can bind at least two sites within HspB1, one in the NTR and one in the β4-β8 groove, and binding in the β4-β8 groove involves competition with the distal region of the NTR.

4.2.3 *Blocking interactions with the β4-β8 groove enhances chaperone activity*

To elucidate the relative contributions of the two tau binding sites in HspB1, we introduced a "groove bump" mutation in the β4-β8 groove to prevent tau from binding to that site. The groove bump mutation S135Q in HspB5 has been previously used to inhibit interactions between the β4-β8 groove and IXI motifs in its own CTR and the CTRs of other human sHSPs (Delbecq et al. 2012). We introduced the homologous mutation, S155Q, into the $HspB1_{ACD}$ and $HspB1_{Dimer}$ constructs and termed the new constructs ACD_{Bump} and $Dimer_{Bump}$. We found that tau4RD caused

CSPs in the ^{15}N HSQC of $HspB1_{ACD}$ in peaks corresponding to the β4-β8 groove, as expected, but that it did not cause CSPs in the spectrum of ACD_{Bump} (Fig. 4.5 A, 4.6). This confirms that the mutation prevents tau from binding to the β4-β8 groove. However, the construct $Dimer_{Bump}$ still causes peak intensity loss in the spectrum of ^{15}N-tau4RD and thus retains the ability to bind tau (Fig. 4.5 B). This binding is only slightly weaker than the binding of $HspB1_{Dimer}$ to tau, indicating that tau is able to bind to full-length HspB1 in a manner that is independent of the β4-β8 groove, presumably through interactions with the NTR. We then asked whether HspB1 carrying the groove bump mutation was still an effective chaperone of tau. Shockingly, we found that $Dimer_{Bump}$ not only retained its chaperone activity against tau but was actually a much more effective chaperone than $HspB1_{Dimer}$, and therefore the groove bump mutation enhances the chaperone activity of HspB1 (Fig. 4.5 C). This clearly demonstrates that although tau is able to bind to both the NTR and the β4-β8 groove, binding to the β4-β8 groove is unnecessary and may be counterproductive, whereas interactions with the NTR are vital for chaperone activity.

It has previously been reported that many chaperones, including HspB1, are less effective against tau that carries the disease-associated mutation P301L (Mok et al. 2018). We asked whether the groove bump mutation could rescue chaperone activity against tau4RD carrying this mutation. $Tau4RD_{P301L}$ has rapid aggregation kinetics and aggregates fully within 2 hours in a heparin-induced, ThT-monitored assay. $HspB1_{Dimer}$ is able to delay this aggregation slightly, but it is less potent than it is against wild-type tau4RD (Fig. 4.7). However, $Dimer_{Bump}$ is able to delay aggregation of $tau4RD_{P301L}$ to a much greater extent than $HspB1_{Dimer}$ (Fig. 4.5 D). The groove bump mutation is therefore able to rescue chaperone activity even against a tau construct that is resistant to many chaperones.

4.2.4 *Releasing the NTR from the β4-β8 groove enhances chaperone activity*

The enhanced chaperone activity of the groove bump mutant could be due to one of two causes. Binding of tau to the β4-β8 groove could disfavor interactions with the NTR by competing with it for the pool of available tau, decreasing the likelihood of productive interactions that lead to chaperone activity. Alternately, the groove bump mutation could affect binding of the NTR to the β4-β8 groove in a manner that enhances the chaperone activity of the NTR. We have previously shown that a peptide consisting of the first 13 residues of HspB1 binds in the β4-β8 groove (Chapter 3). The groove bump mutation is able to block binding of this peptide into the β4-β8 groove of $HspB1_{ACD}$, in a manner similar to the way it blocks tau binding (Fig. 4.8). While these experiments were performed with the peptide added *in trans*, the groove bump mutation likely has the same effect *in cis*, blocking interactions between the β4-β8 groove and the distal NTR within $HspB1_{Dimer}$. We used CD spectroscopy to study whether the bump mutation alters the secondary structure of $HspB1_{Dimer}$ and found that $HspB1_{Dimer}$ and $Dimer_{Bump}$ have very different CD signatures, indicating that the groove bump mutation alters the secondary structure of the protein (Fig. 4.9 D). $HspB1_{Dimer}$ has a characteristic positive peak around 230 nm that is present of in the spectra of phosphorylated HspB1 and HspB1 constructs containing phosphomimetic mutations. $Dimer_{Bump}$ lacks this peak despite containing the three phosphomimetic mutations and has a CD spectrum more similar to wild-type HspB1. We also analyzed the oligomeric propensity of $Dimer_{Bump}$ by SEC-MALS and found that it eluted slightly earlier than $HspB1_{Dimer}$ and formed a population of oligomers larger than dimers, with an average molecular weight around 80 kDa (Fig. 4.9 A). This is consistent with a polydisperse population of oligomers predominantly composed of dimers and tetramers.

We attempted to recapitulate the structural effects of the groove bump mutation by introducing a mutation in the distal region of the NTR that would disrupt interactions between this motif and the β4-β8 groove in a similar manner to the groove bump mutation. We had previously hypothesized that the residue Phe8 was a part of the hydrophobic motif recognized by the groove, so we mutated this residue to a glycine. We found that the construct $Dimer_{F8G}$ was structurally similar to $Dimer_{Bump}$. It had a highly similar CD spectrum and SEC-MALS profile, indicating that the secondary structure and oligomeric propensities of these constructs were similar (Fig. 4.9). This provides strong support that the F8G mutation disrupts distal NTR/β4-β8 groove interactions in a manner similar to the groove bump mutation. However, this mutant has an accessible β4-β8 groove that remains able to bind tau. If the enhanced chaperone activity of the groove bump mutant is due to the release of the distal NTR motif from the β4-β8 groove, we would expect the F8G mutation to also increase chaperone activity. However, if the enhanced activity is due to decreased binding to the β4-β8 groove, we would expect its activity to be the same or diminished, as releasing the NTR from the β4-β8 groove would decrease competition with tau for this groove.

The F8G mutation greatly enhanced the chaperone activity of $HspB1_{Dimer}$, providing strong support for the hypothesis that releasing the distal NTR from the β4-β8 groove enhances chaperone activity toward tau (Fig. 4.10 A). The $Dimer_{F8G}$ mutant also bound much more tightly to tau4RD than $HspB1_{Dimer}$, as monitored by NMR. It caused peaks corresponding to the motifs ^{275}VQIINK^{280} and ^{306}VQIVYK^{311} in tau to disappear from the ^{15}N-HSQC spectrum, in addition to widespread intensity loss in other regions, predominantly at the start of the fourth microtubule-binding repeat (Fig. 4.10 B). This is reminiscent of the intensity loss in this region caused by $HspB1_{ACD}$. It suggests that tau4RD is able to bind the β4-β8 groove in a manner similar to the way it binds the isolated ACD, without competition from the NTR for this groove. However, the intensity loss is

even more widespread than that caused by $HspB1_{ACD}$, likely due to interactions with the released NTR in addition to the β4-β8 groove. Together with the groove bump mutation results, this indicates that HspB1 chaperone activity toward tau is independent of binding to the β4-β8 groove, but strongly dependent on interactions with the NTR.

4.3 Discussion

Overall, the results presented here provide strong evidence that HspB1 achieves its chaperone activity toward tau through transient interactions involving its disordered NTR. Our group and others have noted that the NTR is necessary for chaperone activity, and we were able to identify a direct interaction between tau and the insertion region of the NTR through PRE NMR experiments. HspB1 chaperone activity is enhanced by mutations that release the distal region of the NTR from the β4-β8 groove, suggesting that increased flexibility of this domain results in improved chaperone activity. In contrast, although tau can bind to the β4-β8 groove of the ACD, this binding is independent of HspB1 chaperone activity. The ACD lacks chaperone activity in the absence of the NTR, and the activity of full-length HspB1 can be enhanced by mutations that either diminish or increase the accessibility of the β4-β8 groove.

We have identified at least two regions of the NTR that may be directly involved in binding tau. Our work did not exhaustively sample all regions of the NTR of HspB1. We have previously noted that some regions, particularly the Tryptophan-rich region involving residues 40-55, are sensitive to mutations that enable MTSL conjugation (Chapter 3), so we could not probe interactions between these regions and tau. Therefore, it is possible that additional residues within the NTR play important roles that we were unable to detect. Our PRE results indicate that residue

65 makes close contact with tau4RD. This residue is in an insertion region unique to HspB1, which is not present in other human sHSPs and has been shown to alter oligomeric propensity (Mchaourab et al. 2012; Mishra et al. 2018). The non-conserved nature of this region may indicate that other human sHSPs interact with tau in a manner that is different from HspB1 (Fig. 4.4 A). The only other human sHSP that has been shown to interact with tau is HspB5. In contrast to HspB1, the ACD of HspB5 had chaperone activity in isolation, indicating that the interactions are likely different in nature (Liu et al. 2018).

We also found that the mutation S83C in HspB1 greatly diminished its ability to bind tau, indicating that this residue plays a vital role in the interaction. The adjacent residue, Ser82, undergoes reversible phosphorylation in response to stress. Given the proximity of these residues, one would imagine that interactions with tau may be regulated by phosphorylation. However, previous work from our group and others has found only subtle differences in chaperone activity toward tau between wild-type HspB1 and HspB1 containing three phosphomimetic mutations (Baughman et al. 2018; Freilich et al. 2018). Nevertheless, it is possible that phosphorylation of HspB1 could play an important role under different experimental conditions, especially under more native-like conditions in cells.

The NTR positions we found to be involved in tau binding are separated from the distal region of the NTR by over 50 residues and have not been shown to interact with the β4-β8 groove. Assuming that these interactions are driving chaperone activity, it is intriguing that release of the distal region from the β4-β8 groove is able to enhance the chaperone activity so dramatically. It indicates that changes in the flexibility of the distal region are able to propagate through other regions of the NTR. Binding of the distal region to the β4-β8 groove may constrain the conformational states accessible to the rest of the NTR. The mutations that cause the release of the

distal NTR also alter the CD spectrum of HspB1, suggesting widespread conformational changes and supporting the idea that changes in the distal region can influence other regions of the protein. These results highlight the importance of interplay between the domains of HspB1 in the regulation of local structure and client interactions.

The β4-β8 groove is an important hub for protein-protein interactions in human sHSPs. It has long been known to bind motifs with alternating isoleucine and valine residues (IXI motifs) in the CTRs of sHSPs, and recent work has shown that it can also bind similar motifs in the NTRs of some sHSPs. It is the only well-documented binding site for aggregation-prone clients in human sHSPs. Many recent studies have shown that, in addition to canonical IXI motifs, other non-canonical hydrophobic motifs also can bind (Mainz et al. 2015; Liu et al. 2018; Weeks et al. 2014; Collier et al. 2019). While the β4-β8 groove has some specificity and cannot bind any arbitrary hydrophobic sequence, it is clear that it can tolerate multiple hydrophobic residues in the two pockets within the groove. In HspB1, the β4-β8 groove has been shown to bind the co-chaperone Bag3, an IPV motif in the CTR, and the distal motif in the NTR (Rauch et al. 2017; Hochberg et al. 2014). Given the prevalence of potential interaction motifs in the proteome, it is highly likely that additional interaction partners will be discovered. Therefore, any interactions with the β4-β8 groove likely involve competition between multiple binding partners. Based on the results with our activated mutants, the presence of a binding partner that competes with the NTR for the groove would be predicted to enhance chaperone activity by favoring the release of the NTR (Fig. 4.10 C). Binding to the β4-β8 groove could potentially be a mechanism by which co-chaperones enhance HspB1 activity under conditions of stress. It could also potentially be exploited by a therapeutic agent in the treatment of tauopathies.

Tau is the only client of HspB1 for which a binding site has been mapped at the residue level. However, tau and two other amyloid-forming client proteins, α-synuclein and amyloid-β, have all been shown to bind the β4-β8 groove of HspB5 (Liu et al. 2018; Mainz et al. 2015). While our results clearly demonstrate that binding of tau to the β4-β8 groove of HspB1 is non-functional, this may not be generally true of all sHSP-client interactions. Unlike HspB1, the truncated ACD of HspB5 was able to chaperone all three amyloid-forming clients, suggesting a difference in the mechanism of chaperone activity between these sHSPs. Nevertheless, incorporation of the groove bump mutation in HspB5 still enhanced its chaperone activity toward amyloid-β (Mainz et al. 2015). This result is inconsistent with a simple model in which chaperone activity of HspB5 is solely due to binding of client to the β4-β8 groove. Based on our findings regarding the mechanism of the groove bump mutation in enhancing HspB1 chaperone activity toward tau, we believe it is likely that release of the HspB5 NTR by this mutation is what enhances its activity toward amyloid-β, suggesting that both the NTR and ACD play roles, even if the ACD alone is sufficient for chaperone activity.

In general, the chaperone activity of all human sHSPs likely involves complex interplay between domains, particularly the NTR and ACD. Binding experiments with the isolated ACD tend to give clean results that are easier to interpret than experiments with the full-length proteins (see Fig. 4.5A vs. 4.1B). Given the experimental tractability of isolated ACDs and the complications inherent in structurally characterizing heterogeneous, partially disordered full-length sHSPs, it is no coincidence that the only well-documented binding site for aggregation-prone clients is the β4-β8 groove. The results presented here should serve as a cautionary tale that, although easily detectable, β4-β8 groove binding may be a red herring on the path toward discovering the mechanism of sHSP function. Recent work from our group and others has

documented extensive interactions between the NTR and ACD, such that the activity of either domain in isolation is unlikely to fully capture the nature of sHSP chaperone activity.

Our findings clearly indicate that chaperone activity of HspB1 cannot be explained by the simple binding of tau to the chaperone. In fact, there does not seem to be any correlation between binding affinity and chaperone activity. Our group and others have shown that wild-type HspB1 has chaperone activity toward tau, but binding is undetectable by NMR, whereas the isolated ACD lacks chaperone activity but causes significant intensity loss in the tau4RD NMR spectrum. Rather than acting through a sponge-like mechanism, in which HspB1 binds available tau and prevents aggregation by removing it from solution, it seems that chaperone activity is driven by highly transient interactions between the two proteins. We have been able to identify regions of the NTR that interact with tau and have shown that chaperone activity is enhanced upon release of the distal region of the NTR. However, many important details of this interaction remain to be elucidated. Future studies are needed to determine the nature of these transient interactions and mechanism by which greater NTR flexibility translates into enhanced chaperone activity.

4.4 Materials and Methods

4.4.1 *Protein Expression and Purification*

Tau4RD, $HspB1_{Dimer}$, $HspB1_{NTR\text{-}ACD}$, and $HspB1_{ACD}$ constructs were expressed and purified as described previously (Baughman et al. 2018; Clouser and Klevit 2017; Rajagopal et al. 2015a). $Dimer_{F8G}$ was found to be highly susceptible to proteolysis, so it was expressed at 16°C instead of 22°C and all chromatography steps were performed at 4°C in the presence of protease inhibitors. Additionally, a second anion exchange step was added following elution from the DEAE column. Sample was loaded onto a 5 mL HiTrap Q HP column (GE Healthcare) equilibrated in buffer

containing 20 mM Tris, 30 mM ammonium chloride, and 10 mM magnesium chloride at pH 7.6 and eluted over a 70 mL gradient into the same buffer containing 200 mM NaCl. Sample was then concentrated using a 10,000 MWCO Amicon Ultra Centrifugal Filter prior to size exclusion chromatography. All proteins were quantified by measuring absorbance at 280 nm using a Take3 Micro-Volume Plate on a Biotek Synergy HTX multimode plate reader.

4.4.2 *NMR Spectroscopy*

NMR experiments were performed in buffer containing 25 mM sodium phosphate, 100 mM sodium chloride, and 0.5 mM EDTA at pH 7.4. PRE experiments were conducted in the absence of reducing agent, but all other samples contained 2 mM DTT. All spectra of tau4RD and $HspB1_{NTR\text{-}ACD}$ constructs were collected on a Bruker Avance III 800 MHz magnet equipped with a cryoprobe. Tau4RD spectra all were collected at 10 degrees C, and $HspB1_{NTR\text{-}ACD}$ spectra were collected at 30 degrees C. All spectra of $HspB1_{ACD}$ and $HspB1_{Dimer}$ were collected on a Bruker Avance II 600 MHz magnet equipped with a cryoprobe at 30 degrees C. Previously reported assignments were used for all constructs (Baughman, Clouser, Rajagopal). Data were processed using NMRPipe and analyzed with NMRViewJ.

4.4.3 *PRE Experiments*

Prior to labeling with MTSL, $HspB1_{NTR\text{-}ACD}$ cysteine mutant constructs were incubated in the presence of 2 mM DTT at room temperature for 1 hour. The samples were then run over a 5 mL HiTrap Desalting column (GE Healthcare) equilibrated in NMR buffer (25 mM NaPi, 100 mM NaCl, 0.5 mM EDTA, pH 7.4) to remove the DTT, and 5 molar equivalents MTSL dissolved in DMSO were added to the protein fractions immediately following elution. Samples were incubated at room temperature for 3 hours, then run over the 5 mL HiTrap Desalting column to remove

excess MTSL. Fractions were concentrated to under 400 μL using 10,000 MWCO Amicon Ultra Centrifugal Filters, then dialyzed against 500 mL NMR buffer at 4 degrees C for at least 4 hours to remove remaining MTSL. Samples equilibrated at room temperature for at least an hour before spectra were acquired in the presence of the paramagnetic spin label. Samples were then quenched by the addition of 5 μL 500 mM sodium ascorbate to a final ascorbate concentration of 5 mM. Spectra were collected on the diamagnetic samples within 24 hours of collection of the paramagnetic spectra. PREs were quantified by dividing the intensity of peaks in the paramagnetic spectra by intensity of peaks the diamagnetic spectra.

4.4.4 *Fibril Formation Assays*

Tau4RD fibril formation assays were conducted in a 96-well plate format using a Biotek Synergy HTX multimode plate reader, as described previously (Baughman et al. 2018). Each well contained 200 μL sample with 3.5 μM tau4RD, 6 μM heparin (MP Biomedicals, average molecular mass 3 kDa), 75 μM Thioflavin T (Acros Organics), and varying concentrations of HspB1 in buffer containing 30 mM NaPi, 20 mM NaCl, 5 mM DTT, and 0.5 mM EDTA at pH 7.4. Plates were incubated at 37 degrees C and shaken linearly at 1096 cpm for 1 min every 2.5 min. Fluorescence measurements were taken immediately after shaking using 440- and 485- nm filters for excitation and emission, respectively.

4.4.5 *CD Spectroscopy*

CD spectra of HspB1 constructs were collected on a Jasco J-1500 CD spectrometer. Each sample contained 7.5 μM protein in buffer containing 25 mM sodium phosphate, 50 mM sodium chloride, and 0.5 mM EDTA at pH 7.4. Samples equilibrated at least 2 hours at room

temperature prior to measurement. Measurements were recorded from 260 to 195 nm, and data represent the average of 10 scans.

4.4.6 *SEC-MALS*

Samples containing 50 μM HspB1 were prepared in buffer containing 25 mM sodium phosphate, 100 mM sodium chloride, and 0.5 mM EDTA at pH 7.4 and allowed to equilibrate at room temperature for at least two hours. 100 uL of each sample was injected on a Sepax SRT-C SEC 500 column attached to an Agilent Technologies 1260 Infinity II HPLC coupled to a Wyatt miniDAWN TREOS and Optilab T-rEX differential refractive index detector. Analysis was performed using Wyatt ASTRA VI software. Bovine serum albumin (1 mg/mL) was run before the first sample and after the last and was used to calibrate the curves.

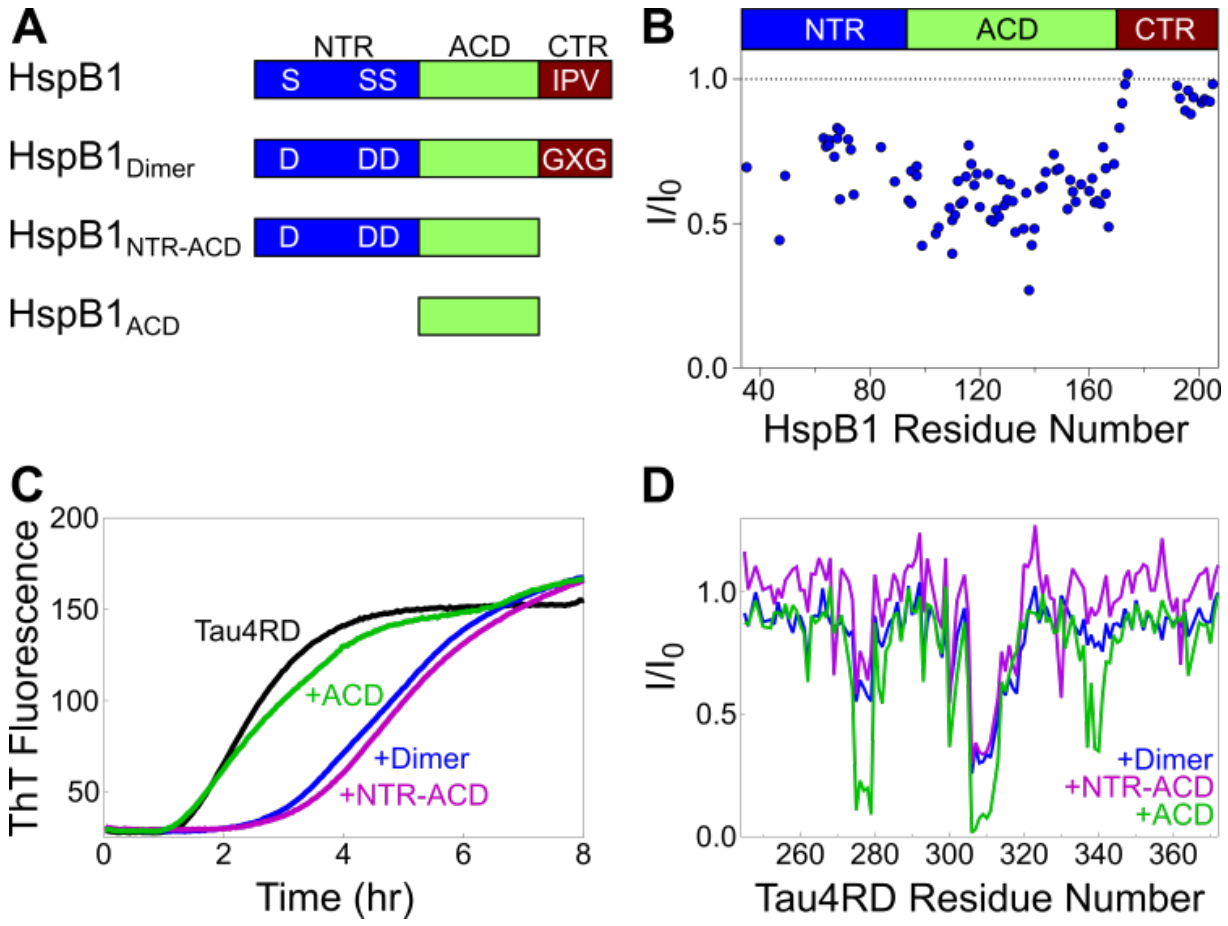

Figure 4.1. The NTR and ACD are implicated in tau binding & chaperone activity

A. HspB1 constructs used in this work. $HspB1_{Dimer}$ was created by mutating the three serine phosphorylation sites in the NTR to aspartate to mimic phosphorylation and mutating the CTR motif ^{179}ITIPV^{183} to GTGPG to inhibit interactions between this motif and the β4-β8 groove of the ACD. $HspB1_{NTR\text{-}ACD}$ consists of the NTR bearing the phosphomimetic mutations as well as the ACD. $HspB1_{ACD}$ lacks both the NTR and CTR.

B. Intensity loss in ^{15}N HSQC spectrum of $HspB1_{Dimer}$ (300 μM) due to binding of tau4RD (300 μM). Tau4RD causes intensity loss in peaks corresponding to residues in both the NTR and ACD, but not the CTR.

C. Heparin-induced tau4RD fibril formation assay monitored by ThT. Tau4RD (3.5 μM) aggregates within six hours, with a lag phase of approximately 1 hour. Addition of 1 molar equivalent $HspB1_{Dimer}$ (blue) or $HspB1_{NTR\text{-}ACD}$ (purple) causes a delay in aggregation of about 2 hours. Addition of $HspB1_{ACD}$ (green) does not alter the aggregation kinetics of tau4RD.

D. Intensity loss in ^{15}N HSQC spectrum of tau4RD (100 μM) due to binding of HspB1 constructs (200 μM). $HspB1_{Dimer}$ (blue) and $HspB1_{NTR\text{-}ACD}$ (purple) both caused similar changes, with peaks corresponding the aggregation prone motifs ^{275}VQIINK^{280} and ^{306}VQIVYK^{311} losing intensity. $HspB1_{ACD}$ caused a greater degree of intensity loss, with peaks corresponding to the motifs ^{275}VQIINK^{280} and ^{306}VQIVYK^{311} losing nearly all their intensity, while peaks corresponding to the region ^{337}VEVKSE^{342} also lost intensity.

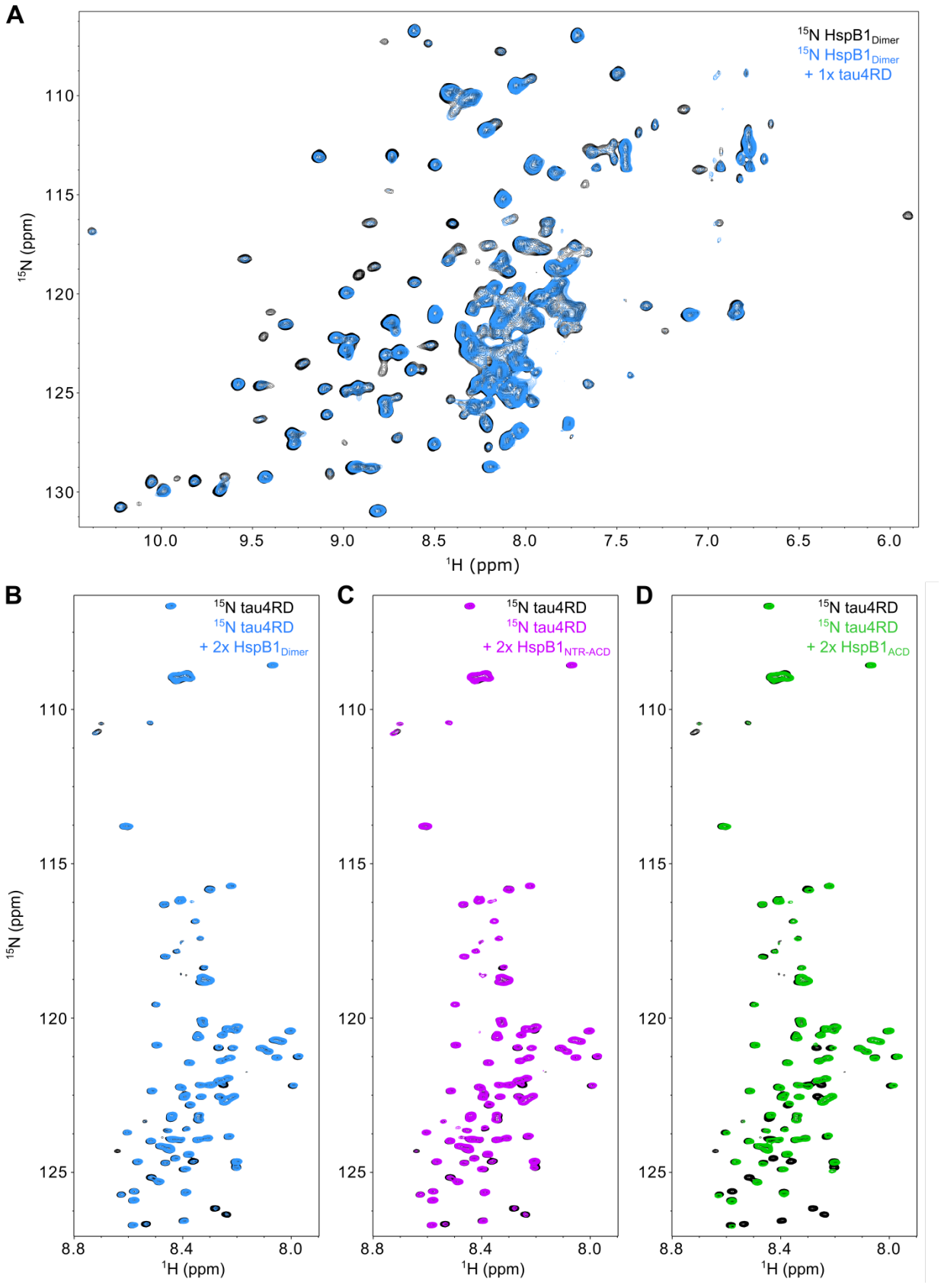
A
^{15}N HspB1$_{Dimer}$
^{15}N HspB1$_{Dimer}$
+ 1x tau4RD
^{15}N (ppm)
^{1}H (ppm)
B
^{15}N tau4RD
^{15}N tau4RD
+ 2x HspB1$_{Dimer}$
C
^{15}N tau4RD
^{15}N tau4RD
+ 2x HspB1$_{NTR-ACD}$
D
^{15}N tau4RD
^{15}N tau4RD
+ 2x HspB1$_{ACD}$

Figure 4.2. NMR spectra of tau/HspB1 complexes

A. ^{15}N HSQC spectrum of 300 μM $HspB1_{Dimer}$ alone (black) and in the presence of 1 molar equivalent tau4RD (blue).
B. ^{15}N HSQC spectrum of 100 μM tau4RD alone (black) and in the presence of 2 molar equivalents $HspB1_{Dimer}$ (blue).
C. ^{15}N HSQC spectrum of 100 μM tau4RD alone (black) and in the presence of 2 molar equivalents $HspB1_{NTR\text{-}ACD}$ (purple).
D. ^{15}N HSQC spectrum of 100 μM tau4RD alone (black) and in the presence of 2 molar equivalents $HspB1_{ACD}$ (green).

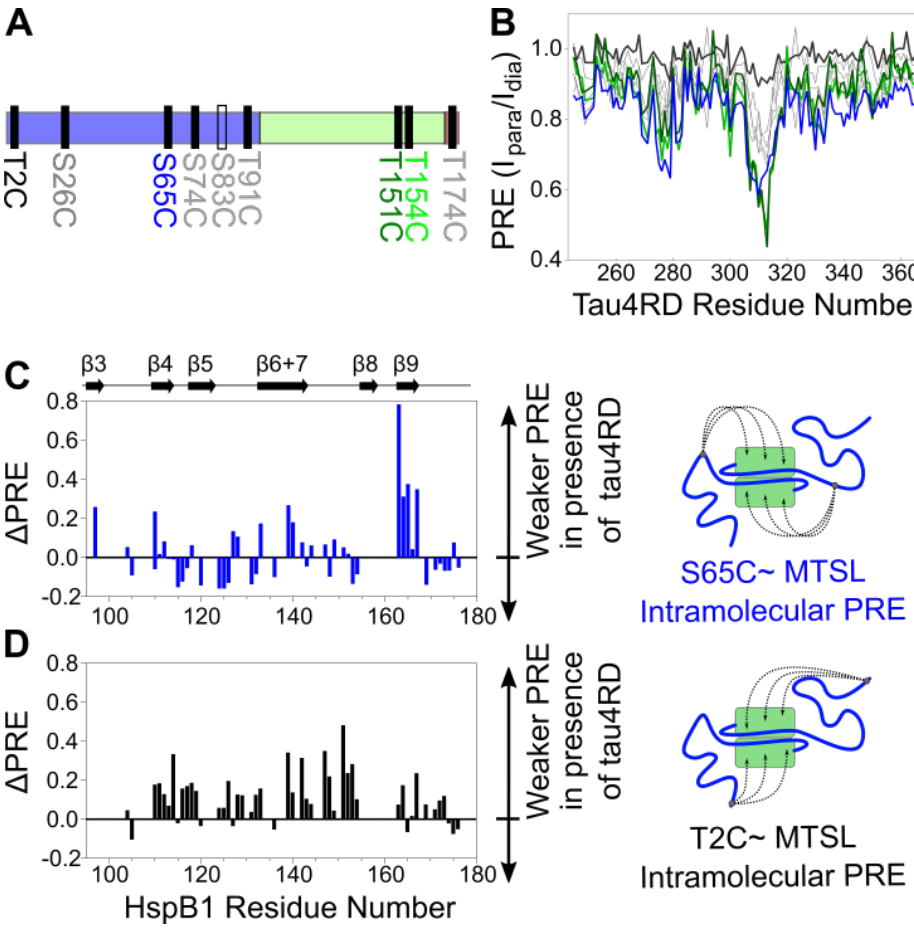

Figure 4.3. Tau4RD interacts with binding sites in both the NTR and the ACD

A. HspB1 constructs used in PRE experiments. Spin label positions were chosen throughout the NTR, near the β8 strand, and at the beginning of the CTR. The mutation at position 83 perturbed binding between tau and HspB1 and was not included in further analysis.
B. Intermolecular PRE data. The constructs with MTSL at positions 65 (blue) 151 (dark green) and 154 (light green) caused significant intensity loss in peaks corresponding to the motifs ^{275}VQIINK^{280} and ^{306}VQIVYK^{311} in the ^{15}N HSQC of tau4RD relative to the spectrum in the which MTSL had been quenched with ascorbate. This indicates that residues 65, 151, and 154 are close in space to these motifs in tau. Constructs with MTSL at positions 26, 74, 91, and 174 caused intermediate intensity loss in these regions. The construct with MTSL at position 2 did not cause intensity loss, indicating that residue 2 does not come in close proximity to tau4RD.
C. Changes in intramolecular PREs upon tau4RD binding with MTSL at position 65. Positive values indicate that PREs in the presence of tau are weaker than in unbound HspB1, meaning that tau binding causes residue 65 to move away from that residue in space. Negative values indicate that tau binding causes residue 65 to move closer to the residue in question. Tau binding caused residue 65 to move away from residues in strand β9 (residues 163-167) but otherwise did not cause major perturbations.
D. Changes in intramolecular PREs upon tau4RD binding with MTSL at position 2. Overall, PREs are weaker in the presence of tau4RD, indicating that tau4RD binding causes residue 2 to move away from the ACD, likely through competition for binding the β4-β8 groove.

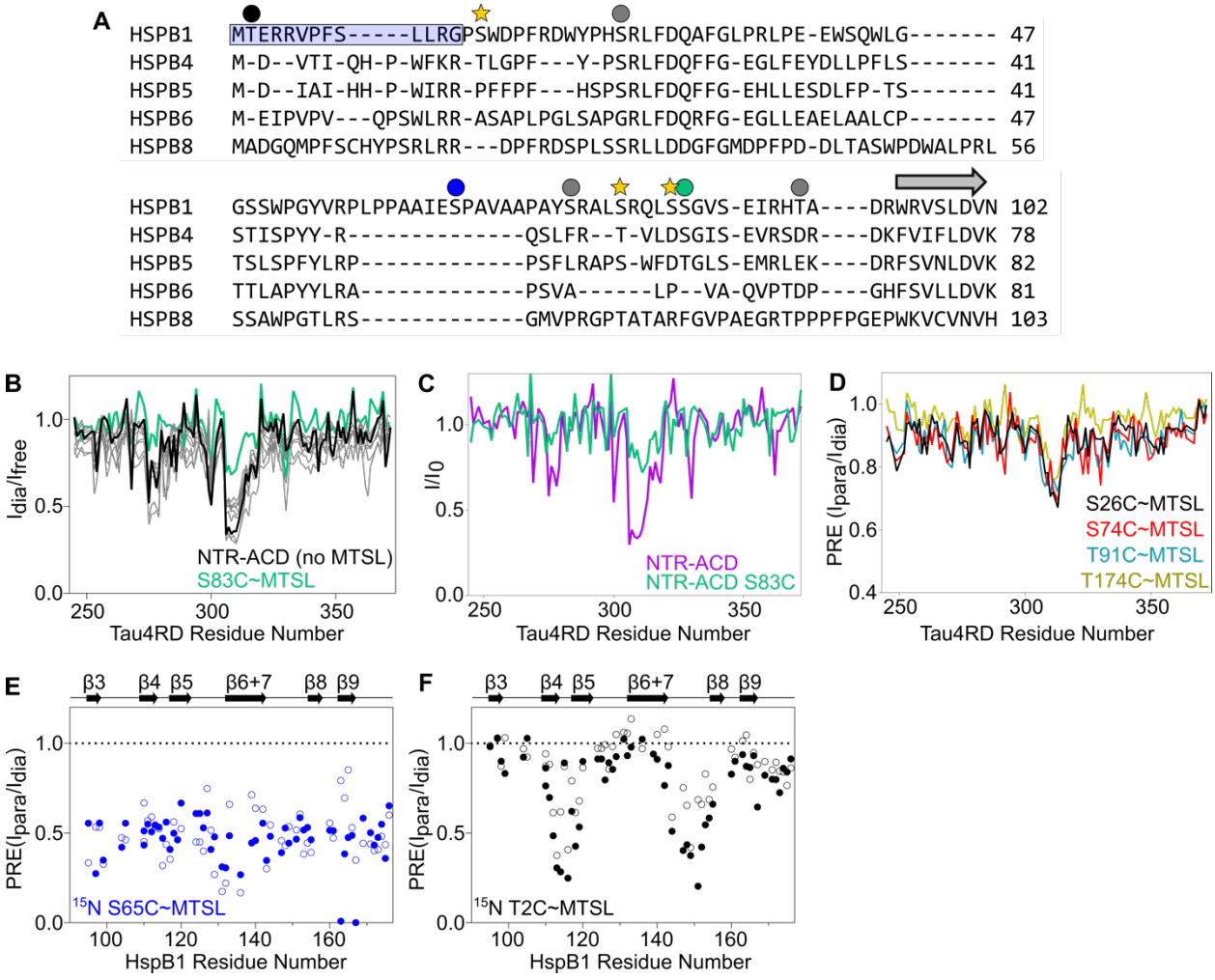

Figure 4.4. Intermolecular and intramolecular PRE experiment controls

A. Sequence alignment of the NTR of HspB1 with other human sHSPs. The circles indicate positions of cysteine mutagenesis and spin label conjugation. The stars indicate phosphorylation sites. The blue box denotes the residues present in the NTR peptide used in Fig. 4.6. The arrow represents strand β3, the first strand in the structured ACD.
B. Intensity loss in the ^{15}N HSQC spectrum of tau4RD (with both native cysteines mutated to serine) due to binding of HspB1$_{NTR-ACD}$ constructs with ascorbate-quenched (diamagnetic) MTSL conjugated at various sites. Eight of the nine constructs (grey lines) caused a similar pattern and magnitude of intensity loss as unlabeled HspB1$_{NTR-ACD}$ (black), indicating that conjugation of MTSL does not disrupt the ability of these constructs to bind tau. The one exception was the construct S83C~MTSL (teal), which showed a diminished ability to bind tau.
C. Intensity loss in the ^{15}N HSQC spectrum of tau4RD due to binding of the HspB1$_{NTR-ACD}$ S83C construct (teal) compared to intensity loss due to binding of HspB1$_{NTR-ACD}$ (purple). The mutant showed a diminished ability to bind tau, indicating that the mutation alone (prior to spin label conjugation) is sufficient to disrupt tau4RD binding.

D. Intermolecular PRE data for the four constructs shown in grey in Fig. 4.3 that cause intermediate PREs. The construct with MTSL at position 26 is shown in black, 74 is shown in red, 91 is shown in blue, and 174 is shown in yellow.
E. Intramolecular PRE data for the construct ^{15}N-HspB1$_{NTR-ACD}$ with MTSL conjugated at residue 65. In the absence of tau, residues throughout the ACD of HspB1lose intensity in the presence of the paramagnetic spin label (closed circles). In the presence of tau4RD (2 molar equivalents), the magnitude of the PREs changes, and they become particularly weak in the β9 strand (open circles).
F. Intramolecular PRE data for the construct ^{15}N-HspB1$_{NTR-ACD}$ with MTSL conjugated at residue 2. In the absence of tau, residues in loops 4/5 and 7/8 lose intensity in the presence of the paramagnetic spin label (closed circles). In the presence of tau4RD (2 molar equivalents), the PREs become weaker, indicating that residue 2 moves away from the ACD (open circles).

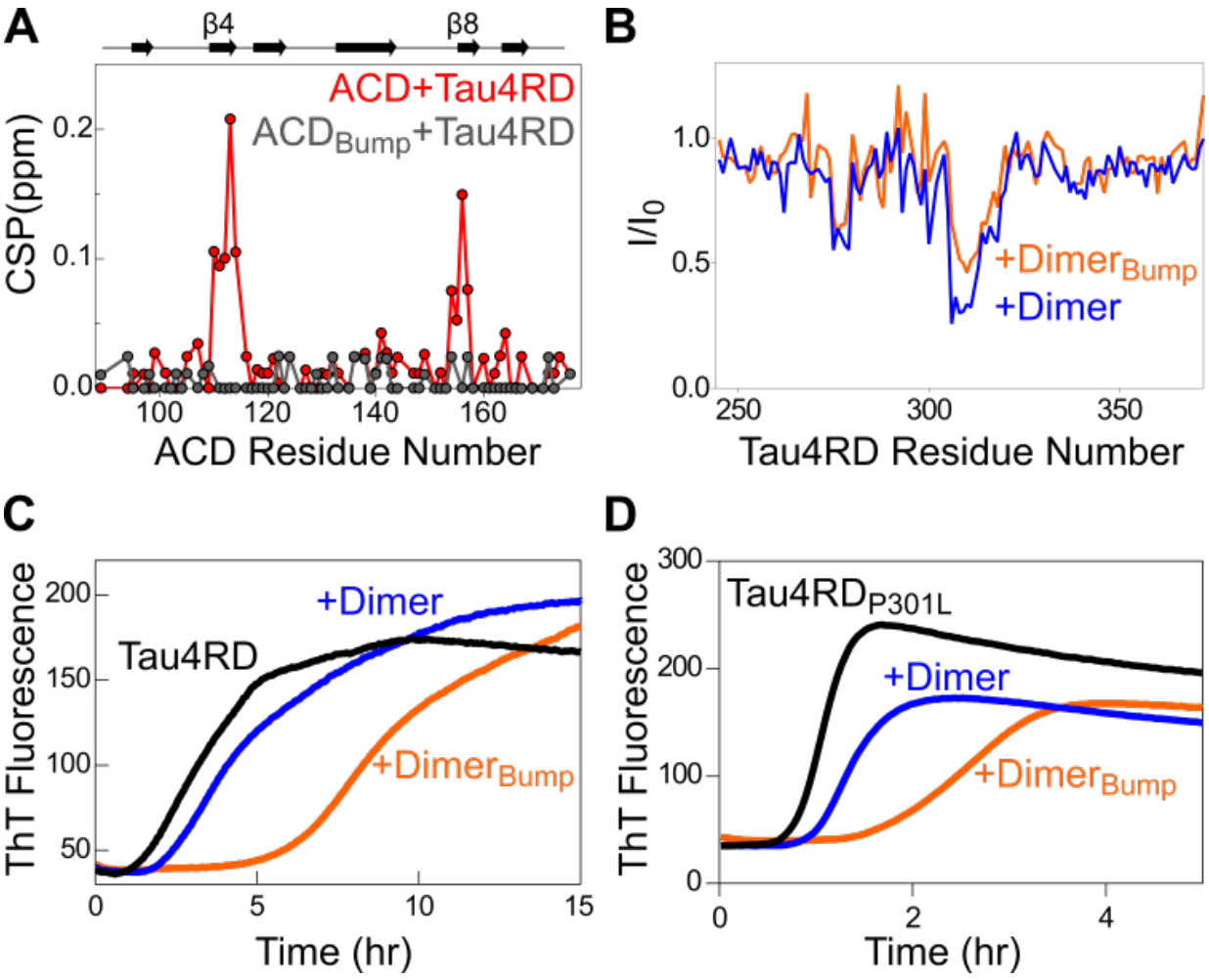

Figure 4.5. The groove bump mutation blocks binding to the β4-β8 groove and enhances chaperone activity

A. Chemical shift perturbations in the ^{15}N HSQC spectrum of 100 μM HspB1$_{ACD}$ due to tau4RD binding. Tau4RD (4 molar equivalents) causes CSPs in peaks corresponding to the β4-β8 groove in the spectrum of wild-type HspB1$_{ACD}$ (red) but not in the spectrum of HspB1$_{ACD, GrooveBump}$ (black).

B. Intensity loss in ^{15}N HSQC spectrum of 100 μM tau4RD due to binding of 2 molar equivalents HspB1$_{Dimer}$ (blue) and Dimer$_{Bump}$ (orange). The groove bump mutation caused only a slight decrease in the ability of HspB1$_{Dimer}$ to bind tau.

C. Tau4RD fibril formation assay in the presence of 0.5 molar equivalents HspB1$_{Dimer}$ (blue) and Dimer$_{Bump}$ (orange). The groove bump mutation caused a significant enhancement in chaperone activity.

D. Tau4RD$_{P301L}$ fibril formation assay in the presence of 1 molar equivalent HspB1$_{Dimer}$ (blue) and HspB1$_{Dimer, GrooveBump}$ (orange). The P301L mutation causes tau4RD to aggregate much more rapidly and decreases the ability of HspB1$_{Dimer}$ to act as a chaperone. The groove bump mutation caused a significant enhancement in chaperone activity against this chaperone-resistant tau mutant.

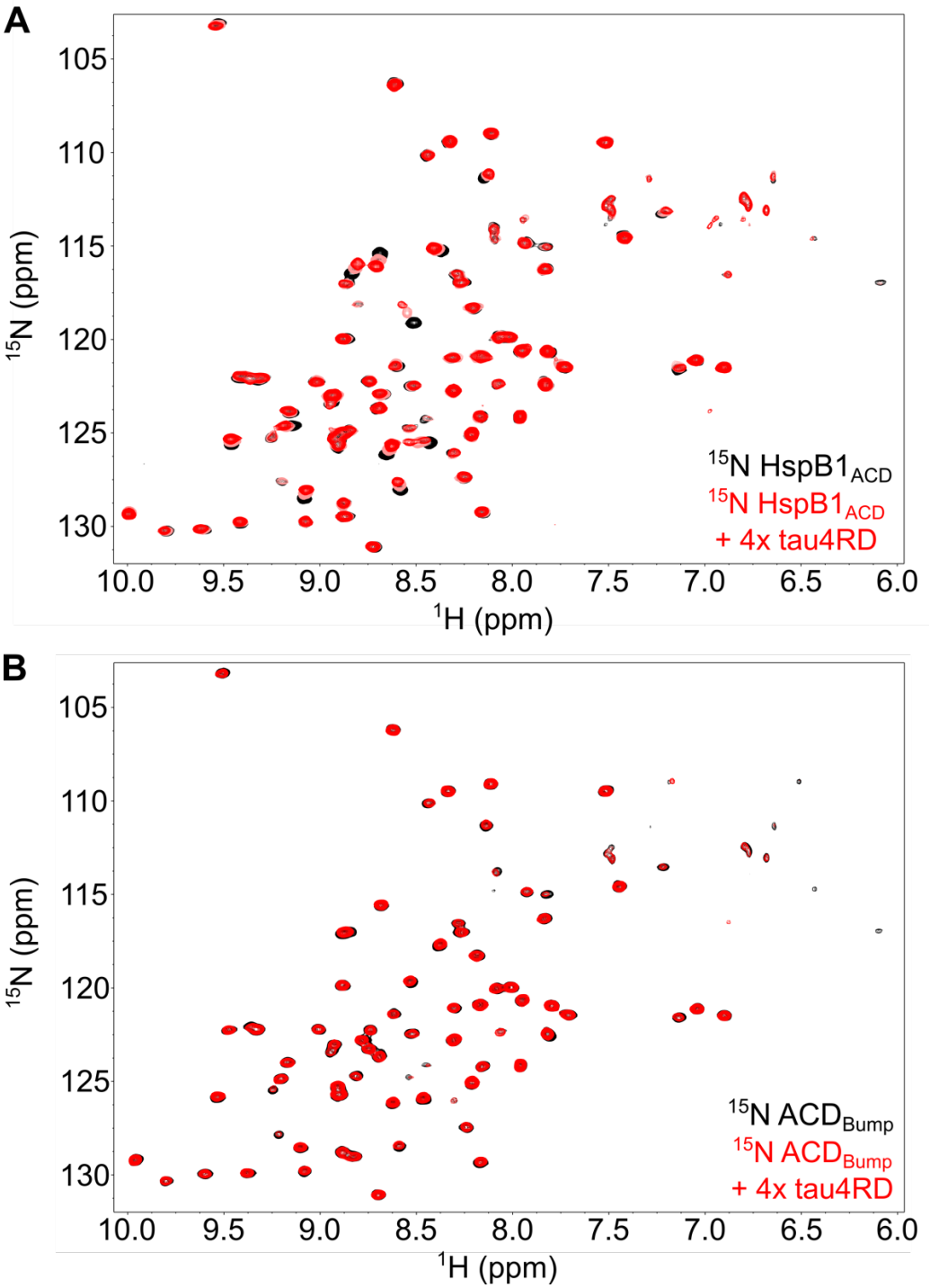

Figure 4.6. Comparison of tau4RD binding by HspB1$_{ACD}$ and ACD$_{Bump}$

A. ^{15}N HSQC spectrum of 100 µM HspB1$_{ACD}$ alone (black) and in the presence of two (pink) and four (red) molar equivalents tau4RD. Tau4RD causes CSPs in residues corresponding to the β4-β8 groove.
B. ^{15}N HSQC spectrum of 100 µM HspB1$_{ACD, GrooveBump}$ alone (black) and in the presence of four molar equivalents tau4RD (red). The groove bump mutation prevents tau4RD from binding in the β4-β8 groove.

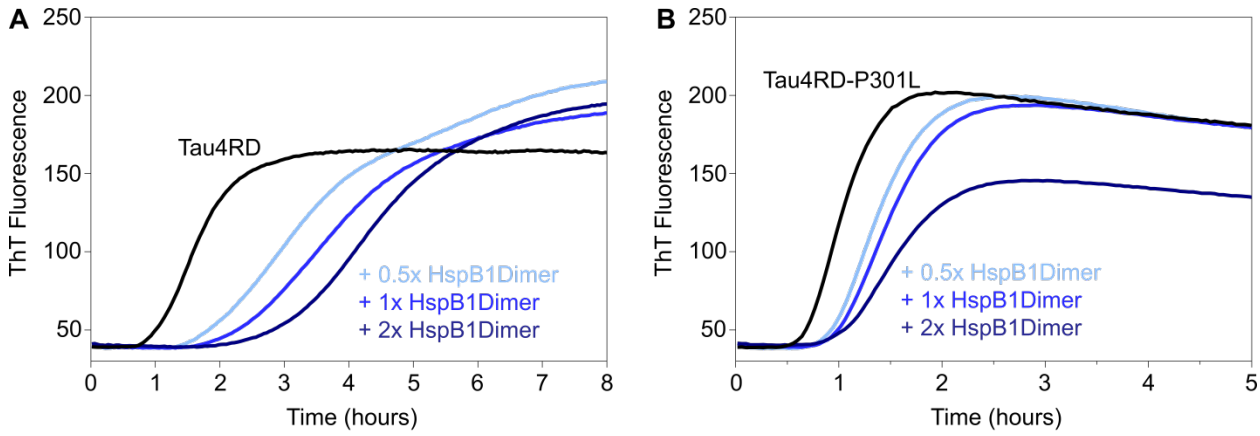

Figure 4.7. Effect of $HspB1_{Dimer}$ on aggregation kinetics of $tau4RD_{P301L}$

A. $HspB1_{Dimer}$ causes a dose-dependent delay in tau4RD (3.5 μM) aggregation, as shown in previous studies.
B. $Tau4RD_{P301L}$ has much faster aggregation kinetics than wild-type tau4RD and aggregates in under two hours. $HspB1_{Dimer}$ is able to delay this aggregation, but it is a less potent chaperone against $tau4RD_{P301L}$ than wild-type tau4RD. Its chaperone activity is also less dose-dependent.

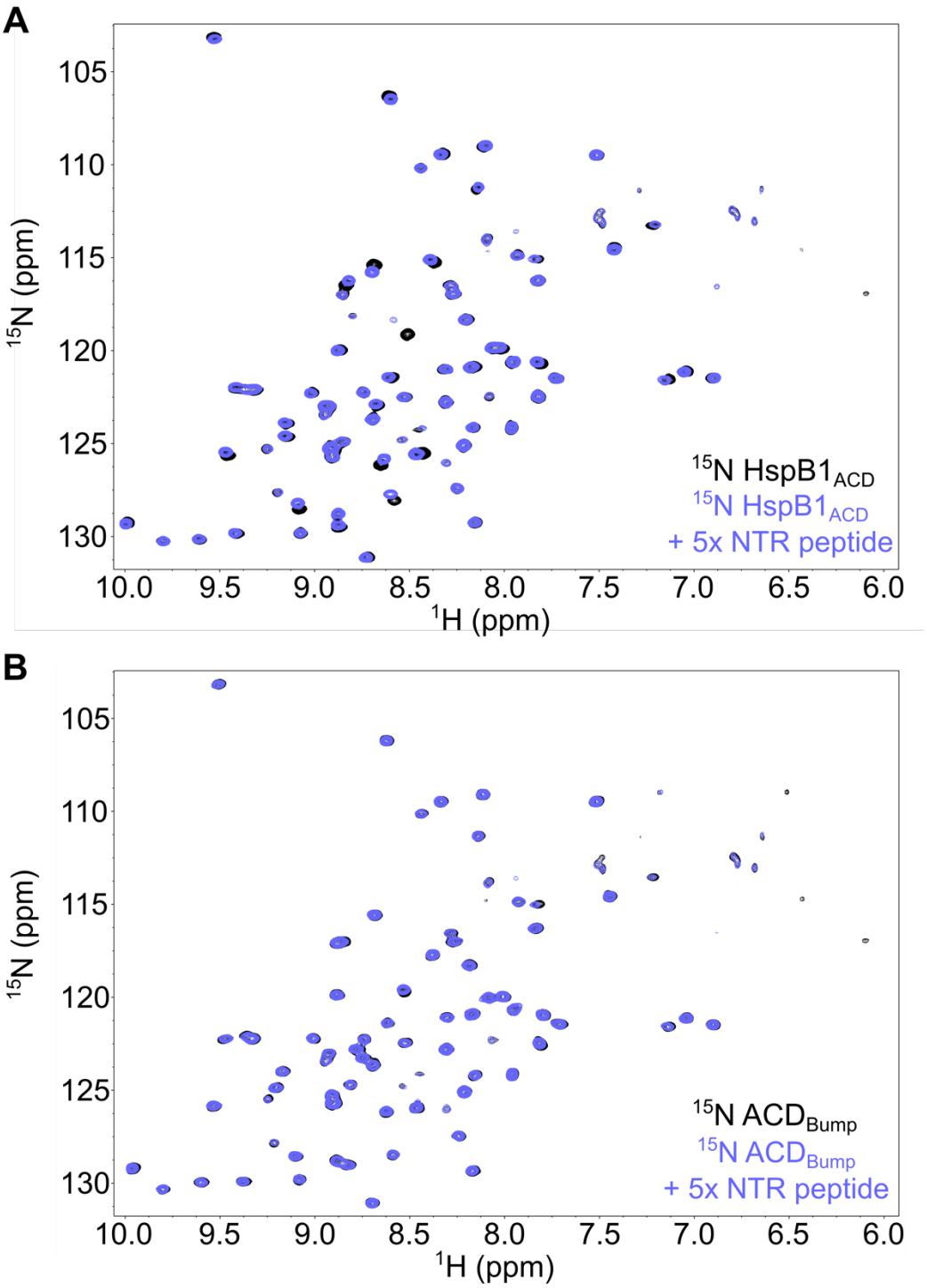

Figure 4.8. Comparison of distal NTR peptide binding by HspB1$_{ACD}$ and ACD$_{Bump}$

A. ^{15}N HSQC spectrum of 100 µM HspB1$_{ACD}$ alone (black) and in the presence of five molar equivalents of the distal NTR peptide (HspB1 residues 1-13, blue). The distal NTR peptide causes CSPs in residues corresponding to the β4-β8 groove.
B. ^{15}N HSQC spectrum of 100 µM HspB1$_{ACD, GrooveBump}$ alone (black) and in the presence of five molar equivalents of the distal NTR peptide (blue). The groove bump mutation prevents this peptide from binding in the β4-β8 groove.

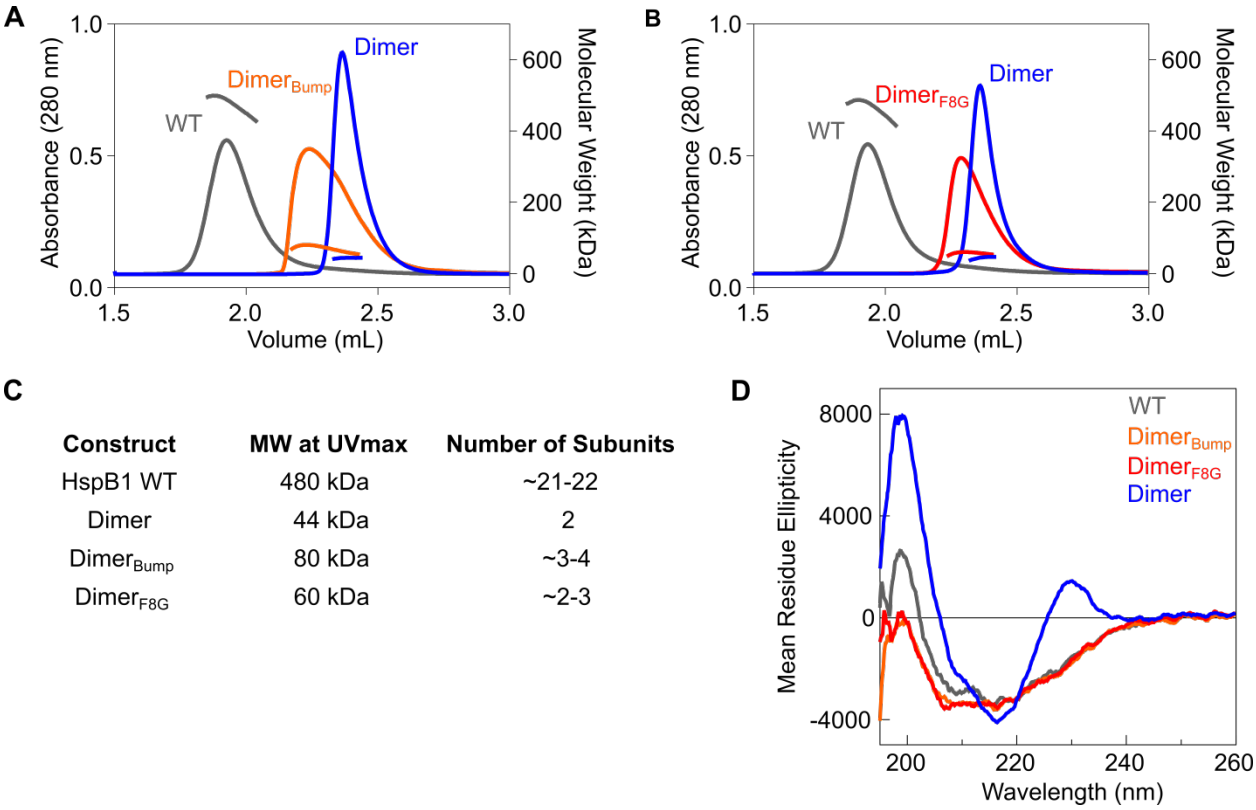

Figure 4.9. Characterization of activated HspB1 mutants

A. SEC-MALS of the $Dimer_{Bump}$ mutant (orange), compared to WT HspB1 (grey) and $HspB1_{Dimer}$ (blue). $Dimer_{Bump}$ elutes slightly earlier than $HspB1_{Dimer}$ and forms an oligomeric ensemble that includes some higher molecular weight species, likely tetramers.
B. SEC-MALS of the $Dimer_{F8G}$ mutant (red), compared to WT HspB1 (grey) and $HspB1_{Dimer}$ (blue). $Dimer_{F8G}$ also elutes slightly earlier than $HspB1_{Dimer}$ and forms an oligomeric ensemble that includes some higher molecular weight species. although the average molecular weight is slightly lower than $Dimer_{Bump}$.
C. Table listing the molecular weight of each HspB1 construct at the maximum of the absorbance peak and the number of subunits corresponding to this molecular weight. $Dimer_{Bump}$ and $Dimer_{F8G}$ both have molecular weights higher than that corresponding to a dimer, indicating that they form higher-order oligomers and exist predominantly as mixtures of dimers and tetramers.
D. Circular dichroism spectra of HspB1 constructs. $HspB1_{Dimer}$ has a positive peak at 230 nm characteristic of HspB1 constructs that have been phosphorylated or contain phosphomimetic mutations. $Dimer_{Bump}$ and $Dimer_{F8G}$ lack this peak, despite carrying the phosphomimetic mutations, indicating a change in the local structure of these constructs. Their CD signal is highly similar to each other and more closely matches HspB1 WT than $HspB1_{Dimer}$.

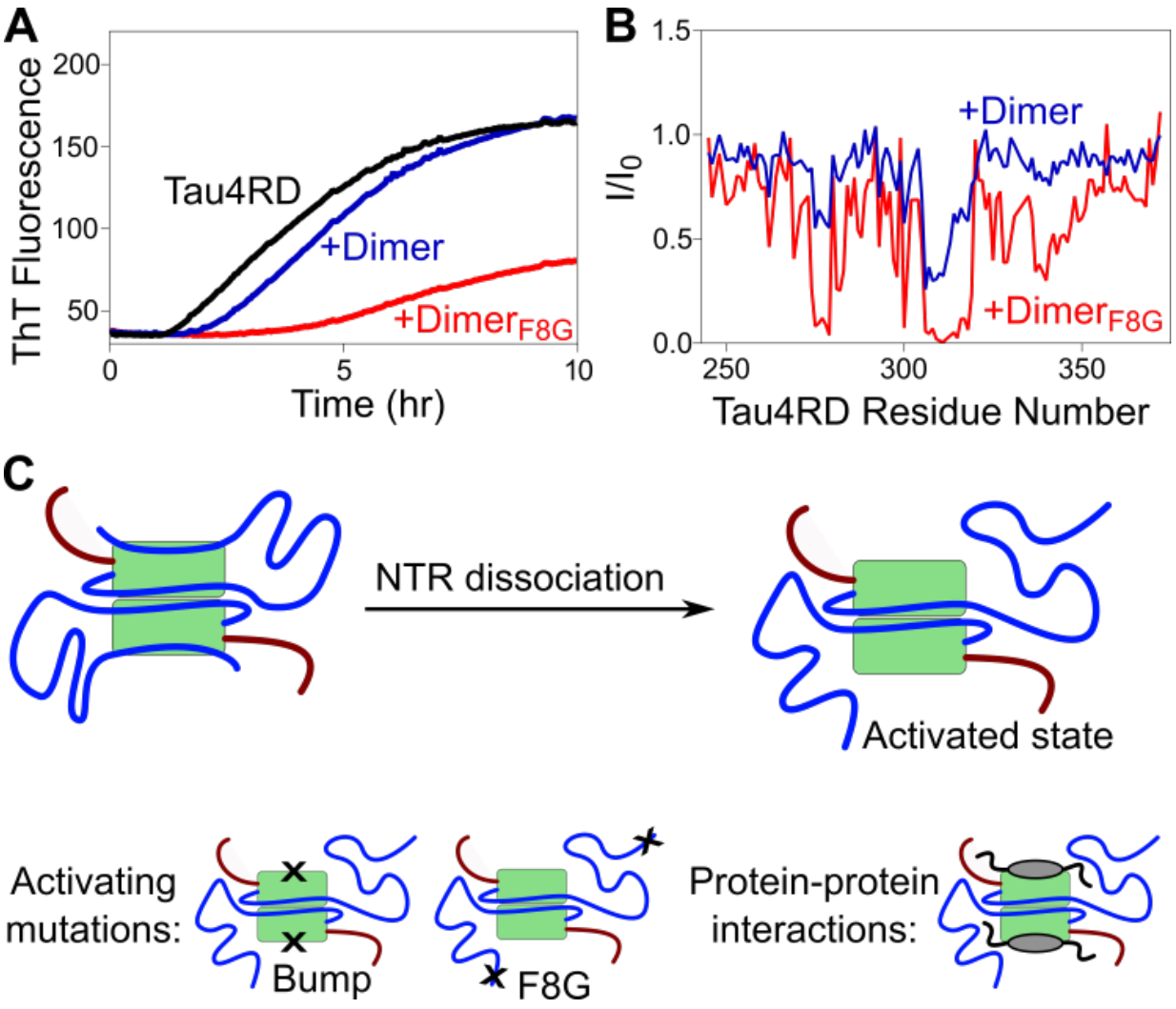

Figure 4.10. Chaperone activity is enhanced by release of the distal region of the NTR

A. Tau4RD fibril formation assay in the presence of 0.5 molar equivalents HspB1$_{Dimer}$ (blue) and Dimer$_{F8G}$ (red). The F8G mutation greatly enhances HspB1$_{Dimer}$ chaperone activity.
B. Intensity loss in ^{15}N HSQC spectrum of tau4RD due to binding of HspB1$_{Dimer}$ (blue) and Dimer$_{F8G}$ (red). Dimer$_{F8G}$ causes significantly more intensity loss, likely due to decreased competition for binding to the β4-β8 groove and enhanced interactions with the released NTR
C. Model of ways in which HspB1 chaperone activity can be enhanced. The groove bump and F8G mutations both enhance HspB1 chaperone activity by releasing the distal region of the NTR from the β4-β8 groove. This effect could be recapitulated by adding a binding partner, such as a co-chaperone or potentially a therapeutic agent to compete with the NTR for the β4-β8 groove.

BIBLIOGRAPHY

Abisambra J, Jinwal UK, Miyata Y, Rogers J, Blair L, Li X, Seguin SP, Wang L, Jin Y, Bacon J, et al. 2013. Allosteric heat shock protein 70 inhibitors rapidly rescue synaptic plasticity deficits by reducing aberrant tau. *Biol Psychiatry* **74**: 367–374.

Abisambra JF, Blair LJ, Hill SE, Jones JR, Kraft C, Rogers J, Koren 3rd J, Jinwal UK, Lawson L, Johnson AG, et al. 2010. Phosphorylation dynamics regulate Hsp27-mediated rescue of neuronal plasticity deficits in tau transgenic mice. *J Neurosci* **30**: 15374–15382.

Alderson TR, Benesch JLP, Baldwin AJ. 2017. Proline isomerization in the C-terminal region of HSP27. *Cell Stress Chaperones* **22**: 639–651.

Aprile FA, Arosio P, Fusco G, Chen SW, Kumita JR, Dhulesia A, Tortora P, Knowles TPJ, Vendruscolo M, Dobson CM, et al. 2017. Inhibition of α-Synuclein Fibril Elongation by Hsp70 Is Governed by a Kinetic Binding Competition between α-Synuclein Species. *Biochemistry* **56**: 1177–1180.

Bagnéris C, Bateman OA, Naylor CE, Cronin N, Boelens WC, Keep NH, Slingsby C. 2009. Crystal Structures of α-Crystallin Domain Dimers of αB-Crystallin and Hsp20. *J Mol Biol* **392**: 1242–1252.

Baldwin AJ, Knowles TPJ, Tartaglia GG, Fitzpatrick AW, Devlin GL, Shammas SL, Waudby CA, Mossuto MF, Meehan S, Gras SL, et al. 2011. Metastability of Native Proteins and the Phenomenon of Amyloid Formation. *J Am Chem Soc* **133**: 14160–14163.

Baldwin AJ, Walsh P, Hansen DF, Hilton GR, Benesch JLP, Sharpe S, Kay LE. 2012. Probing dynamic conformations of the high-molecular-weight αb-crystallin heat shock protein ensemble by NMR spectroscopy. *J Am Chem Soc* **134**: 15343–15350.

Baranova E V, Weeks SD, Beelen S, Bukach O V, Gusev NB, Strelkov S V. 2011. Three-dimensional structure of α-crystallin domain dimers of human small heat shock proteins HSPB1 and HSPB6. *J Mol Biol* **411**: 110–122.

Barre P, Eliezer D. 2013. Structural transitions in tau k18 on micelle binding suggest a hierarchy in the efficacy of individual microtubule-binding repeats in filament nucleation. *Protein Sci* **22**: 1037–1048.

Basha E, O'Neill H, Vierling E. 2012. Small heat shock proteins and α-crystallins: Dynamic proteins with flexible functions. *Trends Biochem Sci* **37**: 106–117.

Baughman HER, Clouser AF, Klevit RE, Nath A. 2018. HspB1 and Hsc70 chaperones engage distinct tau species and have different inhibitory effects on amyloid formation. *J Biol Chem* **293**: 2687–2700.

Berger Z, Roder H, Hanna A, Carlson A, Rangachari V, Yue M, Wszolek Z, Ashe K, Knight J, Dickson D, et al. 2007. Accumulation of Pathological Tau Species and Memory Loss in a Conditional Model of Tauopathy. *J Neurosci* **27**: 3650–3662.

Biancalana M, Koide S. 2010. Molecular mechanism of Thioflavin-T binding to amyloid fibrils. *Biochim Biophys Acta - Proteins Proteomics* **1804**: 1405–1412.

Braun N, Zacharias M, Peschek J, Kastenmuller A, Zou J, Hanzlik M, Haslbeck M, Rappsilber J, Buchner J, Weinkauf S, et al. 2011. Multiple molecular architectures of the eye lens chaperone αB-crystallin elucidated by a triple hybrid approach. *Proc Natl Acad Sci* **108**: 20491–20496.

Carlson SW, Branden M, Voss K, Sun Q, Rankin CA, Gamblin TC. 2007. A complex mechanism for inducer mediated tau polymerization. *Biochemistry* **46**: 8838–8849.

Chaari A, Eliezer D, Ladjimi M. 2016. The C-terminal α-helices of mammalian Hsc70 play a critical role in the stabilization of α-synuclein binding and inhibition of aggregation. *Int J Biol Macromol* **83**: 433–441.

Chiti F, Dobson CM. 2006. Protein Misfolding, Functional Amyloid, and Human Disease. *Annu Rev Biochem* **75**: 333–366.

Clark AR, Vree Egberts W, Kondrat FDL, Hilton GR, Ray NJ, Cole AR, Carver JA, Benesch JLP, Keep NH, Boelens WC, et al. 2018. Terminal Regions Confer Plasticity to the Tetrameric Assembly of Human HspB2 and HspB3. *J Mol Biol* **430**: 3297–3310.

Clouser AF. 2018. Interplay of Local Structure, Dynamics, and Self-Association in HspB1. University of Washington.

Clouser AF, Klevit RE. 2017. pH-dependent structural modulation is conserved in the human small heat shock protein HSBP1. *Cell Stress Chaperones* **22**: 569–575.

Collier MP, Alderson TR, Villiers CP De, Nicholls D, Gastall HY, Allison TM, Degiacomi MT, Jiang H, Mlynek G, Fürst DO, et al. 2019. HspB1 phosphorylation regulates its intramolecular dynamics and mechanosensitive molecular chaperone interaction with filamin C. *Sci Adv* **5**: eaav8421.

Cox D, Selig E, Griffin MDW, Carver JA, Ecroyd H. 2016. Small Heat-shock Proteins Prevent α-synuclein aggregation via transient interactions and their efficacy is affected by the rate of aggregation. *J Biol Chem* **291**: 22618–22629.

Cox D, Whiten DR, Brown JWP, Horrocks MH, Gil RS, Dobson CM, Klenerman D, Van Oijen AM, Ecroyd H. 2018. The small heat shock protein Hsp27 binds -synuclein fibrils, preventing elongation and cytotoxicity. *J Biol Chem* **293**: 4486–4497.

Cremers CM, Knoefler D, Gates S, Martin N, Dahl JU, Lempart J, Xie L, Chapman MR, Galvan V, Southworth DR, et al. 2016. Polyphosphate: A Conserved Modifier of Amyloidogenic Processes. *Mol Cell* **63**: 768–780.

D'Souza I, Poorkaj P, Hong M, Nochlin D, Lee VM-Y, Bird TD, Schellenberg GD. 1999. Missense and silent tau gene mutations cause frontotemporal dementia with parkinsonism-chromosome 17 type, by affecting multiple alternative RNA splicing regulatory elements. *Proc Natl Acad Sci U S A* **96**: 5598–603.

Daebel V, Chinnathambi S, Biernat J, Schwalbe M, Habenstein B, Loquet A, Akoury E, Tepper K, Müller H, Baldus M, et al. 2012. β-sheet core of tau paired helical filaments revealed by solid-state NMR. *J Am Chem Soc* **134**: 13982–13989.

Datskevich PN, Nefedova V V., Sudnitsyna M V., Gusev NB. 2012. Mutations of small heat shock proteins and human congenital diseases. *Biochem* **77**: 1500–1514.

Dawson HN, Ferreira A, Eyster M V, Ghoshal N, Binder LI, Vitek MP. 2001. Inhibition of neuronal maturation in primary hippocampal neurons from tau deficient mice. *J Cell Sci* **114**: 1179–1187.

Delbecq SP, Jehle S, Klevit R. 2012. Binding determinants of the small heat shock protein, αB-crystallin: recognition of the "IxI" motif. *EMBO J* **31**: 4587–94.

Delbecq SP, Rosenbaum JC, Klevit RE. 2015. A Mechanism of Subunit Recruitment in Human Small Heat Shock Protein Oligomers. *Biochemistry* **54**: 4276–4284.

Drubin DG, Kirschner MW. 1986. Tau protein function in living cells. *J Cell Biol* **103**: 2739–46.

Dyson HJ, Wright PE. 2005. Intrinsically unstructured proteins and their functions. *Nat Rev Mol Cell Biol* **6**: 197–208.

Elbaum-Garfinkle S, Rhoades E. 2012. Identification of an aggregation-prone structure of tau. *J Am Chem Soc* **134**: 16607–16613.

Falcon B, Zhang W, Murzin AG, Murshudov G, Garringer HJ, Vidal R, Crowther RA, Ghetti B, Scheres SHW, Goedert M. 2018a. Structures of filaments from Pick's disease reveal a novel tau protein fold. *Nature* **561**: 137–140.

Falcon B, Zhang W, Schweighauser M, Murzin AG, Vidal R, Garringer HJ, Ghetti B, Scheres SHW, Goedert M. 2018b. Tau filaments from multiple cases of sporadic and inherited Alzheimer's disease adopt a common fold. *Acta Neuropathol* **136**: 699–708.

Falcon B, Zivanov J, Zhang W, Murzin AG, Garringer HJ, Vidal R, Crowther RA, Newell KL, Ghetti B, Goedert M, et al. 2019. Novel tau filament fold in chronic traumatic encephalopathy encloses hydrophobic molecules. *Nature* **568**: 420–423.

Fichou Y, Lin Y, Rauch JN, Vigers M, Zeng Z, Srivastava M, Keller TJ, Freed JH, Kosik KS, Han S. 2018. Cofactors are essential constituents of stable and seeding-active tau fibrils. *Proc Natl Acad Sci* **115**: 13234–13239.

Fitzpatrick AWP, Falcon B, He S, Murzin AG, Murshudov G, Garringer HJ, Crowther RA, Ghetti B, Goedert M, Scheres SHW. 2017a. Cryo-EM structures of tau filaments from Alzheimer's disease. *Nature* **547**: 185–190.

Fitzpatrick AWP, Falcon B, He S, Murzin AG, Murshudov G, Garringer HJ, Crowther RA, Ghetti B, Goedert M, Scheres SHW. 2017b. Cryo-EM structures of tau filaments from Alzheimer's disease. *Nature* **547**: 185–190.

Flach K, Hilbrich I, Schiffmann A, Gärtner U, Krüger M, Leonhardt M, Waschipky H, Wick L, Arendt T, Holzer M. 2012. Tau oligomers impair artificial membrane integrity and cellular viability. *J Biol Chem* **287**: 43223–43233.

Fontaine SN, Martin MD, Akoury E, Assimon VA, Borysov S, Nordhues BA, Sabbagh JJ, Cockman M, Gestwicki JE, Zweckstetter M, et al. 2015. The active Hsc70/tau complex can be exploited to enhance tau turnover without damaging microtubule dynamics. *Hum Mol Genet* **24**: 3971–3981.

Fontaine SN, Zheng D, Sabbagh JJ, Martin MD, Chaput D, Darling A, Trotter JH, Stothert AR, Nordhues BA, Lussier A, et al. 2016. DnaJ/Hsc70 chaperone complexes control the extracellular release of neurodegenerative-associated proteins. *EMBO J* **35**: 1537–1549.

Freilich R, Betegon M, Tse E, Mok SA, Julien O, Agard DA, Southworth DR, Takeuchi K, Gestwicki JE. 2018. Competing protein-protein interactions regulate binding of Hsp27 to its client protein tau. *Nat Commun* **9**: 4563.

Friedhoff P, Schneider A, Mandelkow EM, Mandelkow E. 1998. Rapid assembly of Alzheimer-like paired helical filaments from microtubule-associated protein tau monitored by fluorescence in solution. *Biochemistry* **37**: 10223–10230.

Gao X, Carroni M, Nussbaum-Krammer C, Mogk A, Nillegoda NB, Szlachcic A, Guilbride DL, Saibil HR, Mayer MP, Bukau B. 2015a. Human Hsp70 Disaggregase Reverses Parkinson's-Linked α-Synuclein Amyloid Fibrils. *Mol Cell* **59**: 781–793.

Gao X, Carroni M, Nussbaum-Krammer C, Mogk A, Nillegoda NBB, Szlachcic A, Guilbride DLL, Saibil HRR, Mayer MPP, Bukau B. 2015b. Human Hsp70 Disaggregase Reverses Parkinson's-Linked α-Synuclein Amyloid Fibrils. *Mol Cell* **59**: 781–793.

Goedert M, Spillantini MG, Jakes R, Rutherford D, Crowther RA. 1989. Multiple isoforms of human microtubule-associated protein tau: sequences and localization in neurofibrillary tangles of Alzheimer's disease. *Neuron* **3**: 519–526.

Hartl FU, Bracher A, Hayer-Hartl M. 2011. Molecular chaperones in protein folding and proteostasis. *Nature* **475**: 324–332.

Hayes D, Napoli V, Mazurkie A, Stafford WF, Graceffa P. 2009. Phosphorylation dependence of Hsp27 multimeric size and molecular chaperone function. *J Biol Chem* **284**: 18801–18807.

Hochberg GKA, Ecroyd H, Liu C, Cox D, Cascio D, Sawaya MR, Collier MP, Stroud J, Carver JA, Baldwin AJ, et al. 2014. The structured core domain of αB-crystallin can prevent amyloid fibrillation and associated toxicity. *Proc Natl Acad Sci U S A* **111**: E1562-70.

Imhaus A-F, Duménil G. 2014. The number of Neisseria meningitidis type IV pili determines host cell interaction. *EMBO J* **33**: 1767–1783.

Iqbal K, Liu F, Gong C-X, Grundke-Iqbal I. 2010. Tau in Alzheimer disease and related tauopathies. *Curr Alzheimer Res* **7**: 656–64.

Janowska MK, Baughman HER, Woods CN, Klevit RE. 2019. Mechanisms of Small Heat Shock Proteins. *Cold Spring Harb Perspect Biol* a034025.

Jehle S, Vollmar BS, Bardiaux B, Dove KK, Rajagopal P, Gonen T, Oschkinat H, Klevit RE. 2011. N-terminal domain of alphaB-crystallin provides a conformational switch for multimerization and structural heterogeneity. *Proc Natl Acad Sci U S A* **108**: 6409–14.

Jinwal UK, Akoury E, Abisambra JF, O'Leary JC, Thompson AD, Blair LJ, Jin Y, Bacon J, Nordhues BA, Cockman M, et al. 2013. Imbalance of Hsp70 family variants fosters tau accumulation. *FASEB J* **27**: 1450–1459.

Jovcevski B, Kelly MA, Rote AP, Berg T, Gastall HY, Benesch JLPP, Aquilina JA, Ecroyd H. 2015. Phosphomimics destabilize Hsp27 oligomeric assemblies and enhance chaperone activity. *Chem Biol* **22**: 186–195.

Kampers T, Friedhoff P, Biernat J, Mandelkow E-MM, Mandelkow E-MM. 1996. RNA stimulates aggregation of microtubule-associated protein tau into Alzheimer-like paired helical filaments. *FEBS Lett* **399**: 344–349.

Karagöz GE, Duarte AMS, Akoury E, Ippel H, Biernat J, Morán Luengo T, Radli M, Didenko T, Nordhues BA, Veprintsev DB, et al. 2014. Hsp90-tau complex reveals molecular basis for specificity in chaperone action. *Cell* **156**: 963–974.

Kellogg EH, Hejab NMA, Poepsel S, Downing KH, DiMaio F, Nogales E. 2018. Near-atomic model of microtubule-tau interactions. *Science (80-)* **360**: 1242–1246.

Kumar DKV, Choi HS, Washicosky KJ, Eimer WA, Tucker S, Ghofrani J, Lefkowitz A, McColl G, Goldstein LE, Tanzi RE, et al. 2016. Amyloid-β peptide protects against microbial infection in mouse and worm models of Alzheimer's disease. *Sci Transl Med* **8**: 340ra72.

Kundel F, De S, Flagmeier P, Horrocks MH, Kjaergaard M, Shammas SL, Jackson SE, Dobson CM, Klenerman D. 2018. Hsp70 Inhibits the Nucleation and Elongation of Tau and Sequesters Tau Aggregates with High Affinity. *ACS Chem Biol* **13**: 636–646.

Larsen JK, Yamboliev IA, Weber LA, Gerthoffer WT. 1997. Phosphorylation of the 27-kDa heat shock protein via p38 MAP kinase and MAPKAP kinase in smooth muscle. *Am J Physiol* **273**: L930-40.

Lasagna-Reeves CA, Castillo-Carranza DL, Sengupta U, Clos AL, Jackson GR, Kayed R. 2011. Tau oligomers impair memory and induce synaptic and mitochondrial dysfunction in wild-type mice. *Mol Neurodegener* **6**: 39.

Lelj-Garolla B, Mauk AG. 2012. Roles of the N- and C-terminal sequences in Hsp27 self-association and chaperone activity. *Protein Sci* **21**: 122–133.

Li XH, Rhoades E. 2017. Heterogeneous Tau-Tubulin Complexes Accelerate Microtubule Polymerization. *Biophys J* **112**: 2567–2574.

Linding R, Schymkowitz J, Rousseau F, Diella F, Serrano L. 2004. A Comparative Study of the Relationship Between Protein Structure and β-Aggregation in Globular and Intrinsically Disordered Proteins. *J Mol Biol* **342**: 345–353.

Liu Z, Wang C, Li Y, Zhao C, Li T, Li D, Zhang S, Liu C. 2018. Mechanistic insights into the switch of αB-crystallin chaperone activity and self-multimerization. *J Biol Chem* **293**: 14880–14890.

Mainz A, Peschek J, Stavropoulou M, Back KC, Bardiaux B, Asami S, Prade E, Peters C, Weinkauf S, Buchner J, et al. 2015. The chaperone αB-crystallin uses different interfaces to capture an amorphous and an amyloid client. *Nat Struct Mol Biol* **22**: 898–905.

Maji SK, Perrin MH, Sawaya MR, Jessberger S, Vadodaria K, Rissman RA, Singru PS, Nilsson KPR, Simon R, Schubert D, et al. 2009. Functional amyloids as natural storage of peptide hormones in pituitary secretory granules. *Science* **325**: 328–32.

Mandelkow EM, Mandelkow E. 2011. Biochemistry and cell biology of Tau protein in neurofibrillary degeneration. *Cold Spring Harb Perspect Biol* **3**: 1–25.

McDonald ET, Bortolus M, Koteiche HA, McHaourab HS. 2012. Sequence, structure, and dynamic determinants of Hsp27 (HspB1) equilibrium dissociation are encoded by the N-terminal domain. *Biochemistry* **51**: 1257–1268.

Mchaourab HS, Lin Y-L, Spiller BW. 2012. Crystal Structure of an Activated Variant of Small Heat Shock Protein Hsp16.5 NIH Public Access. *Biochemistry* **51**: 5105–5112.

Mishra S, Chandler SA, Williams D, Claxton DP, Koteiche HA, Stewart PL, Benesch JLP, Mchaourab HS. 2018. Engineering of a Polydisperse Small Heat-Shock Protein Reveals Conserved Motifs of Oligomer Plasticity. *Structure* **26**: 1116-1126.e4.

Mok SA, Condello C, Freilich R, Gillies A, Arhar T, Oroz J, Kadavath H, Julien O, Assimon VA, Rauch JN, et al. 2018. Mapping interactions with the chaperone network reveals factors that protect against tau aggregation. *Nat Struct Mol Biol* **25**: 384–393.

Mukrasch MD, Bibow S, Korukottu J, Jeganathan S, Biernat J, Griesinger C, Mandelkow E, Zweckstetter M. 2009. Structural polymorphism of 441-residue Tau at single residue resolution. *PLoS Biol* **7**: 0399–0414.

Mukrasch MD, Biernat J, Von Bergen M, Griesinger C, Mandelkow E, Zweckstetter M. 2005. Sites of tau important for aggregation populate β-structure and bind to microtubules and polyanions. *J Biol Chem* **280**: 24978–24986.

Munishkina LA, Cooper EM, Uversky VN, Fink AL. 2004. The effect of macromolecular crowding on protein aggregation and amyloid fibril formation. *J Mol Recognit* **17**: 456–464.

Muranova LK, Weeks SD, Strelkov S V., Gusev NB. 2015. Characterization of Mutants of Human Small Heat Shock Protein HspB1 Carrying Replacements in the N-Terminal Domain and Associated with Hereditary Motor Neuron Diseases ed. H.H. Kampinga. **10**: e0126248.

Nakatani-Webster E, Nath A. 2017. Inferring Mechanistic Parameters from Amyloid Formation Kinetics by Approximate Bayesian Computation. *Biophys J* **112**: 868–880.

Narayanan RL, Dürr UHN, Bibow S, Biernat J, Mandelkow E, Zweckstetter M. 2010. Automatic assignment of the intrinsically disordered protein Tau with 441-residues. *J Am Chem Soc* **132**: 11906–11907.

Nefedova V V., Muranova LK, Sudnitsyna M V., Ryzhavskaya AS, Gusev NB. 2015. Small Heat Shock Proteins and Distal Hereditary Neuropathies. *Biochem* **80**: 1734–1747.

Nemes Z. 2004. Cross-linking of ubiquitin, HSP27, parkin and -synuclein by -glutamyl- -lysine bonds in Alzheimer's neurofibrillary tangles. *FASEB J* **18**: 1135–7.

Nemes Z, Devreese B, Steinert PM, Van Beeumen J, FÉSÜS L. 2004. Cross-linking of ubiquitin, HSP27, parkin, and α-synuclein by γ-glutamyl-ε-lysine bonds in Alzheimer's neurofibrillary tangles. *FASEB J* **18**: 1135–7.

Oroz J, Chang BJ, Wysoczanski P, Lee CT, Pérez-Lara Á, Chakraborty P, Hofele R V., Baker JD, Blair LJ, Biernat J, et al. 2018. Structure and pro-toxic mechanism of the human Hsp90/PPIase/Tau complex. *Nat Commun* **9**: 4532.

Padmanabhan S, Jost M, Drennan CL, Elías-Arnanz M. 2017. A New Facet of Vitamin B 12 : Gene Regulation by Cobalamin-Based Photoreceptors Photoreceptors: proteins that sense light via a chromophore, which undergoes photochemical transformation and triggers conformational changes in the protein. *Annu Rev Biochem* **86**: 485–514.

Patterson KR, Ward SM, Combs B, Voss K, Kanaan NM, Morfini G, Brady ST, Gamblin TC, Binder LI. 2011. Heat shock protein 70 prevents both tau aggregation and the inhibitory effects of preexisting tau aggregates on fast axonal transport. *Biochemistry* **50**: 10300–10310.

Peschek J, Braun N, Rohrberg J, Back KC, Kriehuber T, Kastenmuller A, Weinkauf S, Buchner J, Kastenmüller A, Weinkauf S, et al. 2013. Regulated structural transitions unleash the chaperone activity of αB-crystallin. *Proc Natl Acad Sci* **110**: E3780–E3789.

Rajagopal P, Liu Y, Shi L, Clouser AF, Klevit RE. 2015a. Structure of the α-crystallin domain from the redox-sensitive chaperone, HSPB1. *J Biomol NMR* **63**: 223–228.

Rajagopal P, Tse E, Borst AJ, Delbecq SP, Shi L, Southworth DR, Klevit RE. 2015b. A conserved histidine modulates HSPB5 structure to trigger chaperone activity in response to stress related acidosis. *Elife* **4**: 1–21.

Rao JL, Reddy PS, Mishra RN, Gupta D, Sahal D, Tuteja N, Sopory SK, Reddy MK. 2010. Thermo and pH stable ATP-independent chaperone activity of heat-inducible Hsp70 from Pennisetum glaucum. *Plant Signal Behav* **5**: 110–121.

Rauch JN, Tse E, Freilich R, Mok SA, Makley LN, Southworth DR, Gestwicki JE. 2017. BAG3 Is a Modular, Scaffolding Protein that physically Links Heat Shock Protein 70 (Hsp70) to the Small Heat Shock Proteins. *J Mol Biol* **429**: 128–141.

Rogalla T, Ehrnsperger M, Preville X, Kotlyarov A, Lutsch G, Ducasse C, Paul C, Wieske M, Arrigo A-PP, Buchner J, et al. 1999. Regulation of Hsp27 Oligomerization , Chaperone Function , and Protective Activity against Oxidative Stress / Tumor Necrosis Factor α by Phosphorylation. *J Biol Chem* **274**: 18947–18956.

Sanders DW, Kaufman SK, DeVos SL, Sharma AM, Mirbaha H, Li A, Barker SJ, Foley AC, Thorpe JR, Serpell LC, et al. 2014. Distinct Tau Prion Strains Propagate in Cells and Mice and Define Different Tauopathies. *Neuron* **82**: 1271–1288.

SantaCruz K, Lewis J, Spires T, Paulson J, Kotilinek L, Ingelsson M, Guimaraes A, DeTure M, Ramsden M, McGowan E, et al. 2005. Tau Suppression in a Neurodegenerative Mouse Model Improves Memory Function. *Science* **309**: 476–481.

Shammas SL, Garcia GA, Kumar S, Kjaergaard M, Horrocks MH, Shivji N, Mandelkow E, Knowles TPJ, Mandelkow E, Klenerman D. 2015. A mechanistic model of tau amyloid aggregation based on direct observation of oligomers. *Nat Commun* **6**.

Sharma AM, Thomas TL, Woodard DR, Kashmer OM, Diamond MI. 2018. Tau monomer encodes strains. *Elife* **7**: e37813.

Shashidharamurthy R, Koteiche HA, Dong J, Mchaourab HS. 2005. Mechanism of chaperone function in small heat shock proteins: Dissociation of the HSP27 oligomer is required for recognition and binding of destabilized T4 lysozyme. *J Biol Chem* **280**: 5281–5289.

Shimura H, Miura-Shimura Y, Kosik KS. 2004. Binding of Tau to Heat Shock Protein 27 Leads to Decreased Concentration of Hyperphosphorylated Tau and Enhanced Cell Survival. *J Biol Chem* **279**: 17957–17962.

Sluchanko NN, Beelen S, Kulikova AA, Weeks SD, Antson AA, Gusev NB, Strelkov S V. 2017. Structural Basis for the Interaction of a Human Small Heat Shock Protein with the 14-3-3 Universal Signaling Regulator. *Structure* **25**: 305–316.

Smet C, Leroy A, Sillen A, Wieruszeski JM, Landrieu I, Lippens G. 2004. Accepting its random coil nature allows a partial NMR assignment of the neuronal Tau protein. *ChemBioChem* **5**: 1639–1646.

Stamer K, Vogel R, Thies E, Mandelkow E, Mandelkow EM. 2002. Tau blocks traffic of organelles, neurofilaments, and APP vesicles in neurons and enhances oxidative stress. *J Cell Biol* **156**: 1051–1063.

Stricher FF, Macri C, Ruff M, Muller S. 2013. {HSPA}8/HSC70 chaperone protein. *Autophagy* **9**: 1937–1954.

Taniguchi-Watanabe S, Arai T, Kametani F, Nonaka T, Masuda-Suzukake M, Tarutani A, Murayama S, Saito Y, Arima K, Yoshida M, et al. 2016. Biochemical classification of tauopathies by immunoblot, protein sequence and mass spectrometric analyses of sarkosyl-insoluble and trypsin-resistant tau. *Acta Neuropathol* **131**: 267–280.

Tompa P, Fuxreiter M. 2008. Fuzzy complexes: polymorphism and structural disorder in protein-protein interactions. *Trends Biochem Sci* **33**: 2–8.

Treweek TM, Meehan S, Ecroyd H, Carver JA. 2015. Small heat-shock proteins: Important players in regulating cellular proteostasis. *Cell Mol Life Sci* **72**: 429–451.

Tyedmers J, Mogk A, Bukau B. 2010. Cellular strategies for controlling protein aggregation. *Nat Rev Mol Cell Biol* **11**: 777–788.

Uversky VN, M. Cooper E, Bower KS, Li J, Fink AL. 2002. Accelerated α-synuclein fibrillation in crowded milieu. *FEBS Lett* **515**: 99–103.

Van Den Berg B, Ellis RJ, Dobson CM. 1999. Effects of macromolecular crowding on protein folding and aggregation. *EMBO J* **18**: 6927–6933.

van der Lee R, Buljan M, Lang B, Weatheritt RJ, Daughdrill GW, Dunker AK, Fuxreiter M, Gough J, Gsponer J, Jones DT, et al. 2014. Classification of Intrinsically Disordered Regions and Proteins. *Chem Rev* **114**: 6589–6631.

Veinger L, Diamant S, Buchner J, Goloubinoff P. 1998. The small heat-shock protein IbpB from Escherichia coli stabilizes stress-denatured proteins for subsequent refolding by a multichaperone network. *J Biol Chem* **273**: 11032–11037.

Von Bergen M, Barghorn S, Li L, Marx A, Biernat J, Mandelkow EM, Mandelkow E. 2001. Mutations of Tau Protein in Frontotemporal Dementia Promote Aggregation of Paired Helical Filaments by Enhancing Local β-Structure. *J Biol Chem* **276**: 48165–48174.

von Bergen M, Friedhoff P, Biernat J, Heberle J, Mandelkow E-MM, Mandelkow E-MM, Kirschner MW. 2000. Assembly of tau protein into Alzheimer paired helical filaments depends on a local sequence motif ((306)VQIVYK(311)) forming beta structure. *Proc Natl Acad Sci U S A* **97**: 5129–5134.

Voss K, Combs B, Patterson KR, Binder LI, Gamblin TC. 2012. Hsp70 alters tau function and aggregation in an isoform specific manner. *Biochemistry* **51**: 888–898.

Ward SM, Himmelstein DS, Lancia JK, Binder LI. 2012. Tau oligomers and tau toxicity in neurodegenerative disease. *Biochem Soc Trans* **40**: 667–671.

Weeks SD, Baranova E V, Heirbaut M, Beelen S, Shkumatov A V, Gusev NB, Strelkov S V. 2014. Molecular structure and dynamics of the dimeric human small heat shock protein HSPB6. *J Struct Biol* **185**: 342–354.

Wickramasinghe SP, Lempart J, Merens HE, Murphy J, Huettemann P, Jakob U, Rhoades E. 2019. Polyphosphate initiates tau aggregation through intra- and intermolecular scaffolding. *Biophys J* **117**: 717–728.

Wolfe MS. 2009. Tau mutations in neurodegenerative diseases. *J Biol Chem* **284**: 6021–6025.

Wszolek ZK, Slowinski J, Golan M, Dickson DW. 2005. Frontotemporal dementia and parkinsonism linked to chromosome 17. *Folia Neuropathol* **43**: 258–270.

Wszolek ZK, Tsuboi Y, Ghetti B, Pickering-Brown S, Baba Y, Cheshire WP. 2006. Frontotemporal dementia and parkinsonism linked to chromosome 17 (FTDP-17). *Orphanet J Rare Dis* **1**: 30.

Wu D, Vonk JJ, Salles F, Vonk D, Haslbeck M, Melki R, Bergink S, Kampinga HH. 2019. The N terminus of the small heat shock protein HSPB7 drives its polyQ aggregation–suppressing activity. *J Biol Chem* **294**: 9985–9994.

Xu L-R, Liu X-L, Chen J, Liang Y. 2013. Protein Disulfide Isomerase Interacts with Tau Protein and Inhibits Its Fibrillization. *PLoS One* **8**: e76657.

Zhang X, Zhang S, Zhang L, Lu J, Zhao C, Luo F, Li D, Li X, Liu C. 2019. Heat shock protein 104 (HSP104) chaperones soluble Tau via a mechanism distinct from its disaggregase activity. *J Biol Chem* **294**: 4956–4965.

Zhao J, Huvent I, Lippens G, Eliezer D, Zhang A, Li Q, Tessier P, Linhardt RJ, Zhang F, Wang C. 2017. Glycan Determinants of Heparin-Tau Interaction. *Biophys J* **112**: 921–932.

Zhou H-X, Rivas G, Minton AP. 2008. Macromolecular Crowding and Confinement: Biochemical, Biophysical, and Potential Physiological Consequences. *Annu Rev Biophys* **37**: 375–397.

Zimmerman SB, Trach SO. 1991. Estimation of macromolecule concentrations and excluded volume effects for the cytoplasm of Escherichia coli. *J Mol Biol* **222**: 599–620.

Żwirowski S, Kłosowska A, Obuchowski I, Nillegoda NB, Piróg A, Ziętkiewicz S, Bukau B, Mogk A, Liberek K. 2017. Hsp70 displaces small heat shock proteins from aggregates to initiate protein refolding. *EMBO J* **36**: 783–796.

VITA

EDUCATION:

B.S. Biological Sciences, Biochemistry Concentration
Cornell University, Ithaca, NY 2012

PhD Medicinal Chemistry
University of Washington, Seattle, WA 2019

PUBLICATIONS:

Baughman HER, Pham THT, Adams CS, Nath A*, Klevit RE*. 2019. Release of a disordered domain enhances HspB1 chaperone activity toward tau [in preparation]

Clouser AF, **Baughman HER**, Basanta B, Guttman M, Nath A, and Klevit RE (2019) "Interplay of disordered and ordered regions in a human small heat shock protein yields an ensemble of 'quasi-ordered' states" [under review]

Janowska MK, **Baughman HER**, Woods CN, Klevit RE. 2019. Mechanisms of Small Heat Shock Proteins. *Cold Spring Harb Perspect Biol* a034025.

Baughman HER, Clouser AF, Klevit RE*, Nath A*. 2018. HspB1 and Hsc70 chaperones engage distinct tau species and have different inhibitory effects on amyloid formation. *J Biol Chem* **293**: 2687–2700

CONFERENCES:

- Protein Society Annual Symposium, Seattle, WA. July 2019
  Poster Presentation, "Release of a disordered domain enhances HspB1 chaperone activity toward tau"
- Intrinsically Disordered Proteins Gordon Research Conference, Les Diablerets, Switzerland, July 2018
  Poster Presentation, "The key role of chaperone disorder in the inhibition of tau aggregation"
- Protein Society Annual Symposium, Montreal, Quebec, Canada, July 2017
  Poster Presentation, "HspB1 and Hsc70 engage distinct tau species and have different inhibitory effects on amyloid formation"
- Biophysical Society Annual Meeting, Los Angeles, CA, February 2016
  Poster Presentation, "The disparate effects of two molecular chaperones on tau amyloid formation"